Texas Commission on Environmental Quality (TCEQ)

Project # 582-10-94307-FY14-06

Flare Performance Optimization: DRE/CE vs. Soot

Phase I Final Report

Prepared by:

Daniel Chen, PI
Helen Lou, Co-PI
Xianchang Li, Co-PI
Peyton Richmond, Co-PI
(Lamar University)
Matthew Johnson, PI
(Carleton University)

Lamar University
Beaumont, TX 77710

August 31, 2014

Distribution List

Jim Smith
TCEQ Project Manager
Air Quality Division
Texas Commission on Environmental Quality
Austin, Texas

Dr. Daniel H. Chen
Principal Investigator
Lamar University,
Beaumont, Texas

General Requirements

This project is a secondary data project. A secondary data project involves the gathering and /or use of existing environmental data for purposes other than those for which they were originally collected. This document is based on EPA's National Risk Management Research Laboratory (NRMRL) QAPP for secondary data project and satisfies a Category III level of QA.

TCEQ **Project # 582-10-94307-FY14-06**
Flare Performance Optimization: DRE/CE vs. Soot

Executive Summary

Current EPA regulations (40CFR60.18) require smokeless flaring, which motivates flare operators to over-steam or over-air to suppress smoke at the expense of combustion efficiency (CE). It is also well known that incipient smoke point (ISP) is a good indicator for good combustion, but the phenomena is neither well understood nor scientifically defined. Further, many factors affect soot emission and unburned/ produced VOC emissions. This leads to a question of how to operate the flares in order to achieve the optimal over-all environmental performance.

From an operations standpoint, there are dual objectives for flares to accomplish: full destruction of hydrocarbons and negligible soot emission. In this project, the challenge of simultaneously addressing these two goals is examined. First, the task performed at Carleton University generated DRE/CE/soot emission data for various fuel/nitrogen mixes by conducting large-scale laboratory flare experiments. Second, a new mechanism that contains soot precursors and C4 species was developed and validated with experimental data. Third, CFD methodology was used to model soot yield and combustion efficiency for CU's lab data and 2010 TCEQ flare tests data. Fourth, response surface models were developed based on controlled flare test data sponsored by EPA (1983, 1984) and TCEQ (2010) for which both soot and CE/DRE data are available.

Laboratory Scale Flare Measurements of Soot, CE, NOx for Alkane Mixtures and Ethylene

Figure E.1 shows a photograph of the laboratory flare in the Energy & Emissions Research Lab at Carleton University. Experimental measurements of flare efficiency and species emission rates were performed using flares of three different diameters (38.1 mm, 50.8 mm, and 76.2 mm), for a range of flare gas compositions summarized in Table E.1. Separate methodologies based on closing the overall carbon mass balance and based on metered injection of tracer into the plume and sampling system were employed, and full mathematical details of

these methods in conjunction with detailed uncertainty analysis procedures have been separately submitted for peer-reviewed journal publication. These methodologies permitted quantitative measurements of flare efficiency, soot emission rates and NOx emission rates as reported with the results.

Figure E.2 provides an overview of flare efficiency test results for the present experiments. Efficiencies were generally high as expected given the quality of the fuels and the quiescent crossflow conditions. Efficiencies for flares burning methane-based natural gas mixtures were all above 99%. Efficiencies were lower when burning ethylene, predominantly due to increased soot emissions. Figure E.3 summarizes sample soot yield measurement results for the 50.8 m diameter flare. Overall, soot emission rate results were shown to have strong dependence on fuel chemistry and comparatively negligible dependence on flare diameter. By contrast, NOx emission rates were shown to have little dependence on fuel chemistry and scaled directly with the fuel consumption rate.

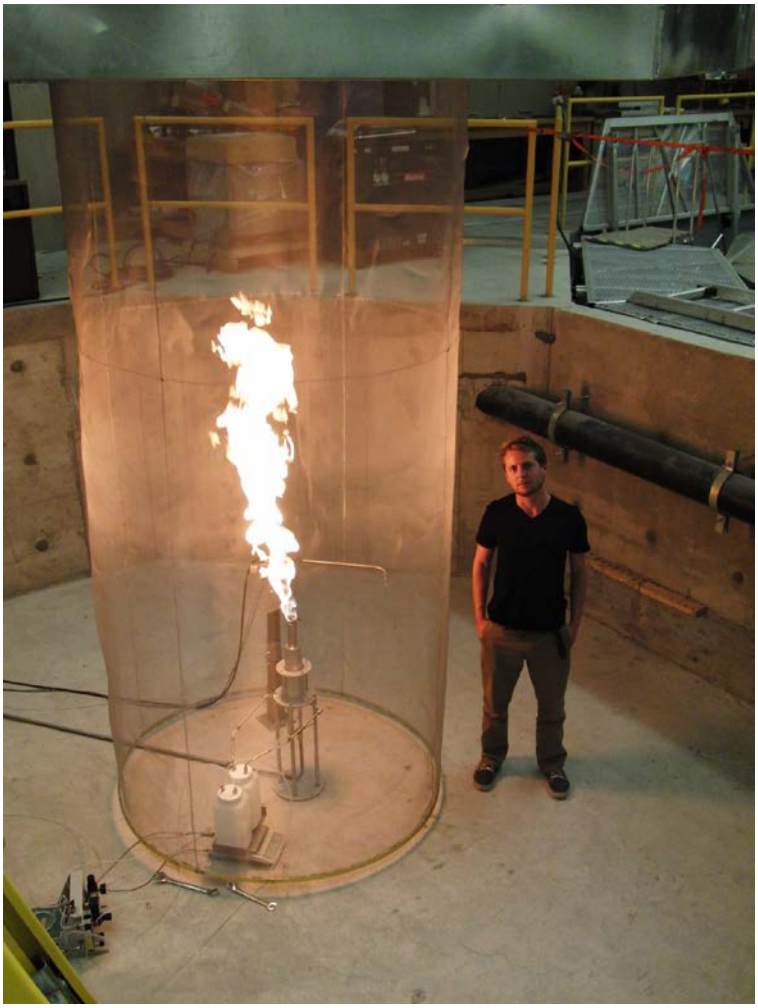

Figure E.1: Photo showing close-up of the flare

Table E.1: Flare Gas Compositions used in Experiments

Species	Purity (%)	Average 6-Mix (%)	Heavy 4-Mix (%)	Ethylene (%)
Methane	99.0	85.24	74.54	-
Ethane	99.0	7.06	15.47	-
Propane	99.0	3.11	6.83	-
Butane	99.0	1.44	3.16	-
Carbon Dioxide	99.0	1.91	-	-
Nitrogen	99.999	1.24	-	-
Ethylene	99.5	-	-	100

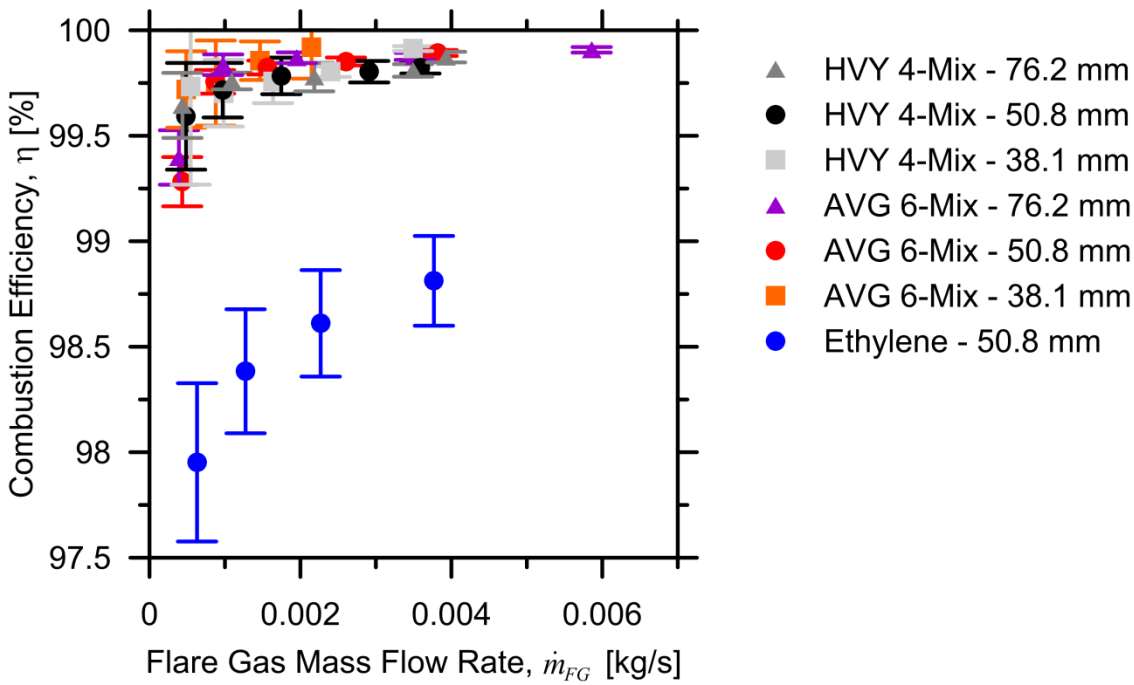

Figure E.2: Combustion efficiency calculated with the carbon balance method for all test cases.

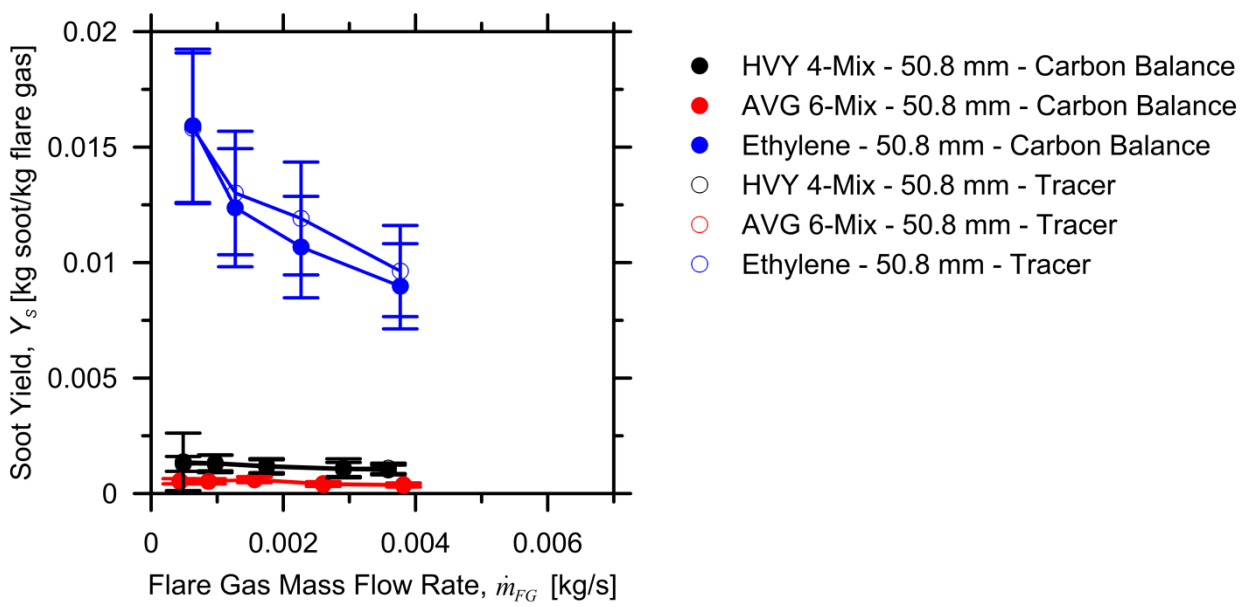

Figure E.3: Soot yield calculated with the carbon balance and tracer injection methods for 50.8 mm burner test cases.

Mechanism Development

A new reduced reaction mechanism LU 3.0.1 was built upon earlier mechanisms (LU 1.0, LU 1.1, and LU 2.0) geared for C_1-C_3 hydrocarbons. LU 3.0.1 contains important soot precursor species and can handle C_1-C_4 hydrocarbons. The important C_4-species included in this mechanism are n-butane, 1-butene and 1,3-butadiene. Since prediction of soot emission from flares using a CFD solver (ANSYS Fluent) is the key objective of this project, soot precursor species (acetylene, ethylene and benzene) employed in ANSYS Fluent (e.g., Moss-Brookes-Hall) soot models are included. Further, the new reduced mechanism also attempts to strike a balance between Volatile Organic Compound (VOC) emissions and soot emissions. A preliminary selection of species that included both VOC and soot precursors was made based on the objectives mentioned above. This preliminary list was further improved by using the reaction path analyzer in CHEMKIN to identify important intermediates and by conducting reaction rate analysis to determine which species had higher rates of production and actively participated in the combustion mechanism. The new mechanism with 50 species and 310 reactions has been compared to the full USC II mechanism and earlier combustion mechanisms for its accuracy. The results show that the predicted concentration of VOC and soot precursor species are comparable to the full USC II and are consistent with previous Lamar mechanisms like LU1.1 and LU2.0. LU3.0.1 has also been validated successfully against experimental performance indicators like laminar flame speed, ignition delay and adiabatic flame temperature using CHEMKIN. LU3.0.1 has been used in conjunction with the Moss-Brooks soot model built in ANSYS Fluent to predict black carbon emission in sooty flames (Task 2 test data by Carleton University and 2010 flare study data provided by Aerodyne Research, Inc.).

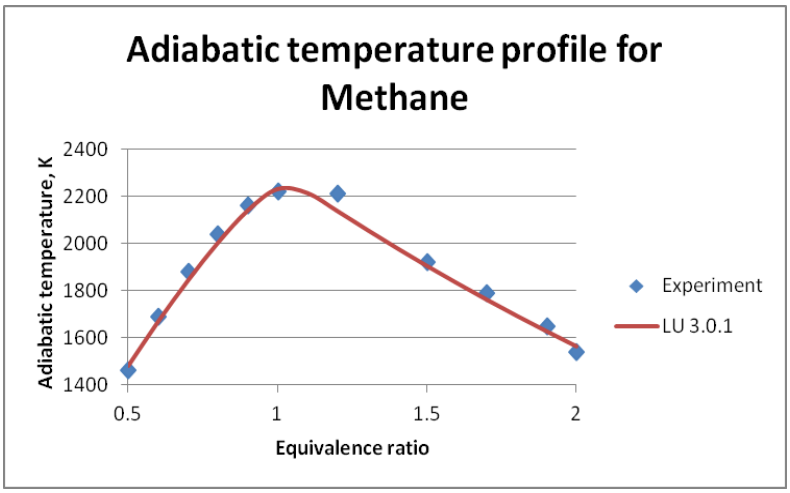

Fig. E.4 Adiabatic flame temperature of Methane

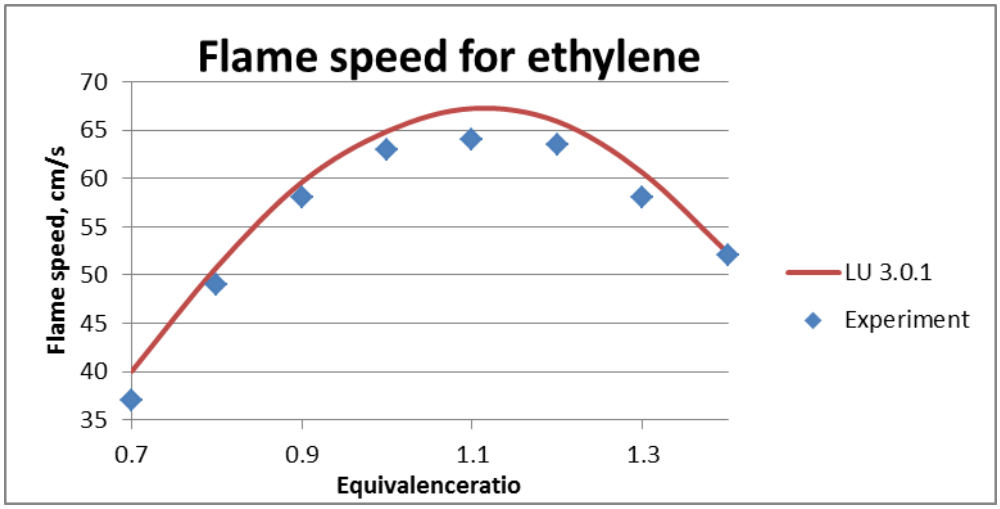

Fig.E.5 Laminar flame speed for different equivalence ratios for Ethylene

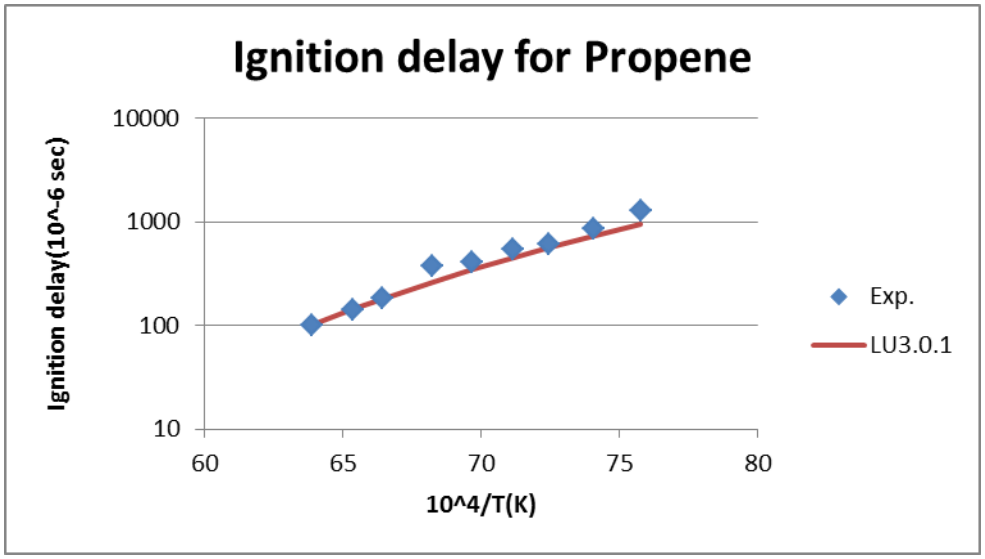

Fig. E.6 Ignition delay time for propene

Table E.2: Comparison of prediction errors of reduced mechanisms for mole fraction of major species at residence time of 1 sec for C_3H_6 fuel

Species	USC II	LU 3.0.1	Abs. error %	LU 1.0	Abs. error %	LU 2.0	Abs. error %
C2H2	1.46E-06	1.32E-06	9.72	1.19E-06	18.53	1.21E-06	17.23
CH4	3.01E-07	3.02E-07	0.23	3.30E-07	9.68	3.91E-07	30.07
CO	5.59E-03	5.70E-03	1.97	6.24E-03	11.68	5.98E-03	7.06
CO2	1.21E-01	1.21E-01	0.20	1.20E-01	0.64	1.21E-01	0.35
H2	1.35E-03	1.37E-03	2.10	1.51E-03	12.31	1.45E-03	7.41
Average abs. error %			2.84		10.57		12.42

<u>CFD Modeling with Soot</u>

Computational fluid dynamics (CFD) analysis of soot yield and combustion efficiency have been performed on controlled flare tests for which DRE/CE/soot data are available (Carleton University's large scale laboratory flares and 2010 TCEQ tests). CU's experiments were performed for a range of controlled conditions with the purpose to quantify combustion efficiency and species yields, within explicitly quantified uncertainties, from turbulent diffusion non-premixed flame burning hydrocarbon mixtures relevant to low-momentum flares abundant in the oil and gas industry. To simulate these experiments for soot in Fluent, a new reduced reaction mechanism LU 3.0.1 that contains important soot precursor species and can handle C_1-C_4 hydrocarbons is developed. LU3.0.1 is used in conjunction with turbulence-chemistry

models like non-premixed model in Ansys FLUENT 13 to simulate CU's experiments and various air assisted flares in 2010 study. Probability Density Function (PDF) turbulence-chemistry interaction approach has been adopted to simulate these flare tests.

For CU's data, soot yield predicted with Fluent-PDF is well within uncertainty limits when the default constants in the Moss-Brooks models are used. However, the trend of soot yield versus exit velocity are off partly due to the late revisions of the Task 2 data and partly due to the need to adjust the model parameters. Corrections to the Moss-Brookes soot model's constants can better fit the trend. However such corrections must be dealt with careful analysis and validation. Combustion efficiencies and CO_2 yields predicted with the CFD model are within the experimental uncertainties.

Table E.3 Simulated (PDF) and experimental combustion efficiency of heavy 4-mix C_1-C_4 alkane mixture

Test no.	Jet Velocity (m/s)	CE % Experimental	CE % Simulation
12	0.28	99.67 (+/-0.31)	99.96
13	0.56	99.70 (+/-0.06)	99.95
14	1.00	99.75 (+/-0.05)	99.93
15	1.67	99.75 (+/-0.04)	99.87

For 2010 study data, the PDF model provided good predictions for soot yield and CE, Figure E.7 and Table E.4. However, the VOC yields are nearly non-existent when PDF model is used. For this reason, the eddy dissipation concept (EDC) model will be further explored in the future.

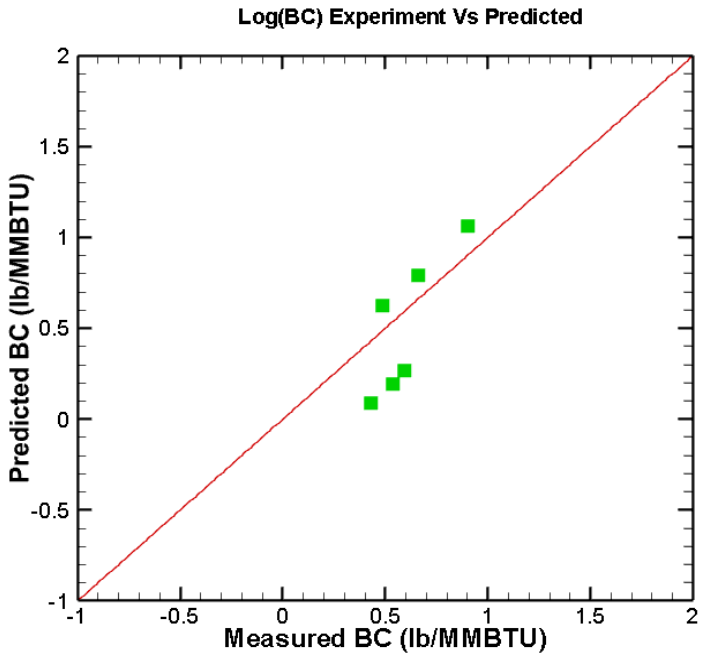

Fig. E.7 Measured vs. Predicted black carbon

Table E.4 Simulated (PDF) and experimental combustion efficiency of air-assisted flares in 2010 flare study

Case no.	CE Experiment (%)	CE Simulation (%)	% error
A1.1	96.9	96.93	0.03
A2.1	95.9	95.09	0.84
A3.1	98.3	98.88	0.59
A4.1	97.1	99.23	2.19
A5.1	95.9	99.37	3.62
A6.1	99.4	92.9	6.54
Avg.			2.3

Flare Test Data Analysis and Response Surface Models

Since soot emission was not considered for the CE calculations in the 2010 flare study, corrections were made and expressed as "corrected CE" or CCE using data provided by ARI. In general, CCE decreased about 3 – 8% (steam assist) and 17 – 22% (air assist) when soot

emissions were taken into account for these smoking flares. From the incipient smoke points identified in the 2010 flare study, the corresponding soot emissions along with the steam and air flow are shown in Table E.5 and E.6, respectively. It can be seen that steam assist in the range of 80 – 110 lb/MMBTU and air assist in the range of 4000 – 13000 lb/MMBTU produce minimum soot at the incipient smoke point.

Table: E.5 Incipient smoke points for steam assisted flare tests in 2010 Study

Test case	S1.5	S4.1	S5.1	S6.1	S8.3
Steam Assist (lb/MMBTU)	94	101	111	84	84.85
Soot (lb/MMBTU)	0.011	0.015	0.683	0.431	1.171

Table: E.6 Incipient smoke points for air assisted flare tests in 2010 Study

Test case	A1.1	A2.1	A3.1	A4.1	A5.1	A6.1	A7.1
Air Assist (lb/MMBTU)	8247	12000	4950	7600	5250	4440	4679
Soot (lb/MMBTU)	3.24	4.44	3.95	2.40	3.90	9.57	0.07

In this work, quadratic response surface (RS) models between DRE/CE/soot emission and the design/operating parameters were developed based on the 2010 TCEQ flare study and 1983/1984 EPA test data using Minitab and MATLAB statistics toolbox. The total number of data points used are 107 for steam assisted flares and 53 for air assisted flares. The following response surface models were developed:

a. log BC versus LHV, VG, S, DB (steam assist flares)

$$\log BC = -2.567 + 0.002904\,LHV - 0.4747\,S - 0.1679\,VG + 4.321\,DB + 0.000001\,LHV*LHV + 0.000078\,LHV*VG - 0.001005\,LHV*DB + 0.4575\,S*DB \quad (E.1)$$

b. log BC versus LHV, V, A, D, DB (air assist flares)

$$\log BC = -2.350 - 0.000001\,LHV*LHV + 0.0501\,A*A + 0.000115\,LHV*D + 0.000187\,LHV*A - 0.01579\,D*A - 0.01203\,D*V + 0.07571\,D*DB - 0.1208\,A*V \quad (E.2)$$

c. CCE vs. S, LHV, V, VG, and D (steam assist flares)

$$CCE = 98.78 + 0.1088\ S - 0.001152\ LHV - 0.00771\ V + 0.0862\ VG - 0.023\ D - 0.000741\ S*S - 0.00620\ D*D - 0.001299\ S*VG + 0.000169\ LHV*D \quad (E.3)$$

d. CCE vs. A, LHV, VG, and DB (air assist flares)

$$CCE = 107.24 - 0.04917\ LHV - 3.18\ A + 1.773\ VG - 6.79\ DB + 0.000021\ LHV*LHV - 1.396\ A*A - 0.000980\ LHV*VG - 0.649\ A*VG + 5.66\ A*DB \quad (E.4)$$

e. DRE vs. LHV, S, VG and D (steam assist flares)

$$DRE = 99.561 - 0.000708\ LHV + 0.0363\ S + 0.0287\ VG - 0.0860\ D - 0.000448\ S*S + 0.000129\ LHV*D - 0.000740\ S*VG \quad (E.5)$$

f. DRE vs. LHV, A, and VG (air assist flares)

$$DRE = 92.835 + 0.002843\ LHV - 5.192\ A - 0.1971\ VG + 0.000983\ LHV*A \quad (E.6)$$

where

LHV….	Lower Heating value (BTU/scf)
D……	Flare tip Dia (inch)
A……..	Air assist flow (lb/MMBTU)
S.....	Steam assist flow (lb/MMBTU)
DB……	Double bond (0/1)
V……..	Exit velocity (ft/s)
BC……	Soot (lb/MMBTU)
VG…..	Vent gas (MMBTU/hr)
CCE ….	Corrected Combustion Efficiency (%)
DRE ….	Destruction and Removal Efficiency (%)

Simultaneous minimization of soot yield and maximization of flare efficiencies is one of the objectives of this study. In order to estimate the region of each operating variable at a higher CCE and a lower soot emission, regression models were developed to present operating variables as a function of performance variables. The inverse response surface model developed for steam and air assists are given below:

$$S = -2718 - 28.3\ logBC + 69.8\ CCE - 5.80\ logBC*logBC - 0.427\ CCE*CCE \quad (E.7)$$

$$A = -252570 - 6968\ logBC + 6806\ CCE - 2166\ logBC*logBC - 43.0\ CCE*CCE \quad (E.8)$$

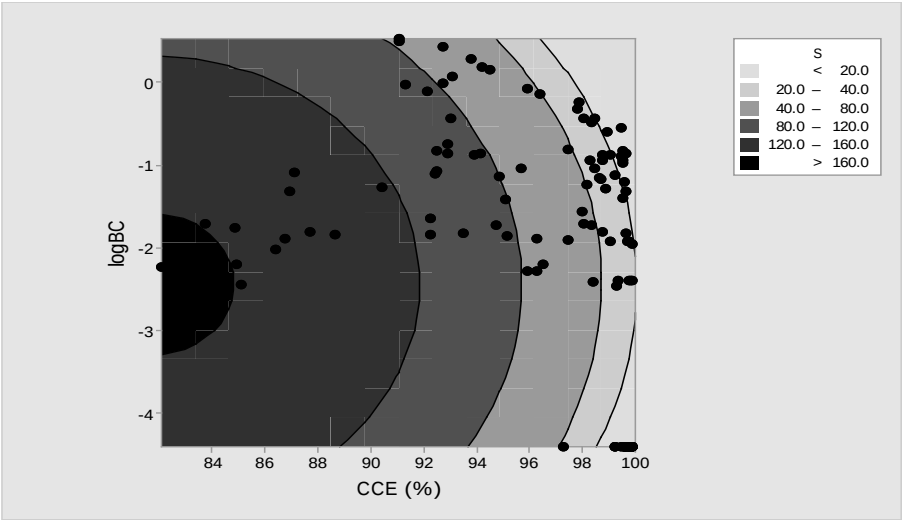

Fig. E.8 2-D Contour plot for the model Steam flow vs. log BC, CCE

2-D and 3-D contour plots were developed using MINITAB and MATLAB statistics toolboxes respectively. From the plots, it was observed that low soot emission (log BC <–1 or BC < 0.1 lb/MMBTU) and high CE (>96%) exist simultaneously in the steam assist range of 20 – 70 lb/MMBTU and in the air assist range of 4000 – 10000 lb/MMBTU. These ranges do not exactly coincide with those of the incipient smoke point as shown in Tables E.1 & E.2. In fact, they are somewhat lower in terms of steam and air assists since they are deduced from Eqns. E.7 & E.8 and 1983/1984 data were also included in the data pool. Further, the regions of interest are also identified in terms of lower heating values (LHV) and vent gas (VG) flow rate. Table E.7 summarizes the region of interest of flare operating variables.

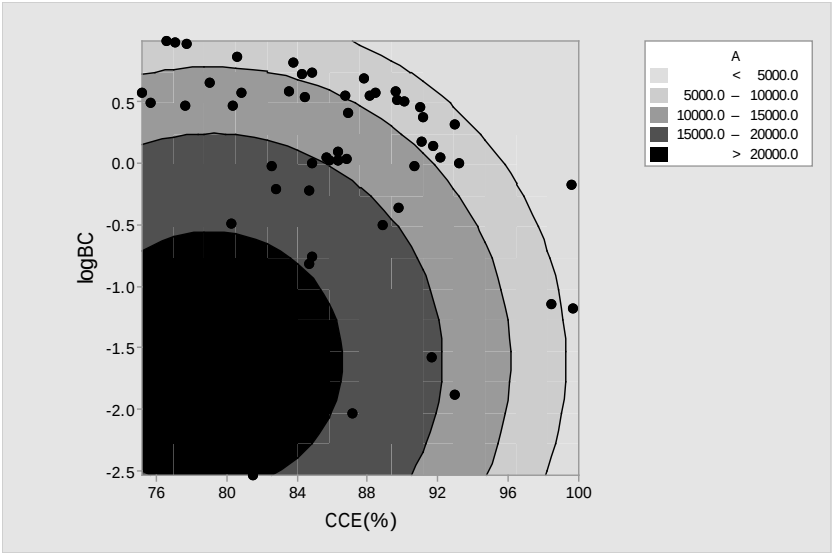

Fig. E.9 2-D Contour plot for the model Air flow vs. log BC, CCE

Table E.7 Optimal range of Flare operating variables based on inverse response surface models

Assist	Variables	Unit	Optimal Range
Steam Assist	S	lb/MMBTU	20 – 70
	LHV	BTU/scf	700 – 1300
	VG	MMBTU/hr	11 – 20
Air Assist	A	lb/MMBTU	4000 – 10000
	LHV	BTU/scf	400 – 600
	VG	MMBTU/hr	1.5 – 4

Table of Contents

		Page No
	Executive Summary	**2**
1	**Project Overview**	**16**
1.1	Project description	16
1.2	Project objectives	18
1.3	List of Project tasks and their status	19
2	**Large-Scale Laboratory Flare Experiments (Task 2)**	**22**
2.1	Introduction and Test Overview	22
2.2	Test Results	26
3	**Soot Models and Combustion Mechanism (Task 3)**	**38**
3.1	Selection of Soot Models from the Fluent Library	38
3.2	Mechanism Development	38
3.3	Mechanism Results and Discussion	50
3.3	Conclusions	60
4	**Model Controlled Flare Tests (Task 4)**	**63**
PART A: CFD Modeling of Large-Scale Laboratory Flare Data		
4.1	Background	63
4.2	Methodology for This Task	65
4.3	Results and Discussion	73
4.4	Conclusions	77
4.5	Future Work	78
PART B: CFD Study of 2010 TCEQ Flare Test Data		
4.6	Model Development for 2010 TCEQ Flare	79
4.7	Results for 2010 TCEQ flare tests	85
4.8	Challenges and Future Work	89
5	**Response Surface Models for DRE/CE/Soot Emissions (Task 5)**	**91**
5.1	Background	91
5.2	Methodology for This Task	91
5.3	Results and Discussion	97
5.4	Conclusions	113
5.5	Future Work	114
6	**Summary Remarks and Future Work**	**115**
	Nomenclatures	**118**
	Appendix	**119**

1. PROJECT OVERVIEW

1.1 Project Description

As indicated in recent TCEQ and EPA reports, the flare destruction and removal efficiency (DRE) and combustion efficiency (CE) can drop below the 98% threshold under certain high air/steam-assisted conditions even in compliance with 40 CFR 60.18. Basic combustion chemistry indicates that many intermediate species including VOCs, HO_x, NO_x, CO, and soot may be formed and emitted during the combustion process in addition to CO_2 and water. Flare operators have a special concern about soot emission, i.e., to avoid visible smoke to comply with EPA's visibility regulations. From an operations standpoint, this means there are dual objectives for flares to accomplish: full destruction of hydrocarbons and negligible soot emission. In this project, the challenge of simultaneously addressing these two goals is examined. Important issues to consider include the width of the operating window for flares to minimize soot emissions (i.e. be "smoke-free") while maintaining high destruction efficiencies (e.g., DRE>98%, CE>96.5%); whether air-assist or steam injection to suppress smoke always lowers destruction efficiencies; whether enough is known about soot formation near high DRE/CE regions to establish a relation between smoke suppression and destruction efficiencies; whether any relations depend on vent gas composition and heating value; and whether turbulence introduced by steam and air injection help to increase DRE/CE and decrease smoke enough to outweigh the negative impact of lowering the heating value in the combustion zone.

In this project, we seek to establish response surface (RS) models based on existing and forth-coming destruction efficiency and soot formation data. Combustion mechanisms with soot precursor species (C, C_2H_2, C_3H_3, C_6H_5, benzene, and PAHs) are developed. We studied soot models built in Fluent and others available in the literature. These models are calibrated with published and forth-coming soot/DRE/CE data. Computational fluid dynamics (CFD) software, CHEMKIN CFD-FLUENT, then is used to fill the data gap and to investigate important flare operating parameters such as steam/air assists, makeup fuel, vent gas composition, exit velocity (V), tip diameter (D), and crosswind (U). The resulting DRE/CE and soot information shall shed light on the interaction between DRE/CE/soot and flare operating parameters. The experimental data together with the simulation results from validated CFD tools is fitted to response surface models for quick scientific/engineering applications.

DRE, CE, and soot emission is expressed as a function of Combustion Zone Heating Value (CZHV), Jet velocity (V), Tip Diameter (D), and Crosswind (U). Note that CZHV here is broadly defined to include the effects of vent gas lower heating value (LHV), makeup fuel/pilot LHV, and assisted steam and air. The impact of fuel composition on DRE/CE/soot is therefore lumped into a single variable of CZHV. Of course, different fuel species may impact the extent of DRE/CE and soot yield even at the same net heating value level. For this reason, the sensitivity of species such as alkene vs. alkane, C_4 vs. C_1 (Carbon Number), and hydrogen to carbon ratio needs to be investigated.

Lamar University has developed a series of 50-species mechanisms for C_1-C_3 hydrocarbon combustion that were validated with key performance indicators like laminar flame speeds, adiabatic flame temperature, and ignition delay tests. The next version of mechanism (USC II + GRI 3.0) with additional butadiene, benzene, toluene, naphthalene, and carbon species is developed and tested for soot formation/oxidation in this proposed project. Lamar's CFD modeling has been validated with several laboratory flame (e.g., Sandia flame and McKenna flat flame) data sets having detailed VOC composition profiles. Further, Lamar's CFD group also modeled the cases in the 2010 Tulsa flare campaign and was able to predict the performance (DRE and CE) within 5% of the measured data.

Carleton University has established a track record in flare black carbon measurements both in the laboratory and in the field. Recent work published by the Energy & Emissions Research Lab has revealed a number of shortcomings with available EPA emission factor data for flare generated particulate matter. There is currently a great deal of uncertainty about the fuel specific soot emission rates of flares under varying operating regimes, and this lack of knowledge is exacerbated by a growing consensus that flares operated to ensure full removal of visible soot emissions may result in lower combustion efficiencies and increased emissions of unburned fuel. Although significant progress has been made in developing technologies capable of measuring flare generated particulate matter in situ, critical models necessary to interpret field data or to predict trends in flare performance over a range of conditions remain elusive. Leveraging a range of ongoing complementary research in the Energy & Emissions Lab at Carleton University, the research outlined in this project can directly address these shortcomings.

In this project, Carleton University provides critical laboratory soot yield and destruction/combustion efficiency data to support development and validation of the soot models

used in CFD. Parametric experiments to quantify soot emission rates, carbon conversion efficiency, destruction removal efficiency, and oxides of nitrogen emissions is performed at the newly commissioned controlled-flare experimental facility in the Energy & Emissions Research Laboratory at Carleton University. The flare facility has been designed to enable controlled experiments on vertical flares with flames up to 4 m in length, over a wide range of operating conditions. A mixed fuel delivery system featuring an array of mass-flow-controllers permits delivery of specified 6-component fuel mixtures consistent with common flare gas compositions. Soot emission rates are quantified within calculated uncertainty limits using laser induced incandescence (LII) while gas phase species in the flare combustion products are accurately measured using Fourier Transform Infrared Spectroscopy (FTIR). After simulating various flare scenarios, the simulated results are used to augment measured data to develop RS models for DRE/CE specification and soot minimization. The combination of Lamar University's modeling efforts with Carleton University's experimental measurements presents a unique opportunity to significantly improve understanding of the potential trade-offs in emissions at different operating conditions, and ultimately to develop optimal control strategies to maximize environmental performance.

1.2 Project Objectives

This project aims to study important flare operating parameters, while summarizing the knowledge base in simple response surface contour maps, and seeking optimal operating regimes for design, operation, and regulatory purposes. The project is to

1) Generate DRE/CE/soot emission data for various fuel/nitrogen mixes by conducting large-scale laboratory flare experiments
2) Develop CFD methodology that is validated/calibrated with controlled flare data and is capable of predicting DRE/CE/soot emission.
3) Search for the acceptable operating window in terms of steam/air injection and makeup fuel in the face of operating variables such as vent gas composition, exit velocity, and crosswind.

1.3 List of Project Tasks

To achieve the project objectives, specific tasks have been proposed and accomplished accordingly. The tasks are outlined below and the accomplishments are detailed in the sections followed.

Task 1 – Grant Activity Description:

The Grantee must submit and obtain approval of a GAD describing the activities to be performed for TCEQ reimbursement.

Status: The TCEQ approved GAD and TCEQ approved Quality Assurance Project Plan (QAPP) were delivered on time

Task 2 – Initiate Large-Scale Laboratory Flare Experiments to Obtain Soot/DRE/CE Data with C_1-C_4 Alkane/ Nitrogen Mixes;

This task consists of performing parametric experiments to quantify soot emission rates, carbon conversion efficiency, and destruction removal efficiency. Following necessary updates to gas handling systems, experiments needs to be performed in the newly commissioned flare experimental facility at Carleton University which features a large diameter hood and variable speed exhaust system that enables full capture of the product plume of the flare. Soot emission rates and DRE/CE data are quantified within calculated uncertainty limits using carbon-balance-based measurement protocols specifically developed for this project based on ongoing diagnostic development work in the Energy & Emissions Research Lab. [57]. Laser induced incandescence (LII) is used to quantify emitted soot, while gas phase species in the flare combustion products are accurately measured using an MKS Instruments Fourier Transform Infrared Spectroscopy (FTIR) gas analyzer. Measured Soot/DRE/CE data are collected for different C_1-C_4 Alkane / Nitrogen fuel mixtures and it is desired to further explore effects of varied flare gas flow rate and flare tip diameter. These experimental results are anticipated to be significant in their own right and are further used to support validation of simulation results as described below and to augment measured data for developing response-surface models for DRE/CE specification and soot minimization.

Status: The Summary Report has been delivered on time and the results of this task are also documented in this final report.

Task 3 – Survey and Select Soot Models from Fluent Library and Initiate the Development of a Combustion Mechanism containing Soot Precursors Species

The grantees studied soot models built in Fluent and others available in the literature. In addition, combustion mechanisms with soot precursor species (C_2H_2, C_3H_3, benzene, and PAHs) are developed. The soot models and the soot-species containing mechanism are employed in Fluent and calibrated with published and forth-coming soot/DRE/CE data. The development of a new mechanism (USC II + GRI 3.0) containing important soot precursor species is initiated to use Fluent library soot models effectively.

Status: The Summary Report has been delivered on time and the results of this task are also documented in this final report.

Task 4 - Model Controlled Flare Tests (1983-2011) for Which DRE/CE/Soot Data are Available:

Model several sets of controlled flare experiments (Carleton University's small and large scale laboratory flares, EPA 1983 tests, and 2010 TCEQ tests), and calibrate the selected soot models and CFD modeling methodology.

Status: The Summary Report has been delivered on time and the results of this task are also documented in this final report.

Task 5 - Develop Response Surface Models using all Available Experimental Data for DRE/CE/Soot Emissions:

Response surface models are developed using Microsoft Excel and MATLAB statistics tool box. DRE, CE, and Soot emission are expressed as a function of Combustion Zone Heating Value (CZHV), Jet velocity (V), Tip Diameter (D) and Crosswind (U). The impact of fuel composition on destruction efficiency and soot formation is assumed to be lumped into a single

variable of CZHV. The developed multi-dimensional response surfaces can be used to identify the optimal operating zones.

Status: The Summary Report has been delivered on time and the results of this task are also documented in this final report.

Task 6 **– Final Report**

A Final Report shall be delivered to the TCEQ Project Manager electronically via e-mail in Microsoft Word format no later than the deliverable due date shown below. The Final Report shall include the following components:

1. An executive summary or abstract.
2. A brief introduction that discusses background and objectives. Include relationships to other studies if applicable.
3. A discussion of the pertinent accomplishments, shortfalls, and limitations of the work completed under each Grant Activities Description task.
4. Recommendations, if any, for what should be considered next as a new study.

The Final Report will provide a comprehensive overview of activities undertaken and data collected and analyzed during the Grant Activity. The Final Report will highlight major activities and key findings, provide pertinent analysis, describe encountered problems and associated corrective actions, and detail relevant statistics including data, parameter, or model completeness, accuracy and precision.

Deliverable 6.1: Project Final Report

Deliverable Date: August 31, 2014

Status: The final report is completed on time.

2. LARGE-SCALE LABORATORY FLARE EXPERIMENTS (TASK 2)

2.1 Introduction & Test Overview

This report summarizes measurements completed as the Energy & Emissions Research Lab. at Carleton University's contributions to the Texas Commission on Environmental Quality sponsored project, "Flare Performance Optimization: DRE/CE vs. Soot" (Project number: 582-10-94307-FY14-06) led by Lamar University. Experimental measurement of the gas-phase composition and black carbon content of combustion products emitted from lab-scale flares have been performed at the Carleton University lab-scale flare facility, which is shown schematically in Figure 2.1, and in photos in Figure 2.2 and Figure 2.3. Experiments were performed for a range of controlled conditions as further detailed below. The purpose of the experiments was to quantify combustion efficiency and species yields, within explicitly quantified uncertainties, from a turbulent diffusion non-premixed flame burning hydrocarbon mixtures relevant to low-momentum flares ubiquitous in the oil and gas industry.

The test facility, measurement instruments, and equations used in the data analysis are described in detail in the attached methodology paper, which has been submitted for peer-reviewed journal publication. Briefly, gaseous flare gas components are mixed to the desired composition using a series of computer-controlled mass flow controllers. A modular burner is situated beneath a large exhaust hood from which suction is provided by a variable speed fan. Evaluation of combustion efficiency and species yields occurs after gas concentrations, soot volume fraction, and various temperatures (sample port, burner exit, duct wall) become stable. The experiments and analysis include measurement of the ambient concentrations of all relevant species before and after the flaring process.

The experiments summarized below investigated a range of flare gas flow rates tested over three burner sizes (38.1, 50.8 and 76.2 mm). Two different methane-based flare gas mixtures (the "Average 6-Mix" and "Heavy 4-Mix") were combusted on all three burners. Additional experiments burned pure ethylene on the 50.8 mm burner. Table 2.1 provides the compositional breakdown of the flare gas mixtures used in the experiments. Certain experiments were repeated numerous times throughout development of the experimental setup and final sampling protocol. Uncertainties for a given operating condition consider the systematic error

inherent in each test instance, as well as precision error based on the repeatability of the experimental outcomes. As such, the uncertainties on some of the outputs (namely those in which the test was repeated only twice) are large due to the larger student-t values.

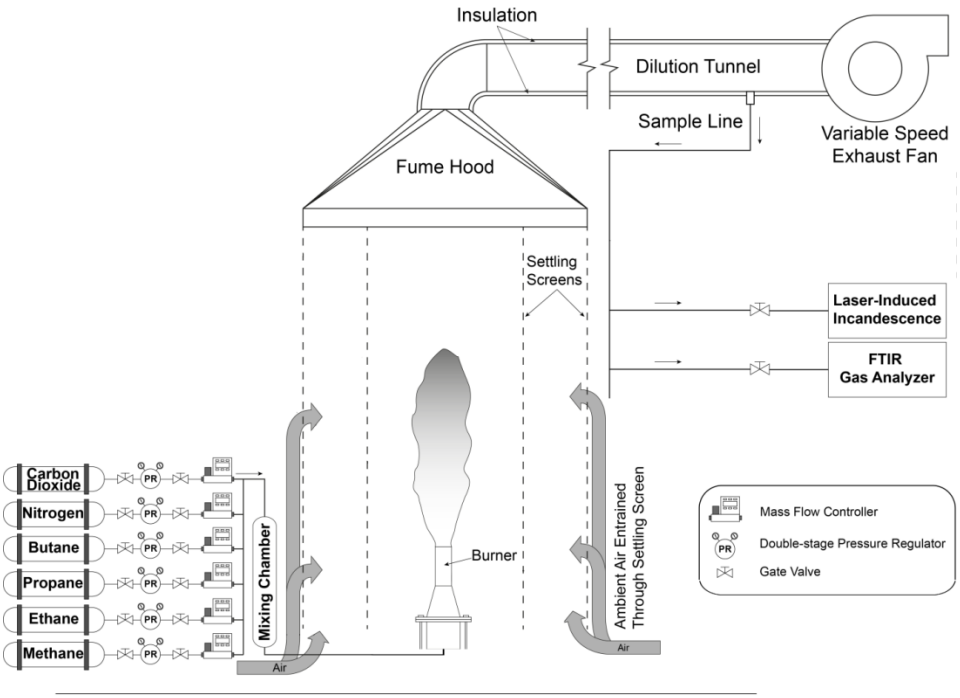

Figure 2.1: Schematic of the Energy & Emissions Research Lab. Flare Facility at Carleton University

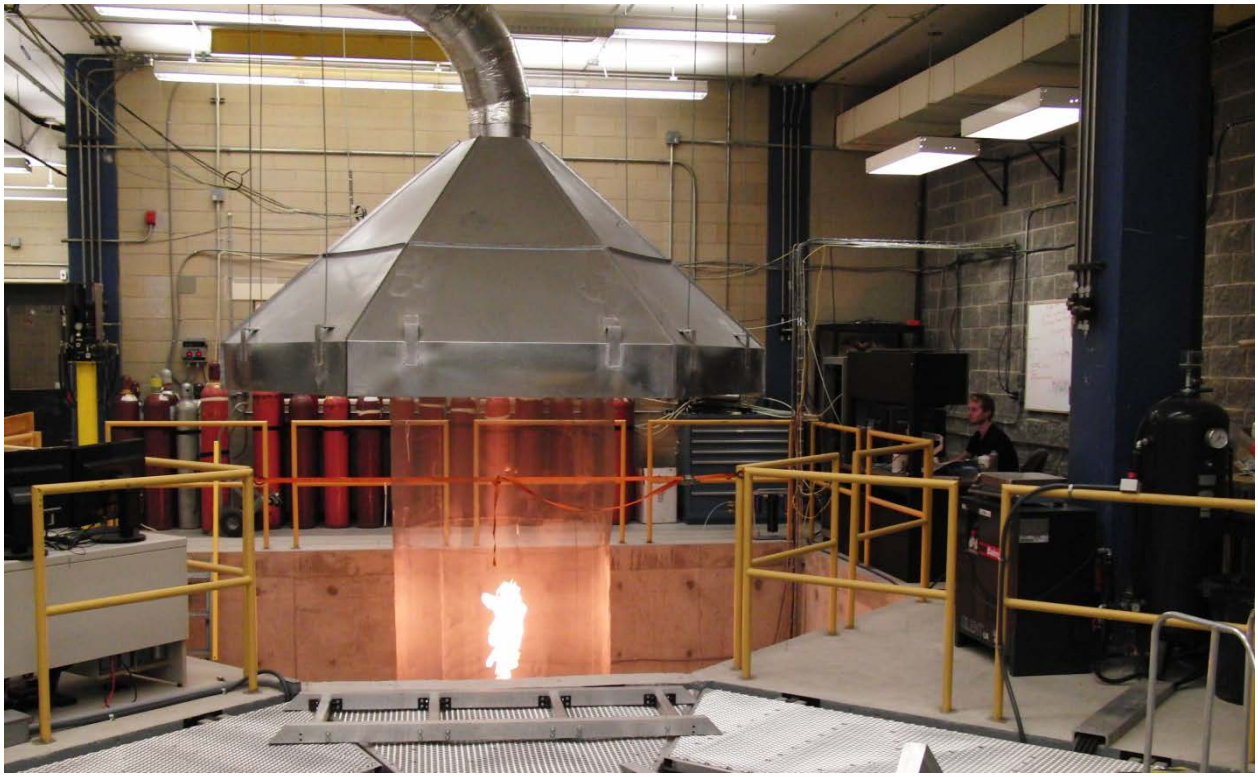

Figure 2.2: Photo showing sampling hood and flare at the Energy & Emissions Research Lab. Flare Facility at Carleton University

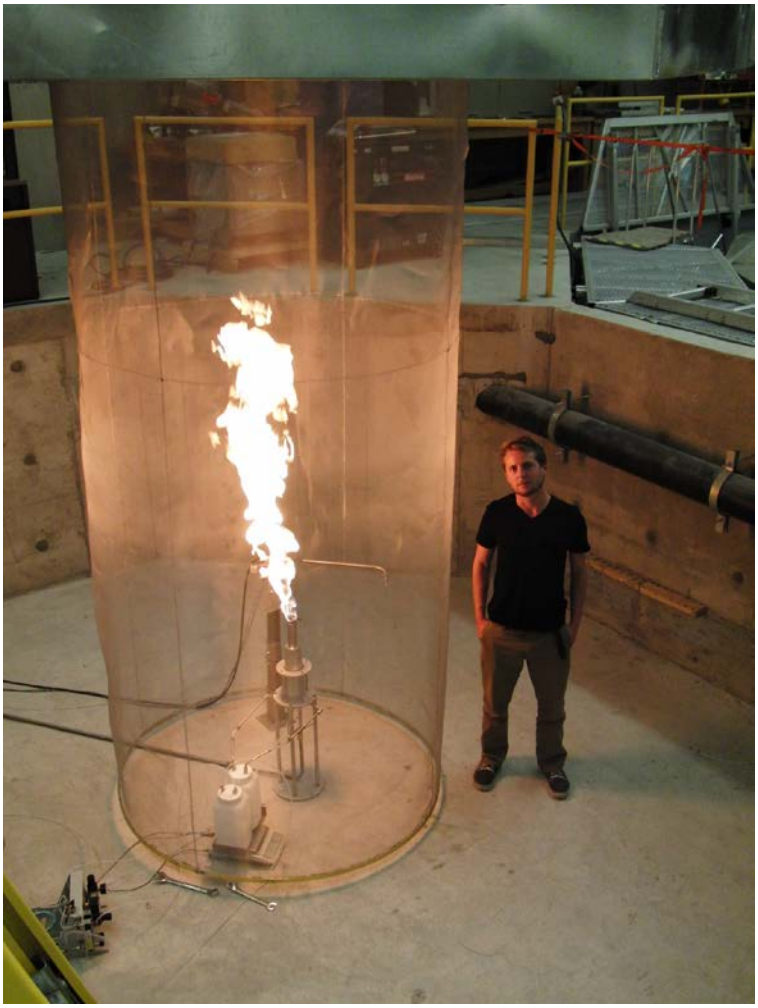

Figure 2.3: Photo showing close-up of the flare

Table 2.2: Flare Gas Compositions used in Experiments

Species	Purity (%)	Average 6-Mix (%)	Heavy 4-Mix (%)	Ethylene (%)
Methane	99.0	85.24	74.54	-
Ethane	99.0	7.06	15.47	-
Propane	99.0	3.11	6.83	-
Butane	99.0	1.44	3.16	-
Carbon Dioxide	99.0	1.91	-	-
Nitrogen	99.999	1.24	-	-
Ethylene	99.5	-	-	100

2.2 Test Results

2.2.1 Combustion Efficiency

A detailed description and analysis of the calculation methodologies for quantifying combustion efficiency, species emissions rates, and associated experimental uncertainties has been separately submitted for peer-reviewed journal publication to the Journal of Industrial & Engineering Chemistry (manuscript id: ie-2014-02914k, submitted July 21, 2014). Combustion efficiencies for all burner sizes and flare gas mixtures were calculated to be greater than 97.5 % using the carbon balance method. The methane-based flare gas mixtures resulted in very high combustion efficiencies (> 99.25 %). Efficiencies of flares burning pure ethylene were lower, primarily due to increased soot production. For tests where the tracer gas method was simultaneously employed, the calculated combustion efficiencies ranged from 92.75 to 108.77 % where the broadened range reflects larger uncertainty bands (~ ± 5% depending on conditions). Combustion efficiency was expected to be near 100% for the quiescent conditions in the lab and both calculation methods agreed within experimentally determined uncertainty limits. The combustion efficiency and uncertainties calculated with the carbon balance method are shown in Figure 2.4. Table 2.2 provides full details of the combustion efficiency measurement results, experimental conditions, and uncertainties for calculations using both the carbon balance and tracer injection methods.

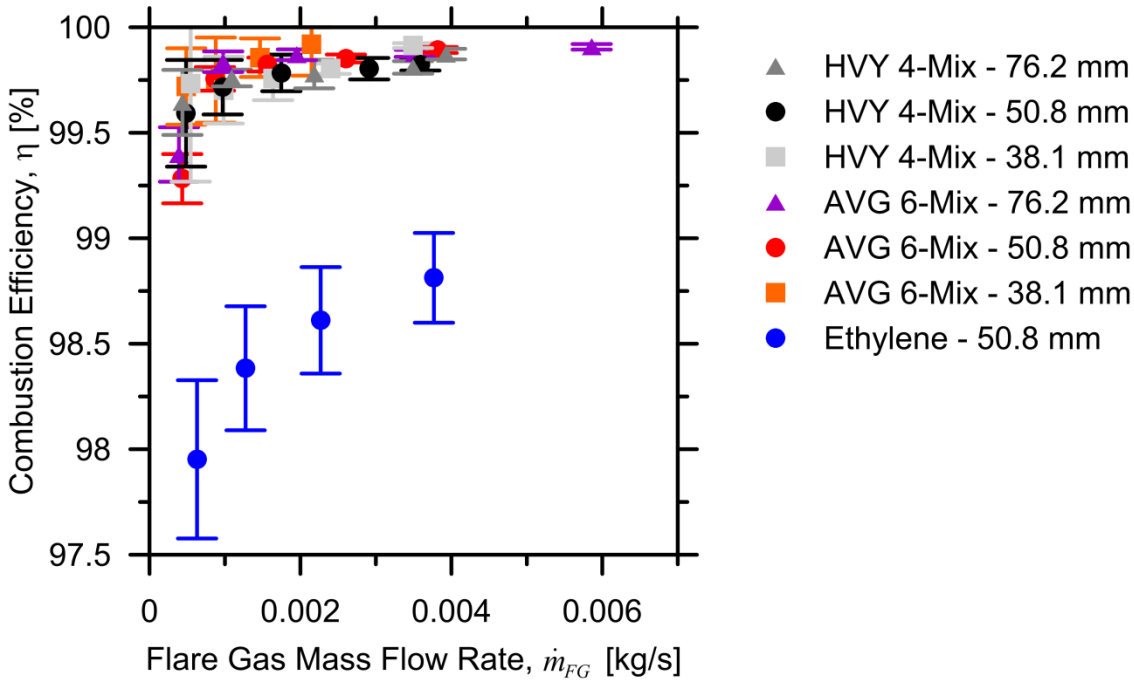

Figure 2.4: Combustion efficiency calculated with the carbon balance method for all test cases.

2.2.2 Soot Yield

Soot yield varied strongly with flare gas flow rate and flare gas composition as shown in Figure 2.5, Figure 2.6, and Figure 2.7. For the 38.1 and 50.8 mm burners, soot yield was found to decline with increasing flare gas flow rate across all mixtures tested. For the 76.2 mm flare, the soot yield trend was generally flat, initially exhibiting a minor increase before decreasing at the highest flow rates. The Heavy 4-Mix flare gas resulted in soot yields approximately twice as large as the Average 6-Mix. This result was consistent across all flow rates and burners tested. The soot yield from the ethylene tests was a full order of magnitude larger than soot yields measured from either of the methane-based flare gas mixtures. These trends are directly indicative of the importance of flare gas chemistry in determining soot production rates and the complex regimes of turbulent non-premixed flames below the transition from buoyancy dominated flames to momentum dominated flames.

Figure 2.5 shows soot yield results for the three flare gas mixtures tested on the 50.8 mm burner. Measurements using both the carbon balance and tracer injection method are displayed

and show agreement well within the error bars. Figure 2.6 and Figure 2.7 show soot yield results across all burners for the Heavy 4-Mix and Average 6-Mix respectively.

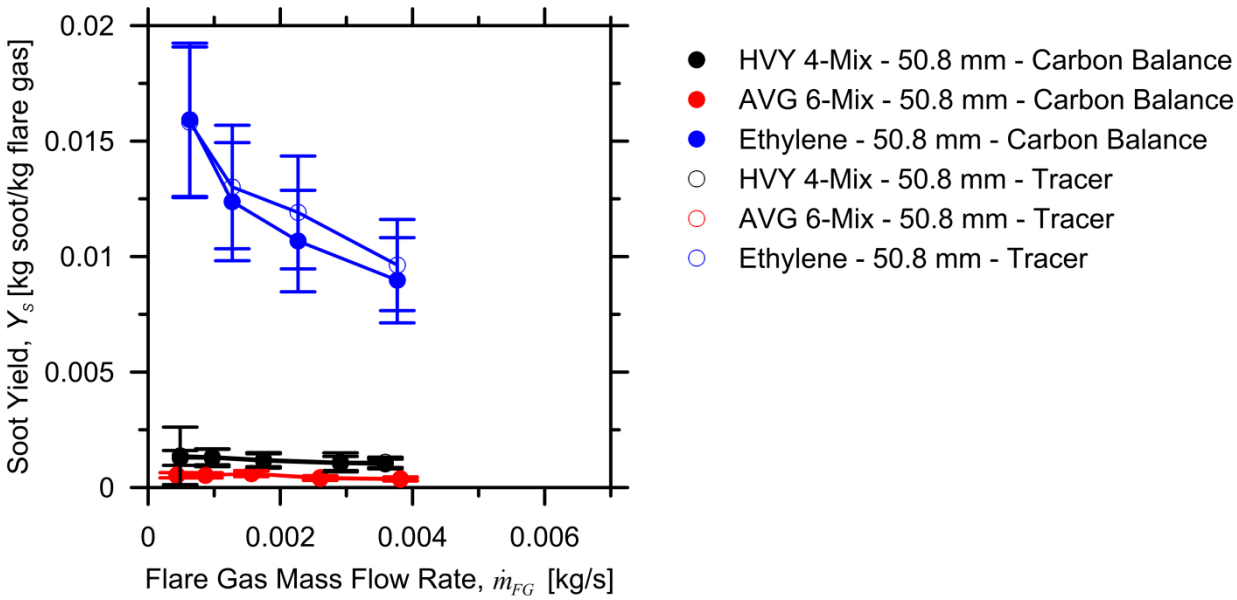

Figure 2.5: Soot yield calculated with the carbon balance and tracer injection methods for 50.8 mm burner test cases.

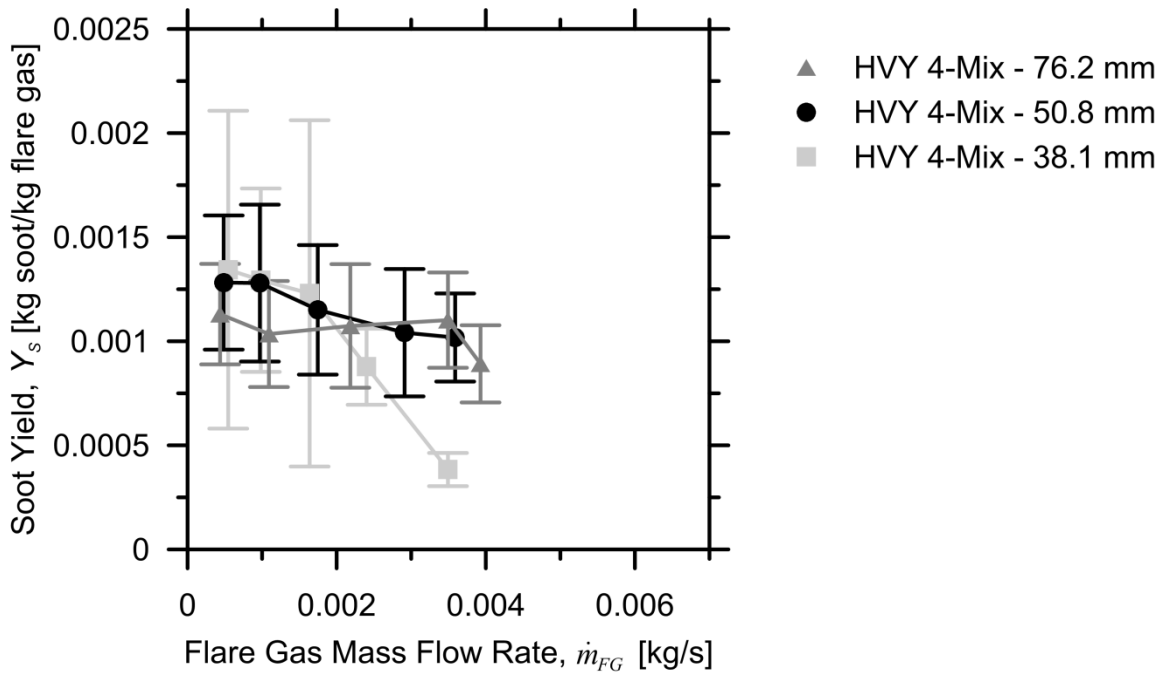

Figure 2.6: Soot yield calculated with the carbon balance method for Heavy 4-Mix flare gas test cases.

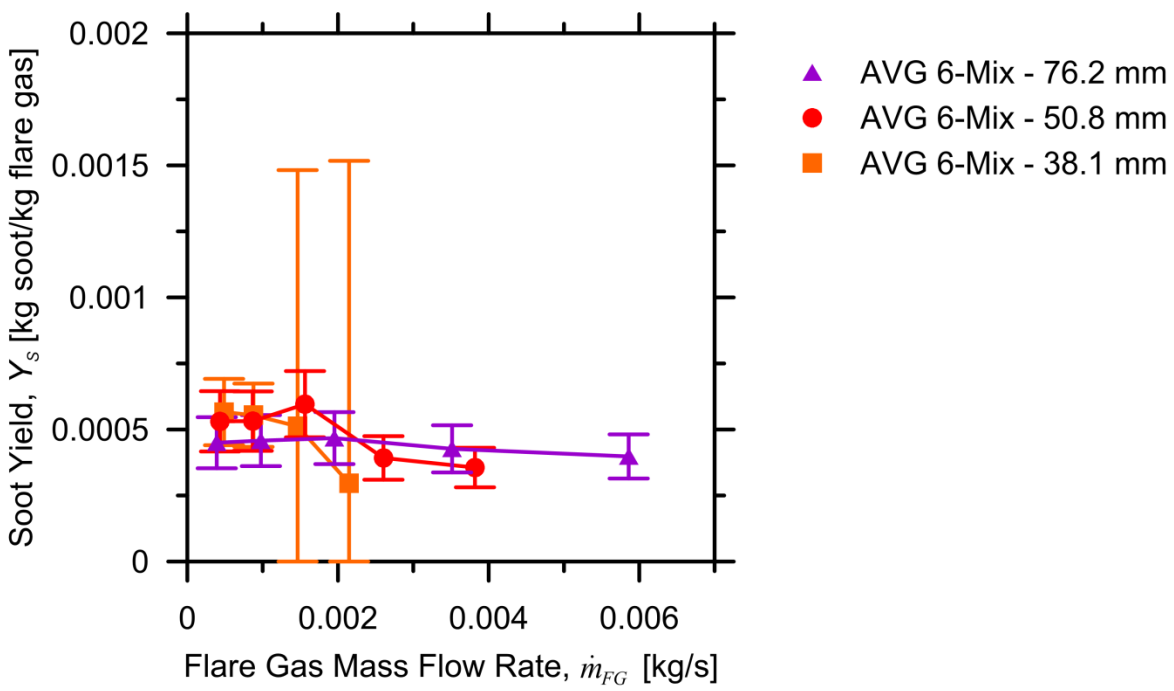

Figure 2.7: Soot yield calculated with the carbon balance method for Average 6-Mix flare gas test cases.

2.2.3 Gas Phase Yields

The main gas species considered for yield analysis were nitrogen oxides, carbon monoxide, and unburned methane. Figure 2.8 shows the results for NO_X yield in mass of NO_2 (moles of NO produced plus moles of NO_2 produced multiplied by the molar mass of NO_2) per mass flare gas. NO_X yield appears to be constant across the range of flow rates tested, independent of flare gas composition or burner size.

As shown in Figure 2.9 and Figure 2.10, both carbon monoxide and methane appear to decrease in yield as the flare gas flow rate increases, with little discernable variation between burner sizes or flare gas composition. The methane yield from the tests in which ethylene was burned are negligible and not displayed. Table 2.3 and Table 2.4 provide further details of the species emission rate measurement results, experimental conditions, and uncertainties for calculations using the carbon balance and tracer injection methods respectively.

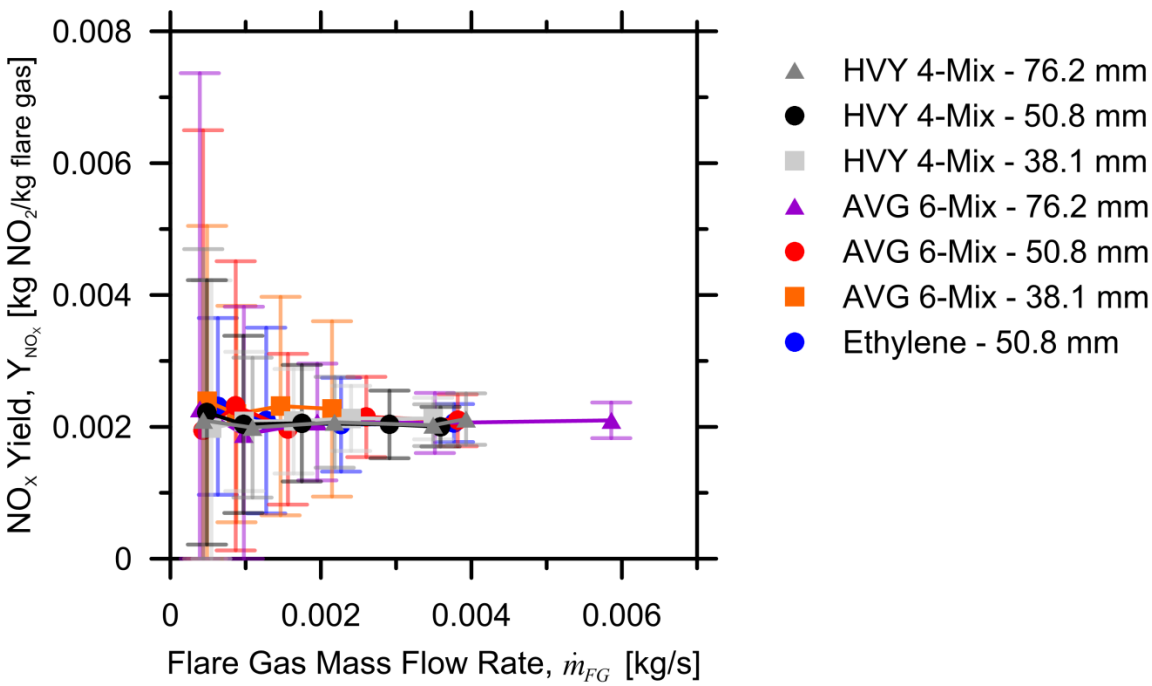

Figure 2.8: NO_X yield calculated with the carbon balance method for all test cases.

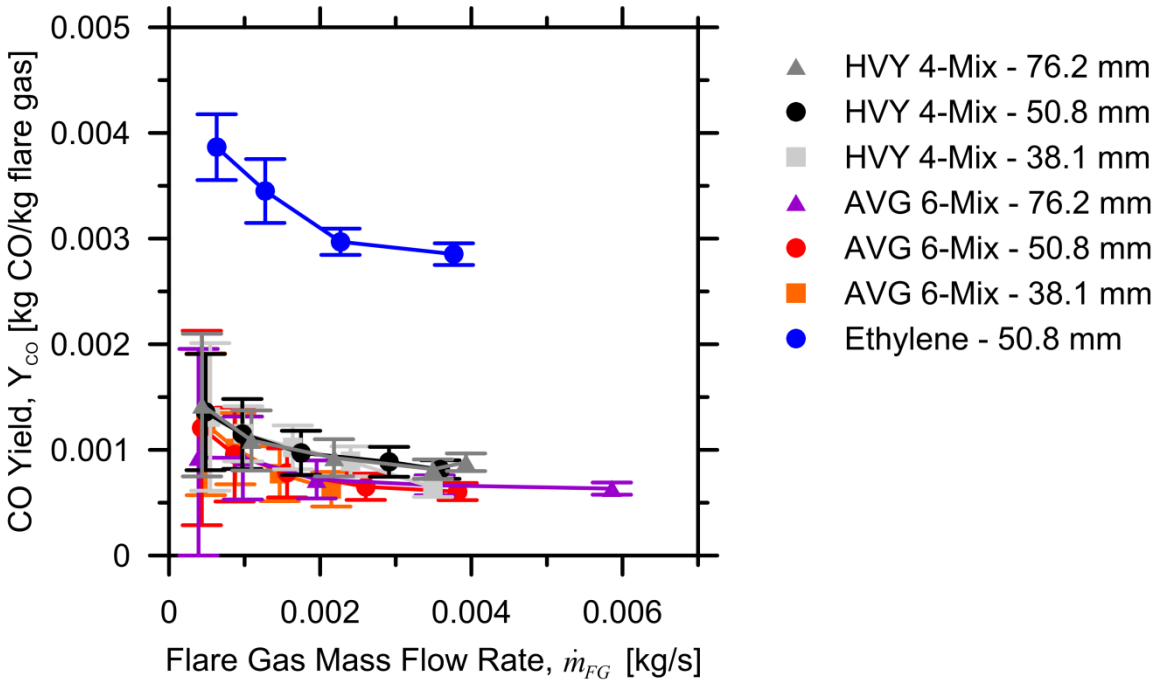

Figure 2.9: CO yield calculated with the carbon balance method for all test cases.

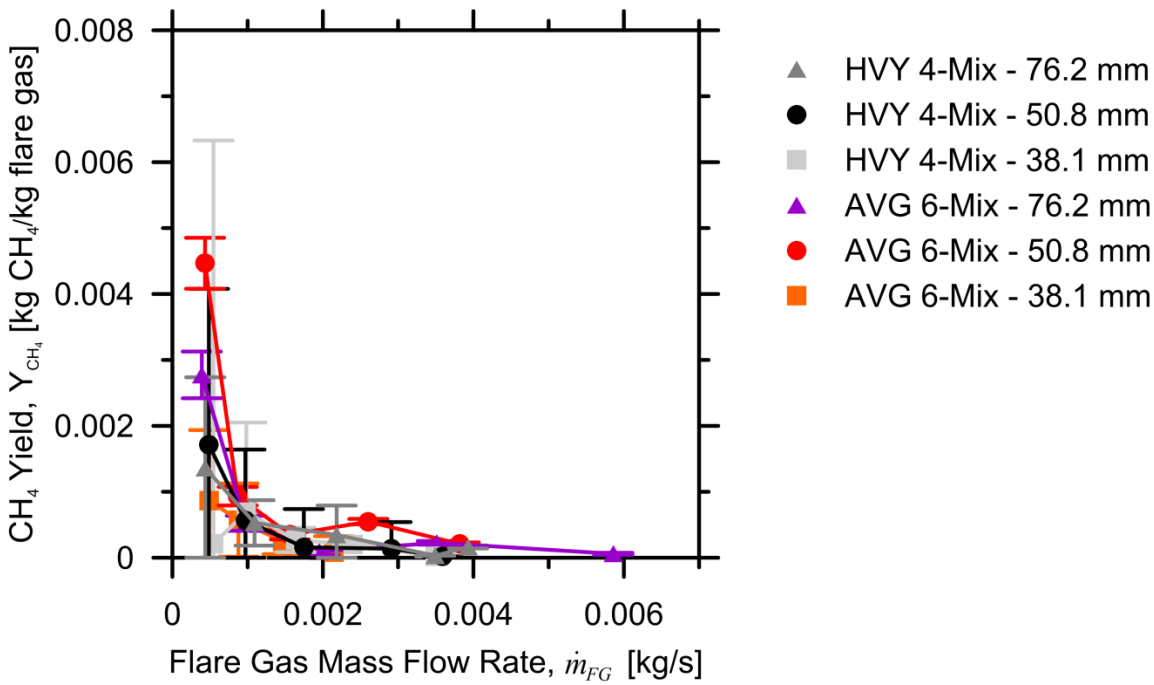

Figure 2.10: CH4 yield calculated with the carbon balance method for all test cases.

Table 2.3: Flare Operating Conditions and Combustion Efficiency Calculated with Carbon Balance and Tracer Injection Methods

Test Condition Number	Number of Times Experiment Repeated	Burner Exit Diameter [mm]	Flare Gas Mass Flow [kg/s]	Fire Froude Number	Reynolds Number	Exit Velocity [m/s]	Duct Flow Rate [m3/s]	Combustion Efficiency [%] - Carbon Balance	Uncertainty [±%]		Combustion Efficiency (%) - Tracer Injection	Uncertainty [± %]	
Average 6-Mix Flare Gas													
1	4	38.1	4.88E-04	5.11E-03	1617.47	0.56	1.02	99.72	0.18	0.18	-	-	-
2	8	38.1	8.78E-04	9.36E-03	2914.44	1.02	1.21	99.75	0.20	0.20	-	-	-
3	2	38.1	1.46E-03	1.52E-02	4857.70	1.66	1.63	99.86	0.09	0.09	-	-	-
4	2	38.1	2.15E-03	2.23E-02	7126.94	2.43	1.56	99.92	0.08	0.15	-	-	-
5	1	50.8	4.34E-04	2.22E-03	0.01	0.28	1.63	99.28	0.12	0.12	99.78	5.65	5.65
6	1	50.8	8.68E-04	4.40E-03	0.01	0.56	1.62	99.76	0.06	0.06	99.43	4.64	4.64
7	1	50.8	1.56E-03	7.92E-03	0.02	1.00	1.57	99.82	0.03	0.03	101.96	4.40	4.40
8	1	50.8	2.60E-03	1.33E-02	0.03	1.67	1.47	99.85	0.02	0.02	108.73	4.52	4.52
9	1	50.8	3.82E-03	1.91E-02	0.05	2.42	1.48	99.89	0.01	0.01	107.20	4.39	4.39
10	1	76.2	3.91E-04	7.59E-04	0.00	0.12	1.64	99.40	0.13	0.13	99.78	5.93	5.93
11	1	76.2	9.76E-04	1.86E-03	0.00	0.28	1.61	99.84	0.05	0.05	99.86	4.57	4.57
12	1	76.2	1.95E-03	3.65E-03	0.01	0.56	1.53	99.87	0.03	0.03	103.67	4.39	4.39
13	1	76.2	3.51E-03	6.67E-03	0.02	1.02	1.55	99.88	0.02	0.02	102.26	4.21	4.21
14	1	76.2	5.86E-03	1.11E-02	0.03	1.70	1.70	99.91	0.01	0.01	92.75	3.79	3.79
Heavy 4-Mix Flare Gas													
15	2	38.1	5.46E-04	3.96E-03	1925.29	0.56	0.78	99.73	0.27	0.47	98.53	4.67	4.67
16	4	38.1	9.82E-04	7.15E-03	3465.65	1.01	1.15	99.70	0.16	0.16	102.97	7.42	7.42
17	2	38.1	1.64E-03	1.18E-02	5777.27	1.68	1.56	99.76	0.10	0.10	103.49	34.14	34.14
18	1	38.1	2.40E-03	1.72E-02	8474.28	2.45	1.52	99.80	0.02	0.02	108.77	4.22	4.22
19	1	38.1	3.49E-03	2.49E-02	12325.22	3.53	1.50	99.91	0.01	0.01	105.87	4.05	4.05
20	4	50.8	4.85E-04	1.70E-03	1283.20	0.28	0.95	99.59	0.25	0.25	102.59	26.55	26.55
21	4	50.8	9.70E-04	3.40E-03	2567.13	0.56	1.28	99.72	0.13	0.13	102.16	4.92	4.92
22	3	50.8	1.75E-03	6.12E-03	4622.57	1.00	1.53	99.78	0.09	0.09	104.92	7.48	7.48
23	3	50.8	2.91E-03	1.02E-02	7704.61	1.67	1.49	99.80	0.05	0.05	103.90	11.56	11.56

Table 2.2: Flare Operating Conditions and Combustion Efficiency Calculated with Carbon Balance and Tracer Injection Methods (*continued*)

Test Condition Number	Number of Times Experiment Repeated	Burner Exit Diameter [mm]	Flare Gas Mass Flow [kg/s]	Fire Froude Number	Reynolds Number	Exit Velocity [m/s]	Duct Flow Rate [m3/s]	Combustion Efficiency [%] - Carbon Balance	Uncertainty [±%]		Combustion Efficiency (%) - Tracer Injection	Uncertainty [± %]	
24	1	50.8	3.59E-03	1.26E-02	9500.66	2.06	1.48	99.82	0.03	0.03	108.59	4.16	4.16
25	3	76.2	4.36E-04	5.74E-04	770.09	0.11	1.03	99.64	0.15	0.15	100.83	4.81	4.81
26	4	76.2	1.09E-03	1.42E-03	1925.63	0.28	1.23	99.76	0.04	0.04	102.72	4.45	4.45
27	3	76.2	2.18E-03	2.86E-03	3851.80	0.57	1.53	99.78	0.07	0.07	104.80	6.38	6.38
28	1	76.2	3.49E-03	4.52E-03	6162.68	0.90	1.51	99.81	0.03	0.03	103.51	3.95	3.95
29	1	76.2	3.93E-03	5.21E-03	6933.12	1.04	1.54	99.87	0.03	0.03	-	-	-
Ethylene Flare Gas													
30	1	50.8	6.30E-04	2.34E-03	1668.35	0.28	0.72	97.95	0.38	0.38	96.96	3.52	3.52
31	1	50.8	1.27E-03	4.72E-03	3370.23	0.57	1.55	98.38	0.29	0.29	104.28	3.24	3.24
32	1	50.8	2.27E-03	8.48E-03	6003.88	1.02	1.47	98.61	0.25	0.25	108.74	2.92	2.92
33	1	50.8	3.77E-03	1.41E-02	9976.05	1.70	1.49	98.81	0.21	0.21	104.61	2.64	2.64

Table 2.4: Species Yields Calculated with the Carbon Balance Method

Test Condition Number	CO_2 Yield [kg / kg_{fuel}]	CO Yield [kg / kg_{fuel}]	Uncertainty [± kg / kg_{fuel}]		CH4 Yield [kg / kg_{fuel}]	Uncertainty [± kg / kg_{fuel}]		Soot Yield [kg / kg_{fuel}]	Uncertainty [± kg / kg_{fuel}]		NOx Yield [kg / kg_{fuel}]	Uncertainty [± kg / kg_{fuel}]	
Average 6-Mix Flare Gas													
1	2.62	1.24E-03	6.71E-04	6.71E-04	8.66E-04	1.07E-03	8.66E-04	5.66E-04	1.26E-04	1.26E-04	2.39E-03	2.66E-03	2.39E-03
2	2.62	1.01E-03	3.38E-04	3.38E-04	5.71E-04	5.56E-04	5.56E-04	5.54E-04	1.20E-04	1.20E-04	2.19E-03	1.64E-03	1.64E-03
3	2.62	7.75E-04	2.60E-04	2.60E-04	2.44E-04	1.89E-04	1.89E-04	5.12E-04	9.70E-04	5.12E-04	2.32E-03	1.66E-03	1.66E-03
4	2.62	6.28E-04	1.64E-04	1.64E-04	8.30E-05	2.43E-04	8.30E-05	2.97E-04	1.22E-03	2.97E-04	2.27E-03	1.33E-03	1.33E-03
5	2.60	1.21E-03	9.20E-04	9.20E-04	4.47E-03	3.86E-04	3.86E-04	5.31E-04	1.14E-04	1.14E-04	1.95E-03	4.55E-03	1.95E-03
6	2.62	9.55E-04	4.44E-04	4.44E-04	9.33E-04	1.40E-04	1.40E-04	5.32E-04	1.12E-04	1.12E-04	2.32E-03	2.19E-03	2.19E-03
7	2.62	7.82E-04	2.32E-04	2.32E-04	3.50E-04	7.28E-05	7.28E-05	5.96E-04	1.25E-04	1.25E-04	1.96E-03	1.14E-03	1.14E-03
8	2.62	6.51E-04	1.24E-04	1.24E-04	5.47E-04	4.20E-05	4.20E-05	3.92E-04	8.25E-05	8.25E-05	2.15E-03	6.09E-04	6.09E-04
9	2.62	6.06E-04	8.12E-05	8.12E-05	2.09E-04	2.43E-05	2.43E-05	3.56E-04	7.48E-05	7.48E-05	2.10E-03	3.94E-04	3.94E-04
10	2.61	9.28E-04	1.03E-03	9.28E-04	2.77E-03	3.54E-04	3.54E-04	4.50E-04	9.68E-05	9.68E-05	2.27E-03	5.09E-03	2.27E-03
11	2.62	9.23E-04	3.92E-04	3.92E-04	5.22E-04	1.14E-04	1.14E-04	4.58E-04	9.66E-05	9.66E-05	1.89E-03	1.94E-03	1.89E-03
12	2.62	7.20E-04	1.80E-04	1.80E-04	9.28E-05	5.11E-05	5.11E-05	4.67E-04	9.83E-05	9.83E-05	2.07E-03	8.86E-04	8.86E-04
13	2.62	6.65E-04	9.43E-05	9.43E-05	2.26E-04	2.76E-05	2.76E-05	4.27E-04	8.92E-05	8.92E-05	2.06E-03	4.56E-04	4.56E-04
14	2.62	6.34E-04	5.76E-05	5.76E-05	5.94E-05	1.52E-05	1.52E-05	3.98E-04	8.35E-05	8.35E-05	2.10E-03	2.70E-04	2.70E-04
Heavy 4-Mix Flare Gas													
15	2.84	1.31E-03	6.98E-04	6.98E-04	2.11E-04	6.12E-03	2.11E-04	1.34E-03	7.64E-04	7.64E-04	1.98E-03	2.24E-03	1.98E-03
16	2.83	1.15E-03	2.61E-04	2.61E-04	6.91E-04	1.36E-03	6.91E-04	1.29E-03	4.40E-04	4.40E-04	2.08E-03	1.06E-03	1.06E-03
17	2.84	1.02E-03	2.08E-04	2.08E-04	2.70E-04	1.85E-04	1.85E-04	1.23E-03	8.32E-04	8.32E-04	2.09E-03	7.93E-04	7.93E-04
18	2.84	8.91E-04	1.42E-04	1.42E-04	2.00E-04	8.07E-06	8.07E-06	8.78E-04	1.83E-04	1.83E-04	2.13E-03	4.94E-04	4.94E-04
19	2.84	6.45E-04	8.98E-05	8.98E-05	2.15E-05	1.40E-06	1.40E-06	3.84E-04	7.98E-05	7.98E-05	2.13E-03	3.15E-04	3.15E-04
20	2.83	1.36E-03	5.50E-04	5.50E-04	1.71E-03	2.36E-03	1.71E-03	1.28E-03	3.22E-04	3.22E-04	2.22E-03	2.01E-03	2.01E-03
21	2.83	1.15E-03	3.31E-04	3.31E-04	5.66E-04	1.07E-03	5.66E-04	1.28E-03	3.77E-04	3.77E-04	2.04E-03	1.34E-03	1.34E-03
22	2.84	9.72E-04	2.09E-04	2.09E-04	1.59E-04	5.79E-04	1.59E-04	1.15E-03	3.11E-04	3.11E-04	2.06E-03	8.84E-04	8.84E-04
23	2.84	8.87E-04	1.41E-04	1.41E-04	1.37E-04	4.04E-04	1.37E-04	1.04E-03	3.06E-04	3.06E-04	2.04E-03	5.13E-04	5.13E-04

24	2.84	8.14E-04	8.79E-05	8.79E-05	1.99E-05	1.22E-06	1.22E-06	1.02E-03	2.12E-04	2.12E-04	2.00E-03	3.01E-04	3.01E-04

Table 2.3: Species Yields Calculated with the Carbon Balance Method (*continued*)

Test Condition Number	CO_2 Yield [kg / kg_{fuel}]	CO Yield [kg / kg_{fuel}]	Uncertainty [± kg / kg_{fuel}]		CH4 Yield [kg / kg_{fuel}]	Uncertainty [± kg / kg_{fuel}]		Soot Yield [kg / kg_{fuel}]	Uncertainty [± kg / kg_{fuel}]		NOx Yield [kg / kg_{fuel}]	Uncertainty [± kg / kg_{fuel}]	
25	2.83	1.42E-03	6.75E-04	6.75E-04	1.36E-03	1.38E-03	1.36E-03	1.13E-03	2.41E-04	2.41E-04	2.10E-03	2.60E-03	2.10E-03
26	2.84	1.09E-03	2.84E-04	2.84E-04	5.29E-04	3.44E-04	3.44E-04	1.03E-03	2.55E-04	2.55E-04	1.99E-03	1.06E-03	1.06E-03
27	2.84	9.25E-04	1.76E-04	1.76E-04	3.46E-04	4.46E-04	3.46E-04	1.07E-03	2.97E-04	2.97E-04	2.07E-03	6.89E-04	6.89E-04
28	2.84	8.17E-04	9.23E-05	9.23E-05	3.17E-05	1.98E-06	1.98E-06	1.10E-03	2.29E-04	2.29E-04	2.03E-03	3.17E-04	3.17E-04
29	2.84	8.83E-04	8.35E-05	8.35E-05	1.63E-04	2.29E-05	2.29E-05	8.91E-04	1.85E-04	1.85E-04	2.12E-03	3.90E-04	3.90E-04
Ethylene Flare Gas													
30	3.07	3.87E-03	3.12E-04	3.12E-04	0.00	-	-	1.59E-02	3.32E-03	3.32E-03	2.31E-03	1.34E-03	1.34E-03
31	3.09	3.45E-03	3.02E-04	3.02E-04	0.00	-	-	1.24E-02	2.56E-03	2.56E-03	2.10E-03	1.41E-03	1.41E-03
32	3.09	2.97E-03	1.24E-04	1.24E-04	0.00	-	-	1.07E-02	2.20E-03	2.20E-03	2.03E-03	7.11E-04	7.11E-04
33	3.10	2.85E-03	1.03E-04	1.03E-04	0.00	-	-	8.97E-03	1.84E-03	1.84E-03	2.06E-03	2.88E-04	2.88E-04

Table 2.5: Species Yields Calculated with the Tracer Injection Method

Test Condition Number	CO_2 Yield [kg / kg_{fuel}]	CO Yield [kg / kg_{fuel}]	Uncertainty [± kg / kg_{fuel}]		CH4 Yield [kg / kg_{fuel}]	Uncertainty [± kg / kg_{fuel}]		Soot Yield [kg / kg_{fuel}]	Uncertainty [± kg / kg_{fuel}]		NOx Yield [kg / kg_{fuel}]	Uncertainty [± kg / kg_{fuel}]	
Average 6-Mix Flare Gas													
5	2.62	1.21E-03	9.23E-04	9.23E-04	4.49E-03	3.04E-04	3.04E-04	5.33E-04	1.11E-04	1.11E-04	1.96E-03	4.57E-03	1.96E-03
6	2.61	9.52E-04	4.41E-04	4.41E-04	9.31E-04	1.34E-04	1.34E-04	5.30E-04	1.10E-04	1.10E-04	2.31E-03	2.18E-03	2.18E-03
7	2.68	7.99E-04	2.35E-04	2.35E-04	3.57E-04	7.29E-05	7.29E-05	6.08E-04	1.26E-04	1.26E-04	2.01E-03	1.16E-03	1.16E-03
8	2.85	7.08E-04	1.33E-04	1.33E-04	5.95E-04	4.02E-05	4.02E-05	4.27E-04	8.83E-05	8.83E-05	2.34E-03	6.57E-04	6.57E-04
9	2.81	6.49E-04	8.39E-05	8.39E-05	2.24E-04	2.47E-05	2.47E-05	3.82E-04	7.90E-05	7.90E-05	2.25E-03	4.14E-04	4.14E-04
10	2.62	9.31E-04	1.03E-03	9.31E-04	2.78E-03	3.16E-04	3.16E-04	4.52E-04	9.38E-05	9.38E-05	2.28E-03	5.11E-03	2.28E-03
11	2.62	9.23E-04	3.91E-04	3.91E-04	5.22E-04	1.12E-04	1.12E-04	4.58E-04	9.47E-05	9.47E-05	1.89E-03	1.94E-03	1.89E-03
12	2.72	7.47E-04	1.85E-04	1.85E-04	9.62E-05	5.29E-05	5.29E-05	4.85E-04	1.00E-04	1.00E-04	2.15E-03	9.16E-04	9.16E-04
13	2.68	6.81E-04	9.33E-05	9.33E-05	2.31E-04	2.70E-05	2.70E-05	4.37E-04	8.99E-05	8.99E-05	2.11E-03	4.60E-04	4.60E-04
14	2.43	5.89E-04	4.92E-05	4.92E-05	5.52E-05	1.40E-05	1.40E-05	3.70E-04	7.65E-05	7.65E-05	1.95E-03	2.41E-04	2.41E-04
Heavy 4-Mix Flare Gas													
15	2.80	1.30E-03	6.58E-04	6.58E-04	2.10E-04	6.05E-03	2.10E-04	1.33E-03	7.20E-04	7.20E-04	1.96E-03	2.17E-03	1.96E-03
16	2.93	1.18E-03	3.06E-04	3.06E-04	8.67E-04	2.62E-03	8.67E-04	1.25E-03	5.33E-04	5.33E-04	2.18E-03	9.91E-04	9.91E-04
17	2.94	1.06E-03	3.25E-04	3.25E-04	2.79E-04	1.01E-04	1.01E-04	1.28E-03	1.27E-03	1.27E-03	2.16E-03	1.21E-03	1.21E-03
18	3.09	9.71E-04	1.51E-04	1.51E-04	2.18E-04	4.74E-06	4.74E-06	9.56E-04	1.97E-04	1.97E-04	2.32E-03	5.32E-04	5.32E-04
19	3.01	7.00E-04	9.17E-05	9.17E-05	3.41E-05	1.55E-06	1.55E-06	3.97E-04	8.19E-05	8.19E-05	2.30E-03	3.24E-04	3.24E-04

20	2.92	1.52E-03	1.64E-03	1.52E-03	2.33E-03	2.05E-02	2.33E-03	1.37E-03	1.25E-03	1.25E-03	2.53E-03	3.18E-03	2.53E-03
21	2.90	1.19E-03	3.45E-04	3.45E-04	6.25E-04	1.25E-03	6.25E-04	1.33E-03	3.45E-04	3.45E-04	2.08E-03	1.38E-03	1.38E-03
22	2.98	1.02E-03	2.18E-04	2.18E-04	1.61E-04	6.27E-04	1.61E-04	1.21E-03	3.04E-04	3.04E-04	2.17E-03	9.60E-04	9.60E-04
23	2.95	9.26E-04	1.39E-04	1.39E-04	1.48E-04	4.03E-04	1.48E-04	1.09E-03	4.12E-04	4.12E-04	2.12E-03	6.25E-04	6.25E-04
24	3.09	8.84E-04	9.05E-05	9.05E-05	1.93E-05	1.39E-06	1.39E-06	1.09E-03	2.24E-04	2.24E-04	2.20E-03	3.17E-04	3.17E-04
25	2.87	1.49E-03	7.07E-04	7.07E-04	1.46E-03	1.29E-03	1.29E-03	1.13E-03	3.88E-04	3.88E-04	2.16E-03	2.61E-03	2.16E-03
26	2.92	1.13E-03	2.89E-04	2.89E-04	5.45E-04	3.54E-04	3.54E-04	1.06E-03	2.60E-04	2.60E-04	2.03E-03	1.08E-03	1.08E-03
27	2.98	9.77E-04	1.82E-04	1.82E-04	3.64E-04	4.76E-04	3.64E-04	1.13E-03	3.50E-04	3.50E-04	2.20E-03	7.40E-04	7.40E-04

Table 2.4: Species Yields Calculated with the Tracer Injection Method (*continued*)

Test Condition Number	CO_2 Yield [kg / kg_{fuel}]	CO Yield [kg / kg_{fuel}]	Uncertainty [± kg / kg_{fuel}]		CH4 Yield [kg / kg_{fuel}]	Uncertainty [± kg / kg_{fuel}]		Soot Yield [kg / kg_{fuel}]	Uncertainty [± kg / kg_{fuel}]		NOx Yield [kg / kg_{fuel}]	Uncertainty [± kg / kg_{fuel}]	
28	2.94	8.47E-04	9.09E-05	9.09E-05	3.77E-05	2.57E-06	2.57E-06	1.15E-03	2.36E-04	2.36E-04	2.12E-03	3.19E-04	3.19E-04
29	-	-	-	-	-	-	-	-	-	-	-	-	-
Ethylene Flare Gas													
30	3.04	3.89E-03	2.83E-04	2.83E-04	0.00	0.00	0.00	1.58E-02	3.26E-03	3.26E-03	2.35E-03	1.32E-03	1.32E-03
31	3.27	3.68E-03	3.06E-04	3.06E-04	0.00	0.00	0.00	1.30E-02	2.67E-03	2.67E-03	2.12E-03	1.48E-03	1.48E-03
32	3.41	3.30E-03	1.21E-04	1.21E-04	0.00	0.00	0.00	1.19E-02	2.44E-03	2.44E-03	2.30E-03	7.83E-04	7.83E-04
33	3.28	3.04E-03	9.48E-05	9.48E-05	0.00	0.00	0.00	9.63E-03	1.97E-03	1.97E-03	2.18E-03	3.02E-04	3.02E-04

3. SOOT MODELS AND COMBUSTION MECHANISM (TASK 3)

3.1 Selection of Soot Models from the Fluent Library

ANSYS FLUENT has four different models to estimate the formation of soot. FLUENT [1] can predict soot in combustion systems with these models.

1. **One-step Khan and Greeves model**: Rate of soot formation is calculated based on simple empirical rate
2. **Two-step Tesner model**: Rate of soot formation is estimated based on the formation of nuclei particles.
3. **Moss-Brookes model**: Rate of soot formation is estimated for CH_4 and higher hydrocarbon flames by solving respective transport equations for normalized nuclei concentration and mass fraction of soot. This model is not very empirical and gives higher accuracy compared to one-step and two-step models which are empirically-based approximate soot models.
4. **Moss-Brookes Hall model**: This is an extension to Moss-Brookes model which is applicable to higher hydrocarbons like kerosene, The work of Hall is based on a soot inception rate due to two-ringed($C_{10}H_7$) and three-ringed($C_{14}H_{10}$) aromatics, as opposed to the Moss-Brookes assumption of a soot inception due to acetylene or benzene (for higher hydrocarbons)[2]

Moss-Brookes model was chosen for experimental simulation after detailed analysis of the various models . The detailed description of this soot model is given in Section 4.2.2 FLUENT Setup and Soot Model.

3.2 Mechanism Development

The flaring process is complicated, since its performance is affected by many operating and meteorological conditions. If not operated appropriately, the flare’s destruction efficiency may be lower than the 98% threshold value and, in the meantime, the flaring produces unwanted intermediates and radicals (e.g., HCHO, OH, NO) in addition to unburned parent compounds. A case in point is flare operators' special concern on soot emission, i.e., to avoid visible smoke to comply with EPA's visibility regulation [3,4], leads to over-steaming or over-aeration at the

expense of flare combustion efficiency. Quantitative understanding of the soot growth and oxidation mechanisms in flames is critical to the development of CFD modeling as well as effective control of soot emissions. The detailed combustion mechanisms are too complicated for the speciation study of flaring events with CFD. In addition, the more rigorous ANSYS FLUENT Eddy-Dissipation Concept (EDC) model, which describes turbulence-chemistry interaction, can handle a maximum of only 50 species. To alleviate this computational difficulty, a 50-species-reduced mechanism is needed.

For light hydrocarbon combustion, the two most commonly accepted combustion mechanisms are GRI 3.0[5] and USC II[6]. GRI 3.0 has 53 species optimized for methane combustion. The USC II mechanism uses 111 species, including species and reactions required for soot formation and oxidation. For soot prediction, the Moss-Brookes-Hall model is only available in Fluent when C_2H_2, C_6H_6, C_6H_5 and H_2 are present in the gas phase species list [1]. On the other hand, a few aspects of natural gas combustion chemistry are not described by GRI-Mech 3.0[5]; these include soot formation and the chemistry involved in the selective non-catalytic reduction of NO. Since GRI 3.0 does not contain some of the species required for the formation of soot precursors, the USC II mechanism was used as the base mechanism for the LU3.0.1 reduced mechanism.

In this project period, a 50-species reduced mechanism was developed from USC II[6] while balancing between species important for VOC emissions and soot precursors to be used in the Moss-Brookes-Hall model[1].

3.2.1 Preliminary Selection of 50-species

A species list was developed from LU1.0 and LU2.0 mechanisms[7,8,9] which were developed earlier by this group to study the formation of VOCs and NO_x from the combustion of light hydrocarbons. A common 34 species set from both LU1.1 and LU2.0 was taken first. Important species related to the generation of VOCs, including HCHO, CH_3CHO, CH_2CHO, were kept. Then, in order to include the soot precursor species (C_6H_6 and C_6H_5) for use in Fluent

Moss-Brooks and Moss-Brooks-Hall models, the species required for the formation of Benzene ring were identified based on literature survey and added to form the initial 50 species list.

The initial 50-species list includes C_1-C_3 hydrocarbons like methane (CH_4), acetylene (C_2H_2), ethylene (C_2H_4), ethane (C_2H_6) propene (C_3H_6), and propane (C_3H_8), as most of the modeling work has been performed with these fuels. Additional species, like propyne (C_3H_4) and butadiene (C_4H_6), are also included as their decomposition will lead to propargyl (C_3H_3,), allyl (C_3H_5), and butadienyl (C_4H_5) radicals involved in the formation of the first aromatic ring[10][11]. Also the formation of mono-substituted aromatics from small molecules needs to be considered in the formation of the first aromatic ring[12]. The formation of C_3 species from small hydrocarbons is achieved through a series of reactions. Davis et al. [13] proposed the methyl addition to acetylene which leads to the formation of both C_3H_4 and C_3H_5 isomers. Another possibility for the initial ring formation is the reaction between propargyl and acetylene to form a cyclopentadienyl radical[14].

$C_3H_3 + C_2H_2 = c\text{-}C_5H_5$

This pathway combines the benefits of the two reactant types discussed above: highly stable radical, propargyl, and the most abundant ‘‘building block’’, acetylene. Once formed, cyclopentadienyl reacts rapidly to form benzene[15]. However, this list can be further checked using CHEMKIN[16] to determine individual species’ contribution to the fuel combustion and soot precursor formation.

The formation and growth of aromatic species bridge the chemistry in the main combustion zone and soot formation. In addition, aromatic molecules are themselves toxic and subject to environmental regulations. The primary focus is on the formation of the first aromatic ring from small aliphatics, because this step is perceived by many to be the rate-limiting step in the reaction sequence to larger aromatics[17].

3.2.2 Reaction Path Analyzer

The Reaction Path Analyzer is a feature in CHEMKIN to provide visualization of the inner relationship of the chemistry model and to provide a fundamental understanding of reaction mechanism dependencies. The Reaction Path Diagram displays species as well as reaction pathways connecting the species. The relative size of the connecting pathways is related to the relative contribution of that pathway to the net rate of production of the species. Path widths with the minimum rate of production correspond to a line thickness of one, and the path widths with the maximum rate of production are scaled to the largest allowed line thickness. In the current study, reaction paths between fuel components and the major products (CO, CO_2, HCHO, C_6H_6, C_6H_5) were analyzed; the major contributing reactions and participating species were identified. CHEMKIN results for various reaction paths can be shown in a diagram with a maximum number of species count. Results for major species are shown as follows.

Figures 3.1 and 3.2 show the important reaction paths for CH_4 and C_3H_6 to CO and CO_2 conversion, respectively.

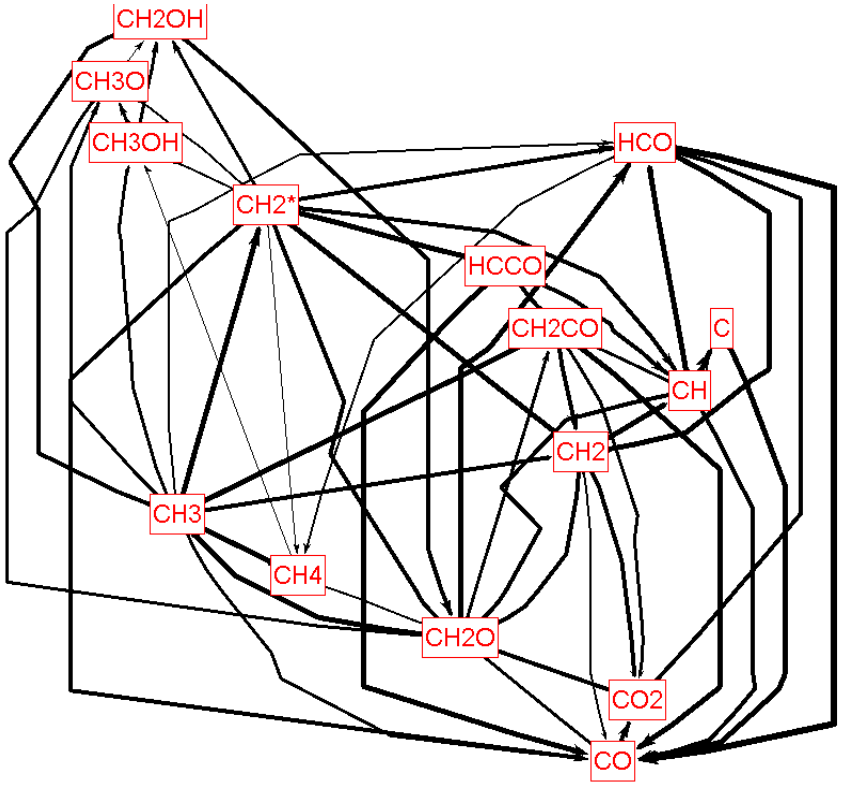

Fig.3.1: Reaction path diagram for CH_4-CO_2 with 15 species

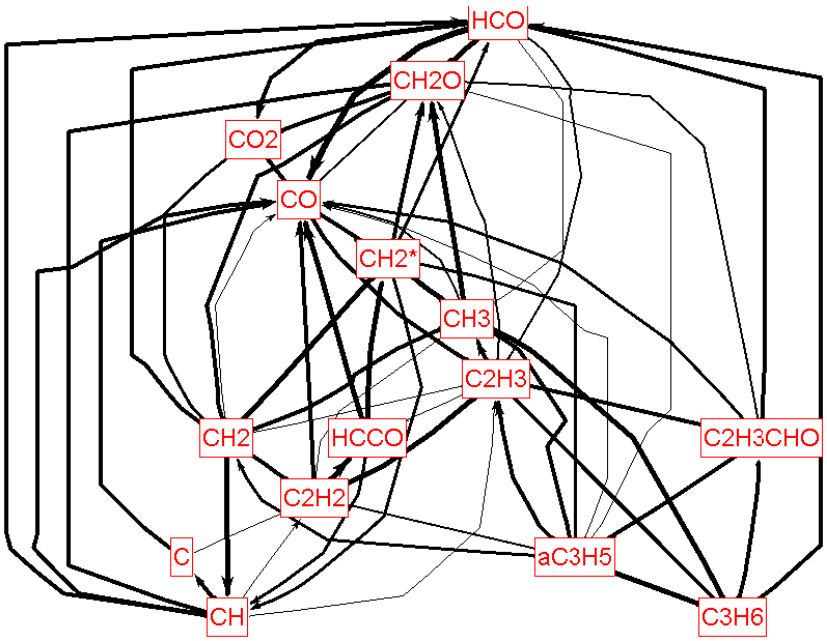

Fig. 3.2: Reaction path diagram for C_3H_6-CO_2 with 15 species

From these two diagrams, it can be seen that C and CH_2* play a very important role in CO and CO_2 production. For propylene fuel, aC_3H_5 (allene) and C_2H_3CHO (acrolein) are the major intermediates for combustion of C_3H_6. Figures 3.3, 3.4, and 3.5 show the important reaction paths for C_4H_{10}, C_3H_8, and C_2H_6 to CO_2 and CO conversion with 15 species, respectively.

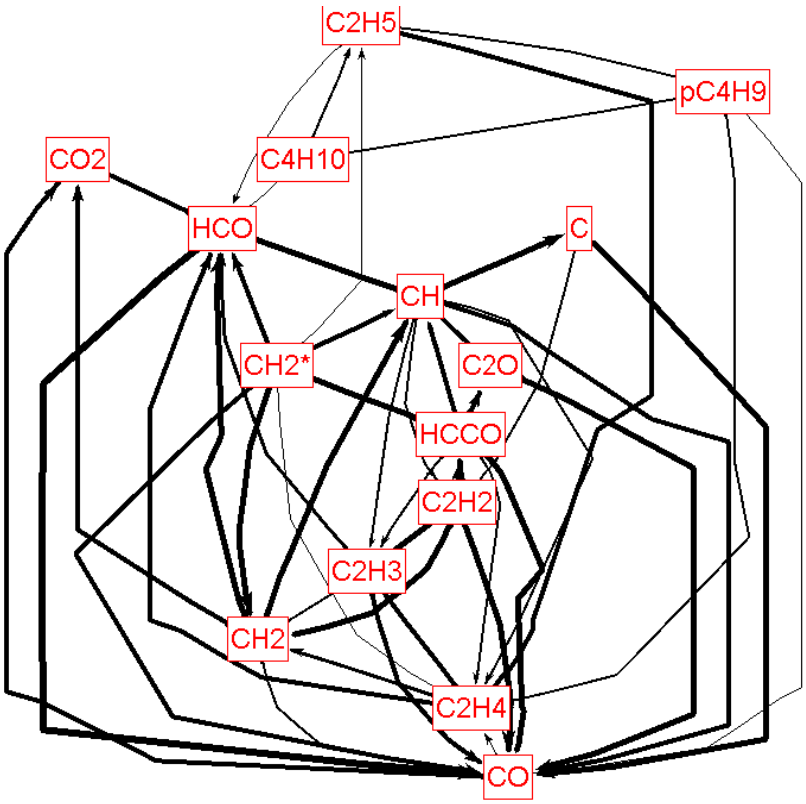

Fig.3.3.: Reaction path for C_4H_{10} to CO and CO_2 with 15 species

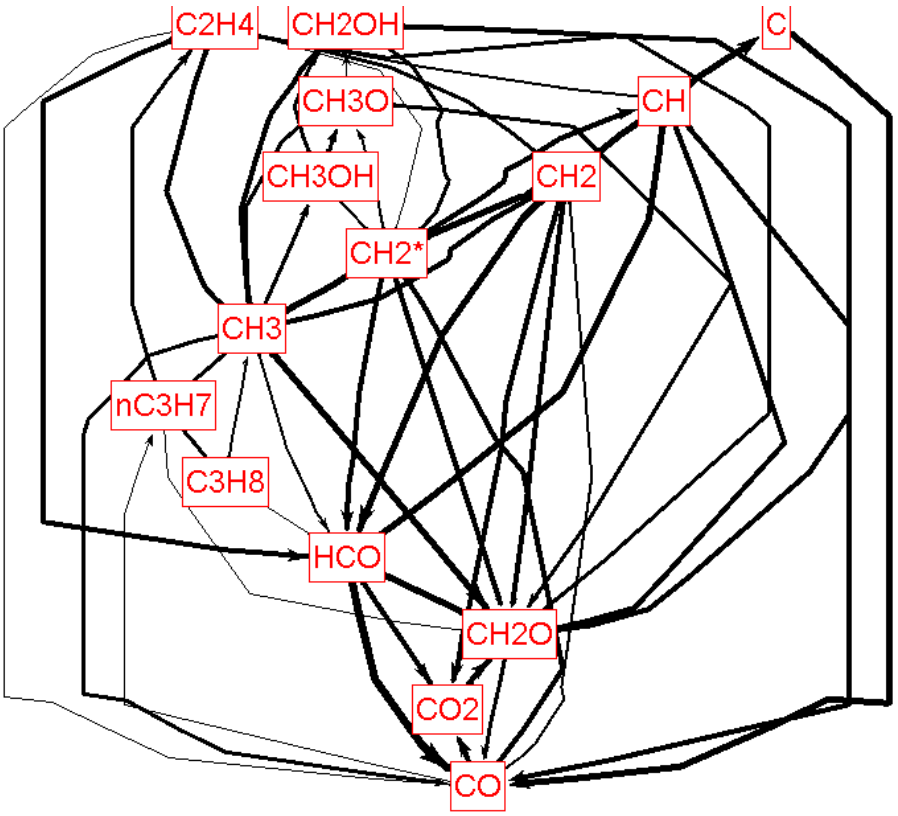

Fig. 3.4: Reaction path for C_3H_8 to CO and CO_2 with 15 species

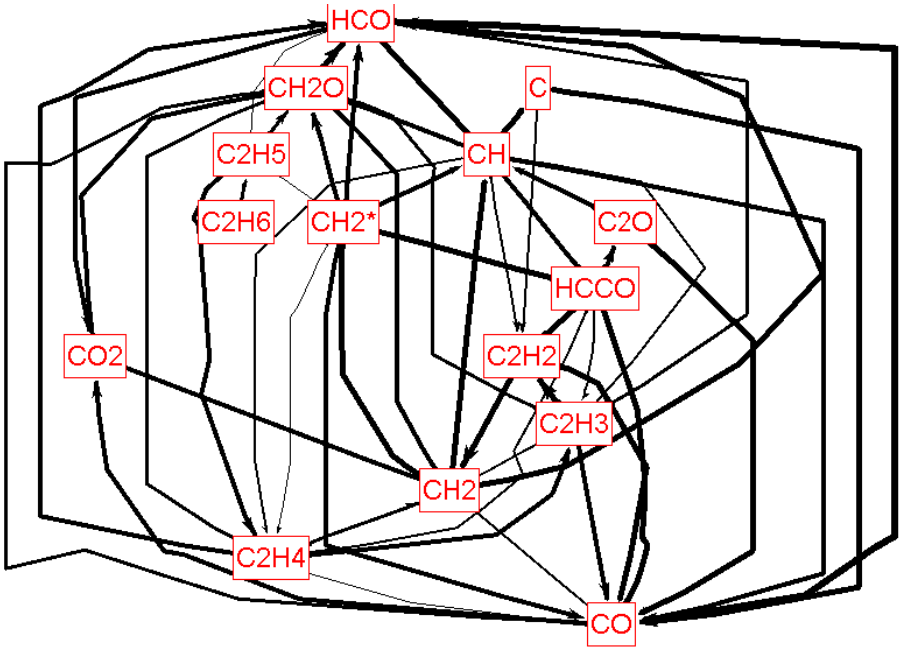

Fig. 3.5: Reaction path for C_2H_6 to CO and CO_2 with 15 species

In Figures 3.3-3.5, the major intermediate species missing for combustion of C_1-C_4 light hydrocarbons are C_2H_5, n-C_3H_7, p-C_4H_9, aC_3H_5, C_2H_3CHO, CH_3O and CH_3OH. Therefore, they are needed in this new mechanism. Figures 3.6 and 3.7 show the absolute rates of production of soot precursor species, C_6H_6 and C_6H_5 from various intermediate species, respectively.

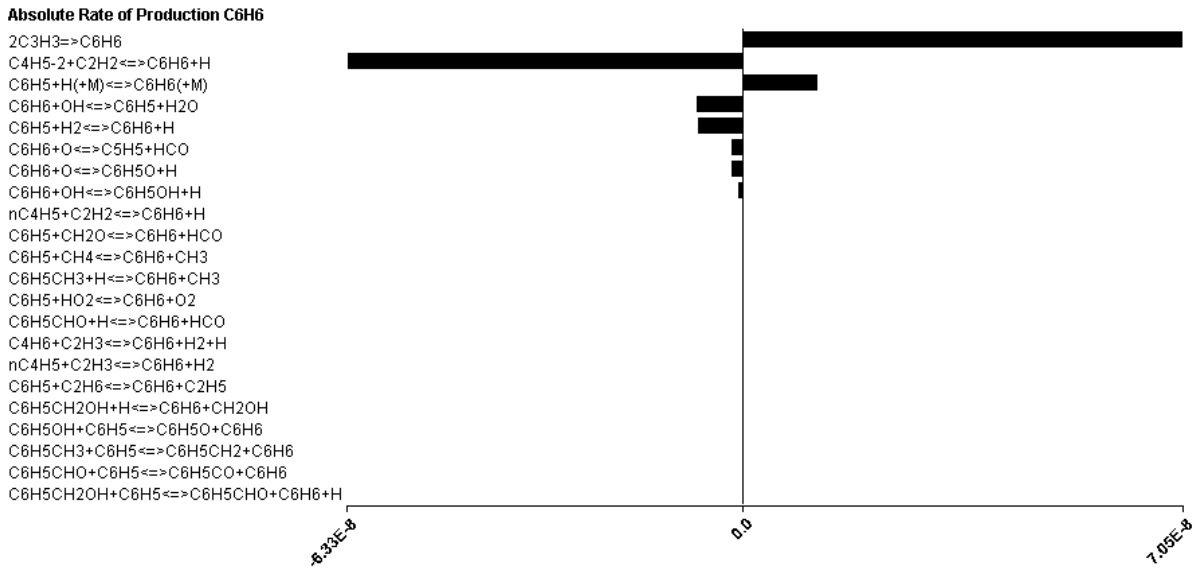

Fig. 3.6: Absolute Rate of Production of C_6H_6

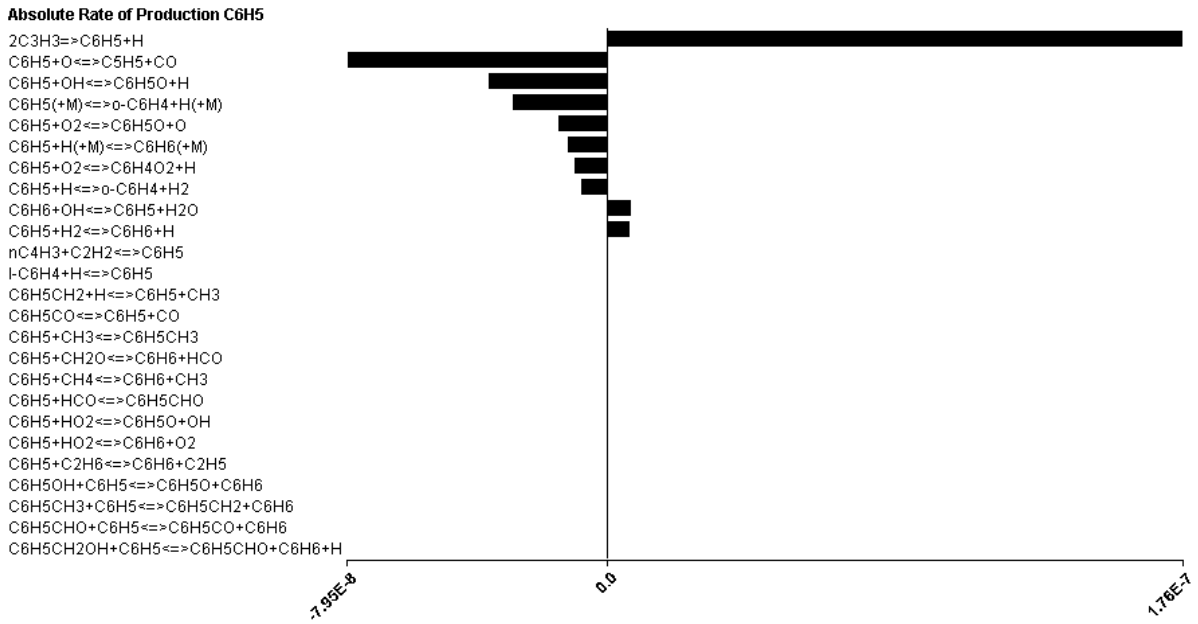

Fig.3.7 : Absolute Rate of Production of C_6H_5

From Figures 3.6 and 3.7, the major intermediates to be considered for the formation of soot precursors C_6H_6 and C_6H_5 are C_3H_3, C_5H_5 and C_6H_5O. The effects of other intermediates are negligible and hence not included in the current mechanism.

Table 3.1a 50-species list for LU3.0.1 combustion mechanism

50 Species selected for reduced mechanism:
Ar N_2 H OH HO_2 H_2 H_2O O O_2 C CO CO_2 CH HCO CH_2 CH_2* CH_2O CH_3 CH_3O CH_2OH CH_4 CH_3OH HCCO C_2H_2 H_2CC CH_2CO C_2H_3 CH_2CHO C_2H_4 CH_3CHO C_2H_5 C_2H_6 C_3H_3 aC_3H_4 C_2H_3CHO aC_3H_5 C_3H_6 nC_3H_7 C_3H_8 iC_4H_3 C_4H_4 C_4H_5-2 C_4H_6 $C_4H_8$1 pC_4H_9 C_4H_{10} C_5H_5 C_6H_5 C_6H_6 C_6H_5O

Table 3.1b C4 species and soot precursors with common name and chemical structure

C_4 Species	**Common name**	**Chemical Structure**
C_4H_{10}	n-Butane	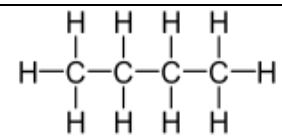
C_4H_6	1,3-Butadiene	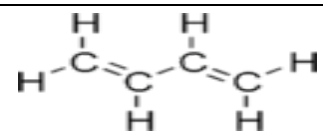
$C_4H_8$1	1-Butene or α-butylene	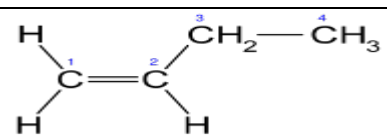
Soot precursors		
C_2H_2	Acetylene	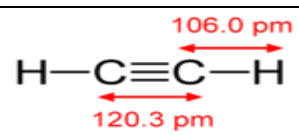
C_6H_6	Benzene	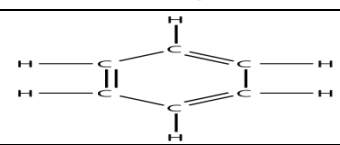
C_2H_4	Ethylene	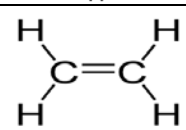

As discussed earlier in this report, C_2H_3CHO, CH_3O and CH_3OH are included for their importance in the reaction paths of C_3H_6 and CH_4 combustion. In the meantime, relatively minor species in the mechanism like H_2O_2, HCCOH, C_2H and C_2O are removed. 1,3-Butadiene(C_4H_6) which is both a fuel and an EPA-Classified carcinogen has been added to this list. Also, 1-Butene (C_4H_81), a Highly Reactive Volatile Organic Compound (HRVOC) defined by the Texas Commission on Environmental Quality (TCEQ), is added to the 50 species list. Table 3.1a shows the 50 species list while Table 3.1b shows important C_4 species and the soot precursors along with their chemical structures.

3.2.3 Reaction Rate Analysis

To validate the afore-mentioned list, the full USC II mechanism was run as a reference combustion model in CHEMKIN. Analysis of the important species was done as a first step by ranking the intermediate species based on their rates of production and destruction; then the reaction path analysis was done for both reactants and products.

For thermal (neutral) systems, perfectly stirred reactor (PSR) models are a common method for testing and developing chemical reaction mechanisms. The CHEMKIN simulation of a PSR was run with the full USC II mechanism to get the CHEMKIN results in the output file, which contains the exit mole concentrations and detailed species balance. In the detailed species balance, it includes the input and output molar flow rates for every species along with the rate of production and rate of destruction for each species. These results are exported to Microsoft Excel to further analyze the role of individual species.

Species rates of production are calculated based on the local chemical state at each time or position point in the solution. Values are given in per volume units for gas-phase reactions. The important intermediate species can be selected based on the active participation of the species in the base mechanism, i.e., USC II. The active participation of the intermediate species can be determined by adding the rate of production and rate of destruction for that particular species. To determine the key intermediate species, an extra column is added in which the rate of production and rate of destruction are added and sorted to get the ranks of the species. So the species with higher rate of production and destruction has higher rank in the species list and is

expected to have more involvement in the reaction mechanism. The highest-ranked species for 80% propene and 20% CH_4 fuel is shown in Table 3.1c. All rates are in moles/sec.

Table 3.6c: Species ranking based on the rates of production and destruction

SPECIES	INLET_FR	OUTLET_FR	GAS_PROD_RATE	GAS_DEST_RATE	SURF_NET_PROD	TOTAL_NET	Total rate
OH	0.00E+00	1.05E+00	4.33E+02	4.32E+02	0	1.35E-13	865
H	0	8.32E-01	2.64E+02	2.63E+02	0	-4.77E-15	527
O	0	6.49E-01	2.33E+02	2.32E+02	0	6.08E-14	465
H_2	0	8.25E-01	1.84E+02	1.83E+02	0	-2.45E-14	367
H_2O	0	4.56E+00	1.84E+02	1.79E+02	0	-4.35E-14	363
O2	9.07E+00	1.70E+00	5.36E+01	6.09E+01	0	-4.53E-14	114.5
CO	0	3.25E+00	2.59E+01	2.27E+01	0	2.22E-15	48.6
CO_2	0	2.61E+00	2.28E+01	2.02E+01	0	-7.55E-15	43
HO_2	0	8.45E-05	4.04E+00	4.04E+00	0	1.11E-15	8.08
HCO	0	7.68E-04	3.07E+00	3.07E+00	0	1.15E-15	6.14
CH_3	0	2.61E-03	2.31E+00	2.31E+00	0	2.95E-16	4.62
CH_2O	0	2.29E-03	1.82E+00	1.82E+00	0	2.14E-16	3.64
C_2H_2	0	2.36E-03	1.72E+00	1.72E+00	0	-9.21E-16	3.44
CH_2	0	4.46E-04	1.62E+00	1.62E+00	0	2.22E-16	3.24
CH_2*	0	1.50E-04	1.45E+00	1.45E+00	0	4.17E-16	2.9
CH	0	3.95E-04	1.23E+00	1.23E+00	0	2.96E-16	2.46
C_2H_3	0	2.14E-04	1.07E+00	1.07E+00	0	1.12E-16	2.14
HCCO	0	6.25E-04	1.04E+00	1.04E+00	0	-2.41E-17	2.08
C_3H_6	1.81E+00	7.54E-04	4.56E-02	1.86E+00	0	-5.33E-15	1.90564
aC_3H_5	0	7.24E-04	9.26E-01	9.26E-01	0	-2.19E-17	1.852
N_2	3.41E+01	3.41E+01	7.37E-01	7.37E-01	0	-1.21E-13	1.474

C_2H	0	1.85E-04	7.02E-01	7.02E-01	0	-2.98E-19	1.404
pC_3H_4	0	1.52E-04	4.97E-01	4.97E-01	0	2.15E-16	0.994
C_3H_3	0	1.92E-03	4.93E-01	4.91E-01	0	-2.86E-16	0.984
aC_3H_4	0	1.65E-04	3.84E-01	3.84E-01	0	5.64E-18	0.768
C_2H_3CHO	0	1.91E-05	3.34E-01	3.34E-01	0	1.85E-16	0.668
C	0	2.52E-04	3.20E-01	3.19E-01	0	-2.38E-17	0.639
CH_4	4.53E-01	1.19E-03	7.46E-02	5.27E-01	0	-1.28E-15	0.60157
CH_2CO	0	4.33E-04	2.80E-01	2.79E-01	0	-6.62E-17	0.559
C_2H_4	0	4.55E-04	2.31E-01	2.31E-01	0	-1.43E-16	0.462
C_2O	0	1.69E-04	1.94E-01	1.94E-01	0	-2.31E-17	0.388
CH_3CHCH	0	1.17E-04	1.94E-01	1.93E-01	0	7.07E-17	0.387
H_2O_2	0	2.11E-05	1.76E-01	1.76E-01	0	6.78E-17	0.352
CH_3CCH_2	0.00E+00	1.13E-04	1.46E-01	1.46E-01	0	5.92E-17	0.292
H_2CC	0	5.77E-05	9.98E-02	9.98E-02	0	2.30E-17	0.19962
C_2H_5	0	1.17E-05	7.52E-02	7.52E-02	0	6.16E-17	0.15035
HCCOH	0	3.53E-05	4.79E-02	4.79E-02	0	-4.99E-18	0.09582
CH_2OH	0	2.88E-05	4.26E-02	4.26E-02	0	-6.71E-18	0.08516

Here, INLET_FR is the Inlet Flow Rate(moles/sec), OUTLET_FR is the outlet Flow Rate(moles/sec), GAS_PROD_RATE is the gas production rate(moles/sec), GAS_DEST_RATE is the gas destruction rate(moles/sec).

From the ranking of the list, it can be seen that most of the species in the combustion process are already selected from earlier versions of the mechanisms. However, some of the species (CH_2*, a-C_3H_5, C, HCCOH) which have both higher rate of production and destruction are missing from the common species list of LU 1.0 and LU 1.1.

3.3 Mechanism Results and Discussion

3.3.1 Comparison with the Full Mechanism USCII

Comparison of the new reduced mechanism with USC II and LU 1.0 at the residence time of 1 sec and at temperature 2000 K (same inlet conditions) is given below. It is noted that the mechanisms (LU 1.0, LU 1.1 & LU 2.0) developed earlier by this group were mainly focused on the important VOC species like HCHO and NO_x species. Also LU 1.0 and LU 1.1 differ from each other by a single species, NO_2. So only LU 1.0 and LU 2.0 were chosen for comparison with the newly developed mechanism. GRI 3.0, which is good for methane combustions, is ideal for low temperature combustions and gives good NO_x species predictions. These results were reported by LU 1.0, 1.1 and 2.0 mechanisms in recent years [7,8,9]. The current new mechanism is good for high temperature combustions since the base mechanism for this is USC II, which holds for high combustion temperatures. Major emphasis was put on the intermediate species for benzene formation and important C_1-C_4 fuel combustions, along with the lighter VOC's, excluding NO_x species. The absolute errors in the estimation of various intermediate species from different mechanisms with reference to USC II are shown in Tables 3.2 and 3.3.

Table 3.2: Comparison of prediction errors of reduced mechanisms for mole fraction of major species at residence time of 1 sec for C_3H_6 fuel

Species	USC II	LU 3.0.1	Abs. error %	LU 1.0	Abs. error %	LU 2.0	Abs. error %
C2H2	1.46E-06	1.32E-06	9.72	1.19E-06	18.53	1.21E-06	17.23
CH4	3.01E-07	3.02E-07	0.23	3.30E-07	9.68	3.91E-07	30.07
CO	5.59E-03	5.70E-03	1.97	6.24E-03	11.68	5.98E-03	7.06
CO2	1.21E-01	1.21E-01	0.20	1.20E-01	0.64	1.21E-01	0.35
H2	1.35E-03	1.37E-03	2.10	1.51E-03	12.31	1.45E-03	7.41
Average abs. error %			2.84		10.57		12.42

Table 3.3: Comparison of prediction errors of reduced mechanisms for mole fraction of trace species at residence time of 1 sec for C_3H_6 fuel

Species	USC II	LU3.0.1	Error, a factor of	LU 1.0	Error, a factor of	LU 2.0	Error, a factor of
C3H6	4.35E-08	4.67E-08	1.07	4.59E-08	1.05	1.48E-07	3.41
HO2	1.19E-07	1.16E-07	1.02	2.06E-07	1.73	2.51E-07	2.10
OH	1.27E-03	1.33E-03	1.05	1.26E-03	1.00	1.22E-03	1.04
CH3CHO	3.16E-12	4.22E-12	1.34	3.58E-11	11.34	4.44E-13	7.11
CH2O	2.11E-07	1.68E-07	1.25	1.75E-07	1.21	2.02E-07	1.04
C2H4	1.81E-08	3.16E-08	1.74	3.84E-08	2.12	2.47E-08	1.36
CH2CHO	8.80E-12	1.10E-11	1.25	1.07E-11	1.21	1.70E-11	1.93
Average error		**1.25**		**2.81**		**2.57**	

The total average absolute error in the prediction of major species by the new reduced mechanism is calculated to be 2.84 % and for the trace species, LU3.0.1 differs from the full USC II mechanism by a factor of 1.25 on an average.

3.3.2 Comparison with Other Mechanisms:

Table 3.4 shows the mole fractions of those important combustion products (CO, CO_2 and OH) obtained from CHEMKIN simulations of various reaction mechanisms at various residence times at 2000 K. It can be observed that the new reaction mechanism has the minimum relative error at many instances compared to LU 1.0 and LU 2.0 for OH and CO, while CO_2 is predicted close to USC II mechanism for all the mechanisms.

Table 3.4: Comparison of combustion products for various mechanisms

Residence time, t (sec)		t=2e-5	Absolute Error (%)	t=9e-5	Absolute Error (%)	t= 0.5	Absolute Error (%)	t= 1	Absolute Error (%)
USC II	CO	0.0806	-	0.0557	-	0.0066	-	0.0056	-
	CO2	0.0306	-	0.0641	-	0.12	-	0.1211	-
	OH	0.0075	-	0.0101	-	0.0015	-	0.0013	-
LU 3.0.1	CO	0.0774	3.87	0.0548	1.57	0.0067	1.7	0.0057	1.97
	CO2	0.0303	0.91	0.064	0.15	0.1197	0.24	0.1208	0.2
	OH	0.0077	2.4	0.0101	0.24	0.0016	4.89	0.0013	4.76
Avg. abs. % error			**2.39**		**0.65**		**2.28**		**2.31**
LU 2.0	CO	0.0776	3.66	0.0554	0.43	0.0071	6.94	0.006	7.06
	CO2	0.0318	3.87	0.064	0.15	0.1195	0.41	0.1206	0.35
	OH	0.0069	8.91	0.0095	5.9	0.0014	3.76	0.0012	3.93
Avg. abs. % error			**5.48**		**2.16**		**3.70**		**3.78**
LU 1.0	CO	0.0779	3.27	0.0552	0.77	0.0073	11.27	0.0062	11.68
	CO2	0.0298	2.49	0.0644	0.42	0.1191	0.73	0.1203	0.64
	OH	0.006	20.48	0.0092	9.45	0.0015	0.24	0.0013	0.14
Avg. abs. % error			**8.75**		**3.55**		**4.08**		**4.15**

3.3.3 Validation with Experimental Data

The new reduced mechanism was checked against experimental data of the key performance indicators including the laminar flame speed, burner stabilized flame, ignition delay and adiabatic flame temperature.

Laminar Flame Speed

Laminar flame speed is the speed at which a laminar flame propagates through a pre-mixture of fuel and air. Flame speed is a fundamental property of a fuel-air mixture which strongly influences design parameters of combustion equipment.

The new mechanism containing 50 species and 310 reactions, along with the thermodynamics file, is pre-processed using CHEMKIN pre-processor. Then the pre-processed solution was used in the flame speed calculation model to evaluate the performance of the reaction mechanism against the experimental values. The experimental results from Davis et al.[18] and Vagelopoulos et al.[19] were used to validate the mechanism for propene and methane laminar flame speeds respectively. For ethylene flame speed, experimental results from Jomaas et al.[20] were compared.

For validation in CHEMKIN, the pressure was taken as 1 atm, and the temperature was 298 K. The equivalence ratio was varied between 0.6 and 1.5 for all the fuels. The model considered was Flame Speed Calculation model. The results obtained for propene, methane and ethylene fuels are given in Table 3.5, 3.6 and 3.7 respectively.

Note: Many properties of combustion processes strongly depend on the stoichiometry of the combustion mixture. Equivalence ratio is defined as the ratio of the actual fuel/oxidizer ratio to the fuel/oxidizer ratio in the stoichiometric equation. Equivalence ratio is the most frequently used parameter to describe the stoichiometry of a mixture.

Table 3.5: Laminar Flame Speed (cm/sec) - Comparison of Simulation and Experimental Results

Equivalence ratio	Experiment	USC II	Abs error %	LU3.0.1	Abs error %
0.7	22	25.7	16.82	27	22.73
0.8	29.5	32.7	10.85	33.7	14.24
0.9	37	38.0	2.70	37.2	0.54
1	42	41.0	2.38	40	4.76
1.1	44.5	41.2	7.42	40	10.11
1.2	44	38.2	13.18	37.1	15.68
1.3	41.5	31.8	23.37	31.3	24.58
1.4	34	23.5	30.88	22.2	34.71
1.5	22	16.4	25.45	16.9	23.18
Ave. absolute error %		14.78		16.73	

The average absolute error in the flame speed calculation of propylene fuel for LU 3.0.1 mechanism is calculated to be 16.73% and for USC II is 14.78% as compared to the experimental data.

Figs. 3.8-3.10 show the graphical representation of the experimental and the new reduced mechanism along with the base mechanism (USC II) for propylene, methane, and ethylene.

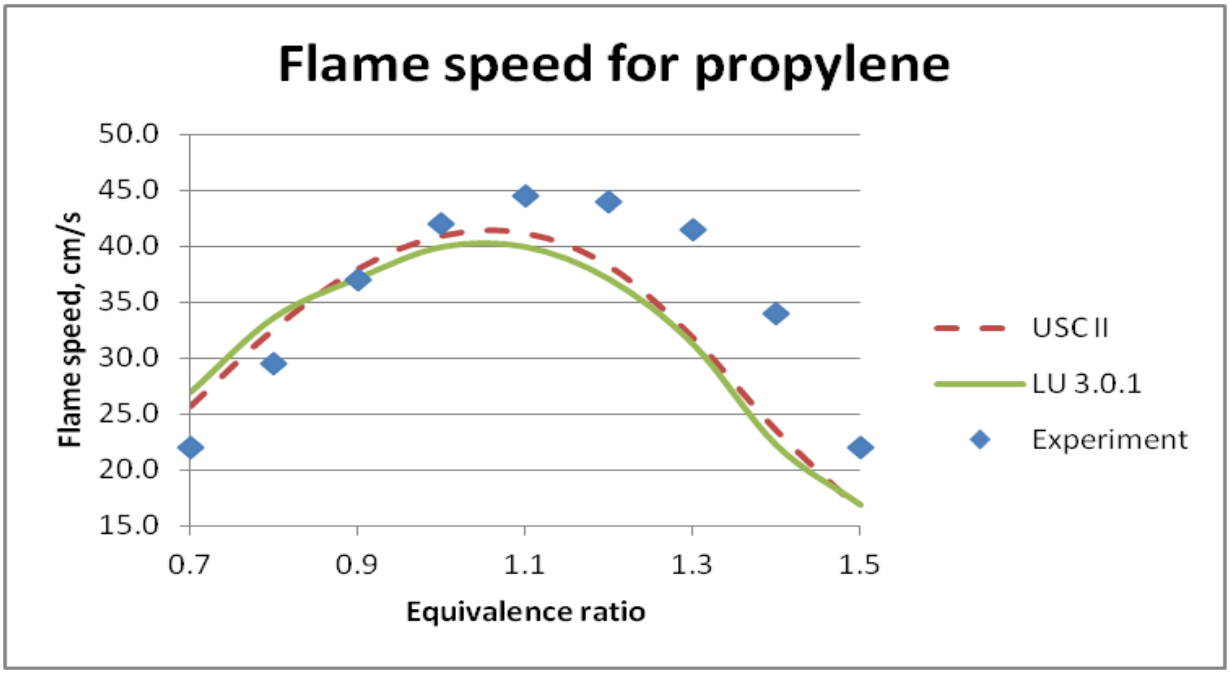

Fig. 3.8: Laminar flame speed for different equivalence ratios for propylene

Table 3.6: Laminar Flame Speed- Comparison of Simulation and Experimental Results for methane

Equivalence ratio	Experiment	LU 3.0.1	Absolute error %
0.6	10	12.6	26.00
0.7	19	21.1	11.05
0.8	25	28.8	15.20
0.9	32	34.5	7.81
1	35	37.5	7.14
1.1	37	36.9	0.27
1.2	30	32.3	7.67
1.3	28	23.2	17.14
1.4	15	14.39	4.07
Average absolute error %			10.71

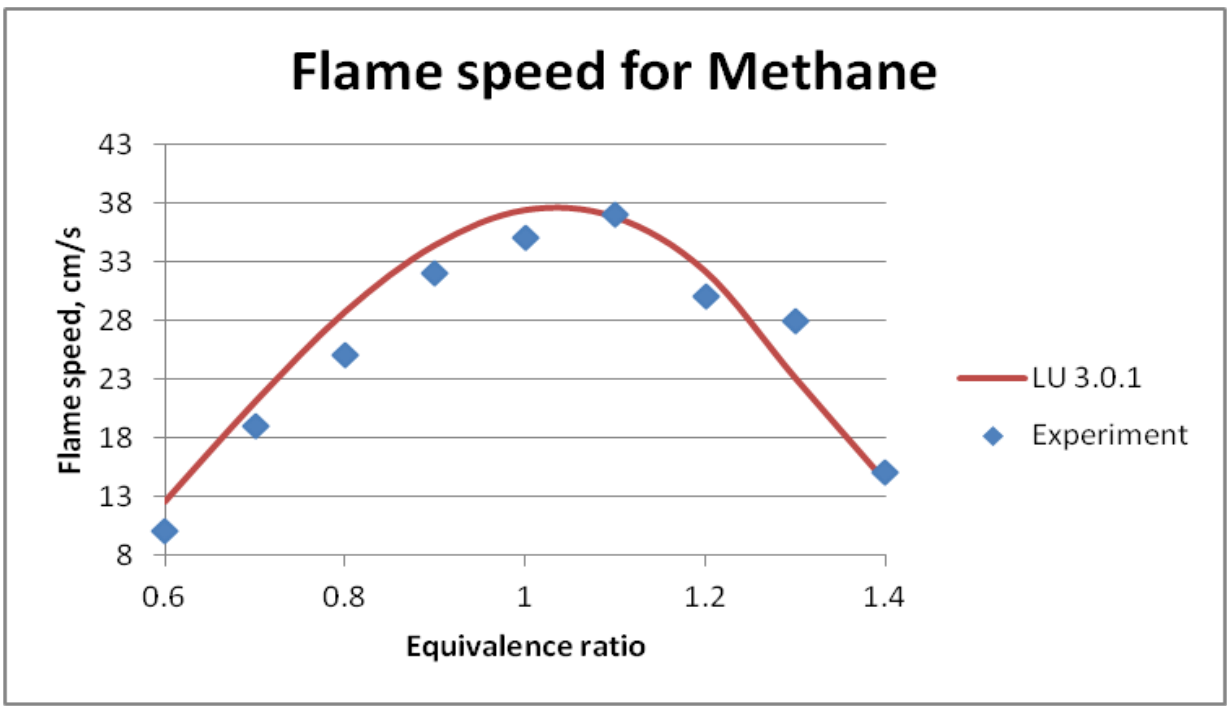

Fig. 3.9: Laminar flame speed for different equivalence ratios for Methane

Table 3.7: Laminar Flame Speed- Comparison of Simulation and Experimental Results for ethylene

Equivalence ratio	Experiment	LU 3.0.1	Absolute error %
0.7	37	40.05	8.24
0.8	49	50.85	3.78
0.9	58	59.63	2.81
1	63	64.89	3.00
1.1	64	67.25	5.08
1.2	63.5	65.9	3.78
1.3	58	60.6	4.48
1.4	52	52.3	0.58
Average absolute error %			3.97

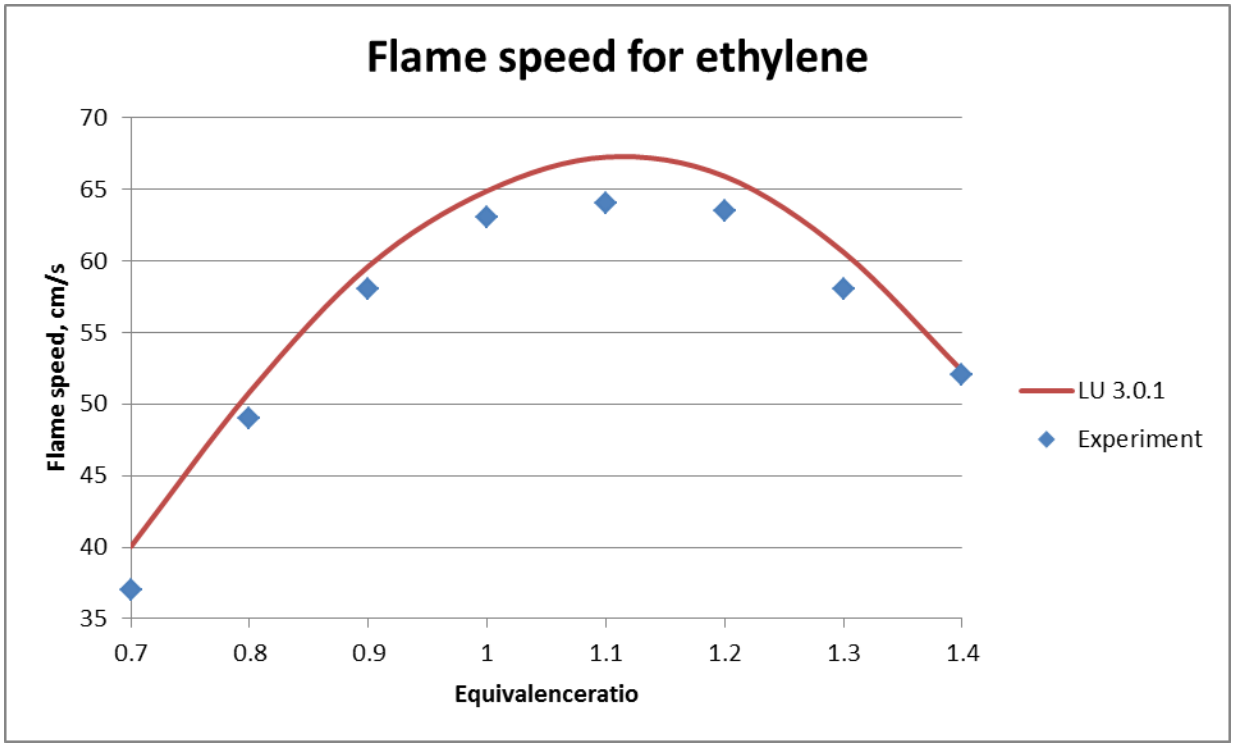

Fig. 3.10: Laminar flame speed for different equivalence ratios for Ethylene

***Ignition delay*:**

The ignition delay time can be defined as the period between the creation of a combustible mixture when the fuel is injected in an oxidizing environment, and the sustained, onset of the rapid reaction phase leading to the rise of temperature and pressure. Ignition delay was tested for propylene fuel. The reduced mechanism with 50 species was tested for ignition

delay in CHEMKIN. This was compared with experimental data from *Qin et al.[21]* For validation in CHEMKIN, the pressure was taken as 4 atm, and the temperature was varied between 1200 K to 1600 K. Fuel composition was $C_3H_6/O_2/Ar$ (3.17% - 7.83% - 89%). The model considered was closed homogenous reactor. The results obtained are shown in Table 3.8:

Table 3.8: Ignition delay Comparison of Simulation and Experimental Results

10^4/T (K)	**Experimental**	**LU3.0.1**	Absolute Error %
	Ignition Delay, μs	Ignition Delay, μs	
75.76	1285	961.49	25.18
74.07	870	742.7	14.63
72.46	615	570.52	7.23
71.17	550	455.89	17.11
69.69	410	346.57	15.47
68.26	375	261.95	30.15
66.45	185	180.2	2.59
65.36	140	142.16	1.54
63.9	100	102.84	2.84

Figure 3.11 shows the graphical representation of the experimental and simulation results between Ignition delay time and 10^4/T for propylene air mixtures with new mechanism.

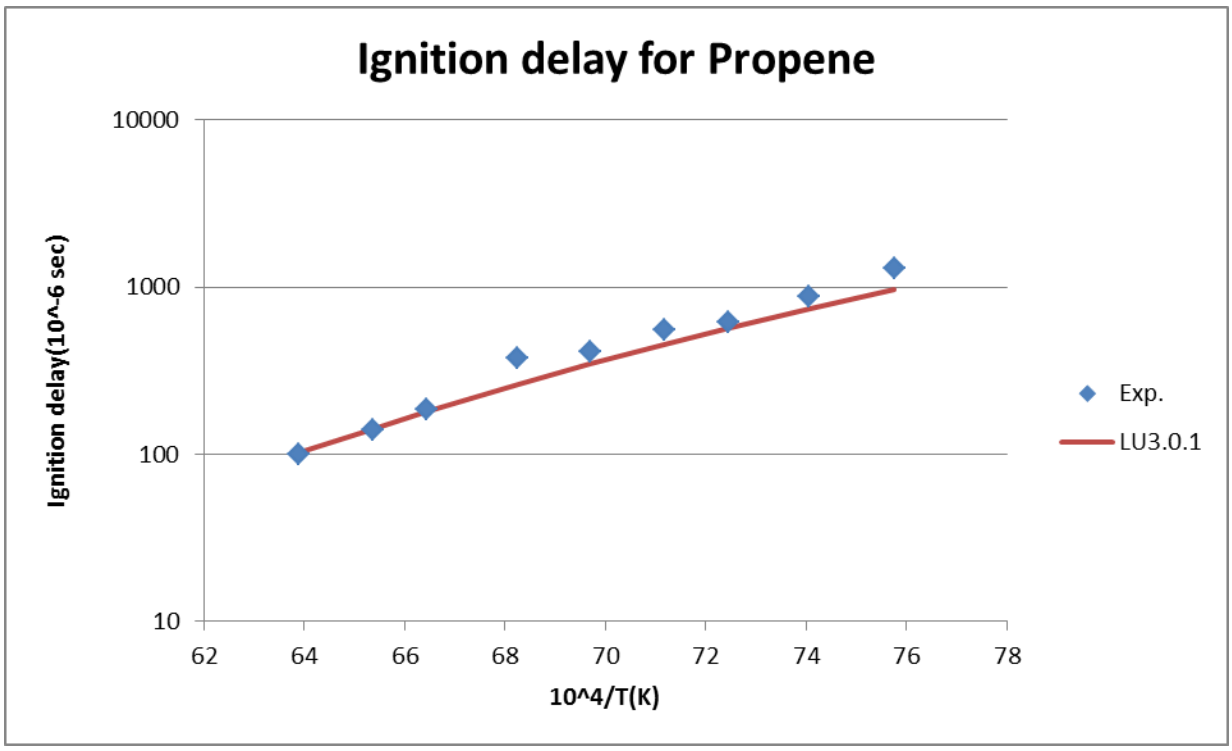

Fig. 3.11: Ignition delay time for propene

***Adiabatic flame temperature*:**

The adiabatic flame temperature is a measure of the maximum temperature that could be reached by combusting a particular gas mixture under a specific set of conditions. In a real system which includes heat losses, chemical kinetic and/or mass transport limitations, the flame temperature is likely to be lower than the adiabatic flame temperature.

For estimating adiabatic flame temperatures, the equilibrium calculation model is used in CHEMKIN. The inlet composition of fuel and air mixtures varies at different equivalence ratios. The initial temperature and pressure were set at 300 K and 1 atm respectively for both methane and ethylene and the estimated temperature was 2000 K. The estimated adiabatic temperature for propene is 2341 K at equivalence ration Φ=1 and the experimental value as determined by *Davis et al* is 2342 K. Fig. 3.12 shows the adiabatic flame temperatures at different values of Φ generated from simulation.

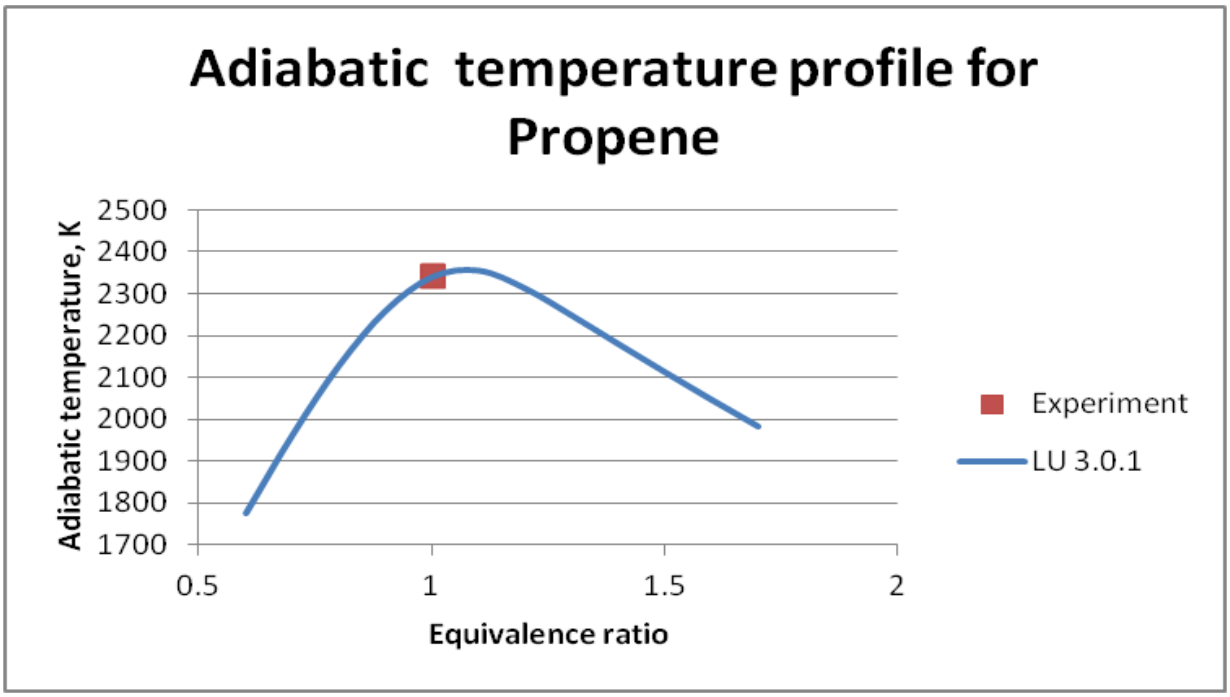

Fig. 3.12: Adiabatic flame temperature of propene

The results from Law et al.[22] were considered to validate the mechanism for methane and ethylene adiabatic flame temperatures. Adiabatic flame temperature comparison of CHEMKIN simulation and experimental results for methane and ethylene flame at different equivalence ratios are shown in Fig. 3.13 and Fig. 3.14 respectively. The equivalence ratio varies in the range of 0.5-2 for either of the cases. In both cases the maximum adiabatic temperature was observed at the equivalence ratio of 1.0-1.1, i.e., towards the leaner side of the fuel.

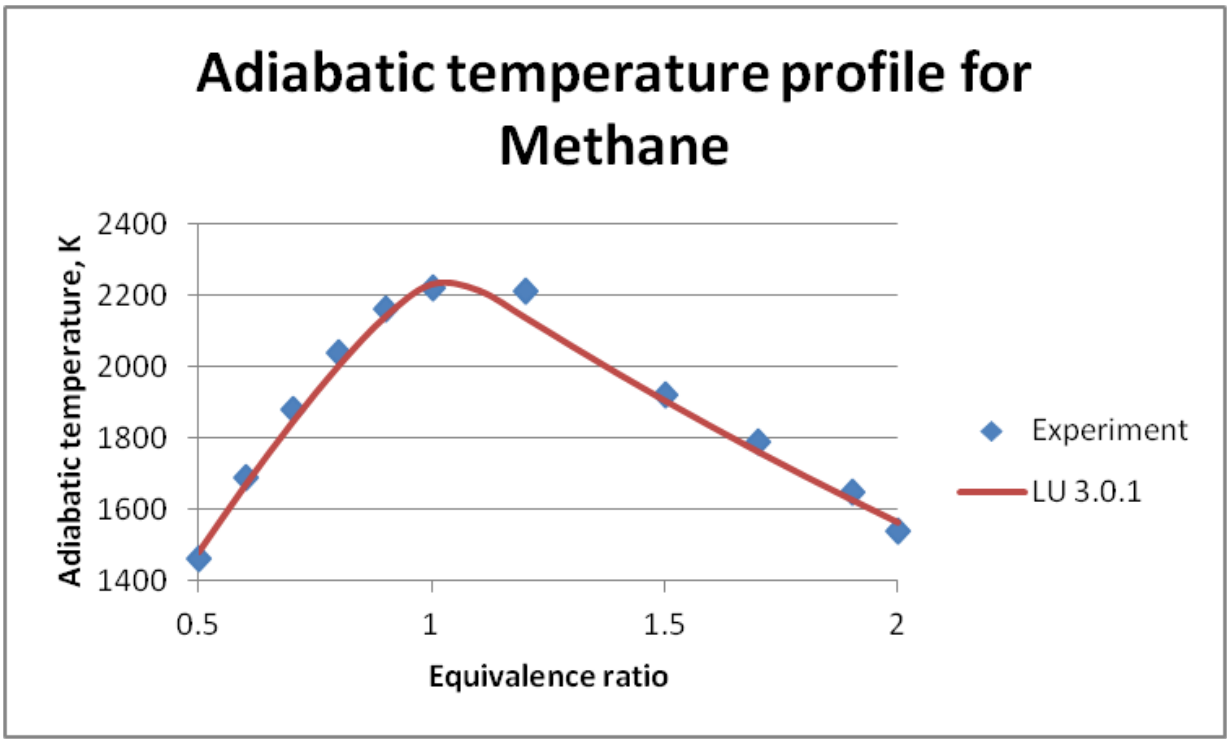

Fig. 3.13: Adiabatic flame temperature of Methane

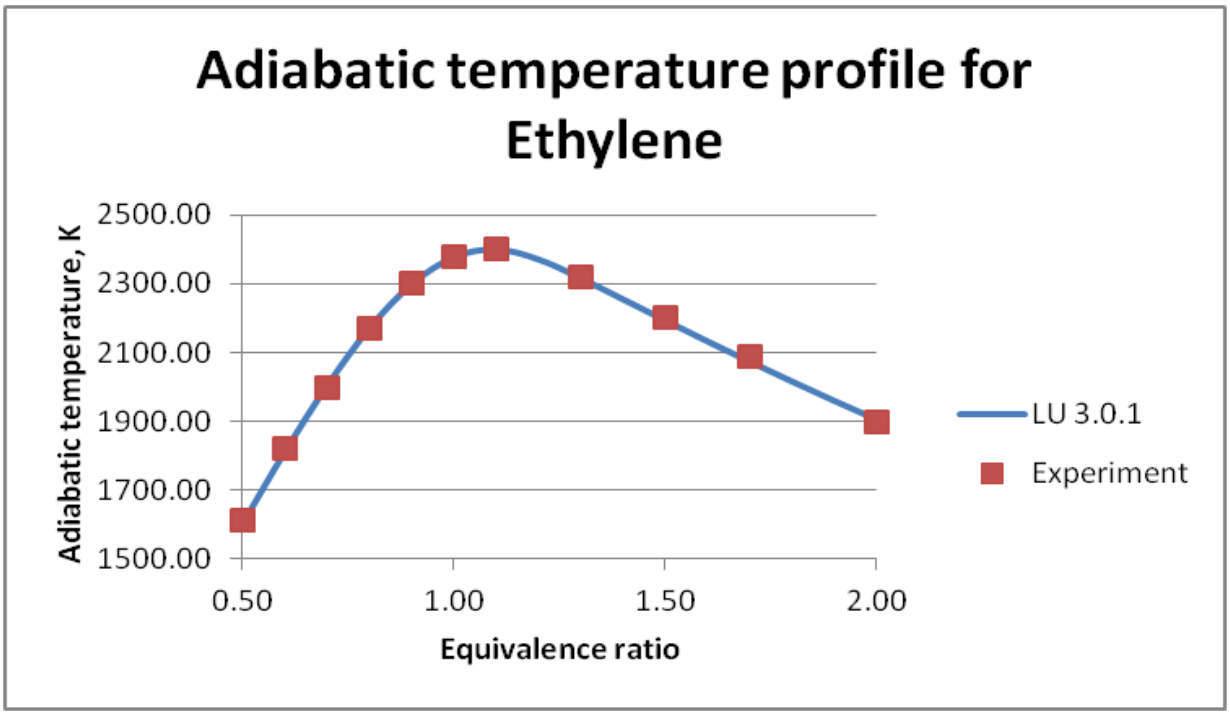

Fig. 3.14: Adiabatic temperature profile of Ethylene

3.4 Conclusions

The new reduced mechanism LU3.0.1 was validated successfully against literature data. From Table 3.9, it can be noted that the new mechanism (LU3.0.1) performs much better in the case of ignition delay and adiabatic flame temperature as compared to the LU 1.0 and LU1.1 mechanisms. In the case of laminar flame speed, LU3.0.1 shows a relatively high deviation from the experimental data, but nonetheless, it is comparable to the full USC II mechanism which has an error percentage of 14.78 %. Overall, the results show that the simulation and experimental literature results are in good agreement for light hydrocarbons.

Table 3.9: Average % Error of the Reduced Mechanisms compared to experimental data

Indicators		**Average Percentage Error**		
		LU 1.0	**LU1.1**	**LU3.0.1**
Laminar Flame Speed	Propylene	11.605	8.058	16.73
Adiabatic Flame Temperature	Ethylene	1.138	0.527	0.2626
Ignition Delay	Propylene	30.68	31.25	12.97

It can be thus concluded that the above chemical mechanism, LU3.0.1, is validated for further applications. CFD simulations are conducted and the mechanism is tested for its complete validation especially for the prediction of soot. The new reduced reaction mechanism is used in conjunction with turbulence-chemistry models like non-premixed model and eddy-dissipation concept model in Ansys FLUENT to simulate various air assisted flares. Controlled flare tests (1983-2011) for which DRE/CE/soot data are available (Carleton University's small and large scale laboratory flares, and 2010 TCEQ tests) were modelled.

References Cited in This Section

[1] ANSYS FLUENT User's Guide Release 14.0 ; Theory Guide Release 14.0; *ANSYS® Academic Research, Release 14.0, ANSYS Workbench User's Guide Release 14.0;* November 2011. ANSYS.Inc.

[2] R. J. Hall, M. D. Smooke, and M. B. Colket. *Physical and Chemical Aspects of Combustion*. Gordon and Breach. 1997

[3] " Method 9-Visual Determination of the Opacity Of Emissions From Stationary Sources,"Environmental Protection Agency, 40 CFR Ch. I (7–1–09 Edition), Pt. 60, App. A–4, Meth.9.

[4] United States Government Code of Federal Regulations - Standards of Performance for New Stationary Sources, General Control Device and Work Practice Requirements, 40CFR § 60.18

[5] GRI-Mech 3.0-Gregory P. Smith, David M. Golden, Michael Frenklach, Nigel W. Moriarty, Boris Eiteneer, Mikhail Goldenberg, C. Thomas Bowman, Ronald K. Hanson, Soonho Song, William C. Gardiner, Jr., Vitali V. Lissianski, and Zhiwei Qin http://www.me.berkeley.edu/gri_mech/

[6] High-Temperature Combustion Reaction Model of H2/CO/C1-C4 Compounds- Prof Hai Wang; Combustion Kinetics Laboratory, Aerospace and Mechanical Engineering, University of Southern California.

6a) Stohl A, Klimont Z, Eckhardt S, Kupiainen K, Shevchenko VP, Kopeikin VM, et al. Black carbon in the Arctic: the underestimated role of gas flaring and residential combustion emissions. Atmos Chem Phys, 2013;13:8833–55.

[7] Helen H. Lou, Christopher B. Martin, Daniel Chen, Xianchang Li, Kyuen Li, Hitesh Vaid,Anjan Tula Kumar, Kanwar Devesh Singh, & Doyle P. Bean, "A reduced reaction mechanism for the simulation in ethylene flare combustion," Clean Technologies and Environmental Policy, **14** (2), pp 229-239, April 2012, doi:10.1007/s10098-011-0394-9.

[8] H. Lou, C. Martin, D. Chen, X. Li, K. Li, H. Vaid, A. Tula, K. Singh,"Validation of a Reduced Combustion Mechanism for Light Hydrocarbons," Clean Technologies and Environmental Policy, **14** (4), pp 737-748, August 2012, DOI 10.1007/s10098-011-0441-6.

[9] Helen H. Lou, Daniel Chen, Christopher B. Martin, Xianchang Li, Kuyen Li, Hitesh Vaid, Kanwar Devesh Singh, Preeti Gangadharan, "Optimal Reduction of the C1-C3 Combustion Mechanism for the Simulation of Flaring, " Industrial & Engineering Chemistry Research, Industrial flares special issue, **51** (39), 12697-12705, DOI: 10.1021/ie2027684, October, 2012.

[10] Studies of aromatic hydrocarbon formation mechanisms in flames: Progress towards closing the fuel gap(2006) (Progress in Energy and Combustion Science 32 (2006) 247–294)

[11] Chemical and statistical soot modeling-Guillaume Blanquart-March 2008 (A dissertation submitted to the department of mechanical engineering and the committee on graduate studies of stanford university)(2008)

[12] A modelling study of aromatic soot precursors formation in laminar methane and ethene flames(2009)(Combustion and FlameVolume 156, Issue 9, September 2009, Pages 1705–1722)Germany

[13] "Propene pyrolysis and oxidation kinetics in a flow reactor and laminar flames" S.G.Davis and K.Law and H.Wang (Combustion and Flame 119, pp. 375-399 (1999))

[14] Michael Frenklach(Phys. Chem. Chem. Phys., 2002, 4, 2028–2037), Department of Mechanical Engineering, University of California at Berkeley

[15] DEFINITIVE STUDIES OF KEY COMBUSTION PROCESSES - Mechanisms of Soot Formation: The Propargyl + Allyl System(C. F. Melius, M. E. Colvin, N. M. Marinov, W. J. Pitz and S. M.Senkan, Proc. Combust. Inst., 1996, 26, 685.)

[16] R.J. Kee, F.M. Rupley, J.A. Miller, et al., CHEMKIN Release 4.1.1, Reaction Design, San Diego, CA, 2007.

[17] Colket, M. B., et al. *The Determination of Rate-Limiting Steps during Soot Formation*. No. UTRC89-13. UNITED TECHNOLOGIES RESEARCH CENTER EAST HARTFORD CT, 1989.

[18] Davis, S. G. and Law, C. K.(1998), "Determination of and Fuel Structure Effects on Laminar Flame Speeds of C1 to C8 Hydrocarbons", Combustion Science and Technology, 140:1,427- 449.
[19] Vagelopoulos, C.M., Egolfopoulos, F.N. Law, C.K. Proc. Combust. Inst. 1994, 25, 1341
[20] Jomaas, G., Zheng, X. L., Zhu, D. L., and Law, C. K. Proc. Combust. Inst. 2005, 30, 193.
[21] Qin.Z, Yang.H, C.Gardiner, " Measurement and modeling of shock-tube ignition delay for propene ", Combustion and Flame ,124,246-254(2001).
[22] C.K. Law, A. Makino, T.F. Lu, On the off-stoichiometric peaking of adiabatic flame temperature, Combustion and Flame, Volume 145, Issue 4, June 2006, Pages 808-819, ISSN 0010-2180

4. MODEL CONTROLLED FLARE TESTS (TASK 4)

PART A: CFD Modeling of Large-Scale Laboratory Flare Data

4.1 Background

Flaring is widely used in many industries to dispose unwanted combustion gases by burning them as a flame. Satellite imagery analysis suggests more than 139 billion cubic meters of gas were flared worldwide in 2008 [1]. Industrial flares are one of the major sources of black carbon, i.e. soot. Despite the very high amount of gas flared all over the world and the requirement to report associated emissions, an analysis of the very few existing black carbon (PM) emission factors has revealed serious limitations enough to suggest that guesstimates of black carbon production from industrial flares based on current emission factors must be interpreted with cautiousness. Soot is considered as a significant health hazard mainly because it's small size [2] and it has been linked to serious respiratory, reproductive, and developmental effects in humans [3]. Soot has also been recognized as a significant source of anthropogenic radiative forcing of the planet's surface [4-6]. Measurement of soot emitted by industrial flares with experimental methods is relatively expensive and complex. Computational fluid dynamics (CFD), based on a validated reaction mechanism and viscous/turbulent-chemistry interaction models, can be a viable alternative to predict soot yield and combustion efficiency (or carbon conversion efficiency). Johnson et al. [7] in Carleton University, Canada conducted a series of alkane mixture flare experiments to measure black carbon, i.e., soot. These quantitative soot emission measurements were performed on lab-scale flares for a range of burner diameters, exit velocities and fuel compositions. The key objective of this task is to analyze the soot data and to present results of CFD simulation aimed at developing a better CFD model in industrial flares.

For this work, CFD is applied to quantitatively model the soot/CE data from non-premixed flares by using basic physics, mechanism, and turbulence/chemistry/soot models. The commercial software package, ANSYS Fluent 13.0, is used for this purpose.

Lab-scale Flare Test Experiments: Experimental measurement of the gas-phase composition and black carbon content of combustion products emitted from lab-scale flares have been performed at the Carleton University lab-scale flare facility. Photos and schematics of experiments are shown in Figures 4.1 and 4.2 respectively.

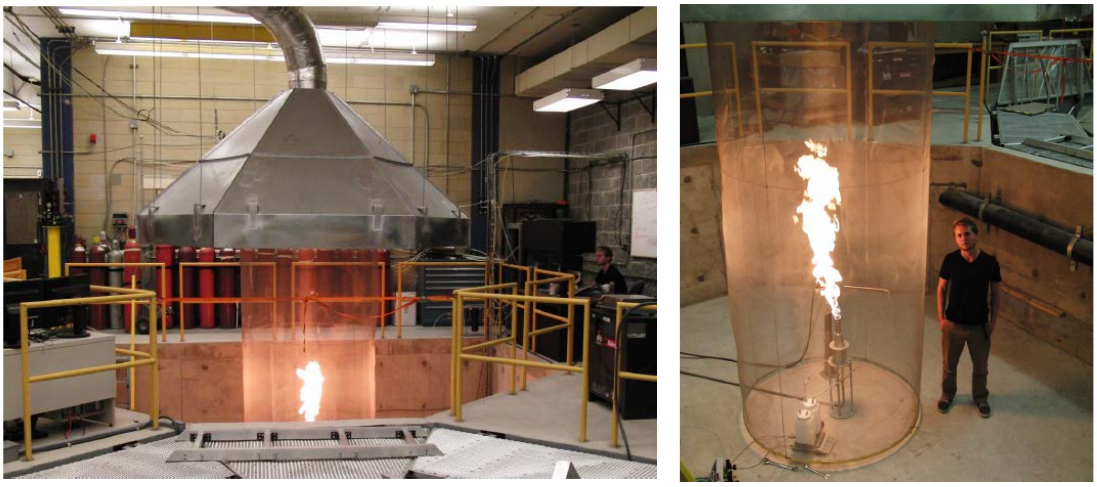

(a) **(b)**

Figure 4.1: a) Photo showing sampling hood and flare at the Energy & Emissions Research Lab. Flare Facility at Carleton University b) Photo showing close-up of the flare

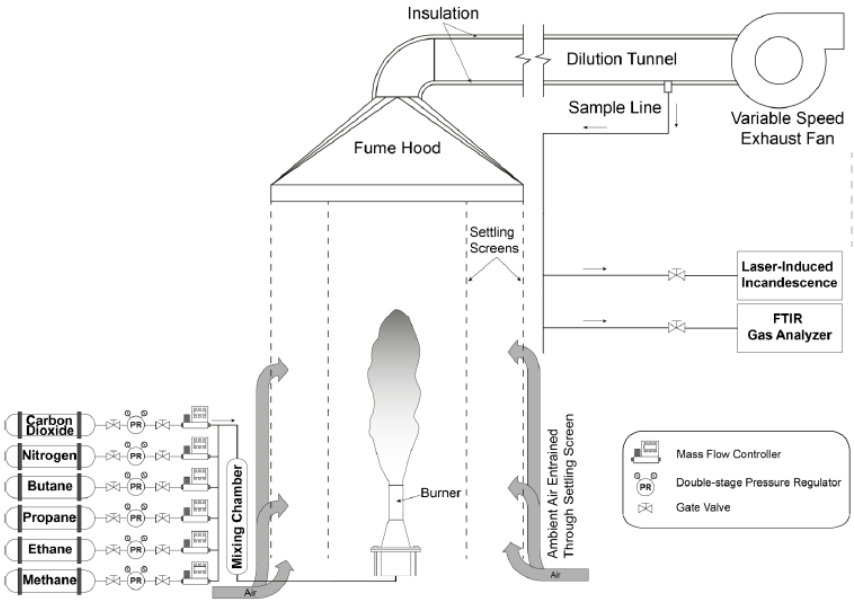

Figure 4.2: Schematic of the Energy & Emissions Research Lab. Flare Facility at Carleton University

In these flare tests, gaseous fuel components are mixed to the desired result using a series of computer-controlled mass flow controllers. A modular burner is situated beneath a large

exhaust hood from which suction is provided by a variable speed fan. The experiments consist of a measurement of the ambient concentrations of all relevant species before and after the flaring process. Evaluation of combustion efficiency and species yields occurs after gas concentrations, soot volume fraction, and various temperatures (sample port, burner exit, and duct wall) become stable. These experiments were performed at a range of flare gas flow rates and over three burner sizes. Methane and Ethane are major components for all fuel mixtures. Certain experiments have been repeated numerous times throughout development of the experimental setup and sampling protocol. Uncertainties for a given operating condition consist of the systematic error inherent on each test instance of that condition as well as precision error based on the repeatability of the experimental outcomes.

Lamar University acquired the operating and design data of these lab-scale flare experiments. These input data include the geometry, fuel mixture and fuel exit velocities. The flare performance data provided primarily include soot yield (kg/kg) and Combustion Efficiency (CE).

Combustion efficiency is defined as the percentage of flare emission that are completely oxidized to CO_2. It can be written mathematically as:

$$\%CE = \frac{CO_2}{CO_2 + CO + THC + Soot} \tag{4.1}$$

Where

CO_2 — flow rate of carbon dioxide in kg/s

CO — flow rate of carbon monoxide in kg/s

THC — flow rate total hydrocarbon exiting from the flare in kg/s

Soot — flow rate of soot black carbon (soot) in kg/s

4.2 Methodology for This Task

For this CFD study, ANSYS-Workbench is used to create a three-dimensional geometry. Figure 4.3 shows three-dimensional geometry with sloped meshing for lab-scale flare simulations. As shown, air is supplied from the side wall of a cylinder, and fuel inlet is given from center stack. The geometry consists of two axially concentric cylinders and nozzle domain

at the top. Diameter of the large cylinder is 1 m and overall height is 4.5 m. Diameter and height of stack inlet is 0.7 m and 0.0508m respectively. Outlet is placed at top of the computational nozzle domain.

Geometry is built in the Geometry section of workbench. A circle with diameter 1m is constructed at origin and extruded for height of 4 m by using *add material* command. Then another circle of 50.8 mm is constructed and the stack of 0.7 m height is created by using *cut material* command. The geometry then divided in various parts by using *freeze* and *slice* command to create effective meshing. New single part is formed by using *Form New Part* command. Then this geometry is saved and imported in meshing section of workbench. In meshing section, *Edge Sizing* command is widely used. Circular edges of cylinder are divided in 60 equal parts. Whereas height above stack is divide in 100 parts with high bias factor. Because of it, mesh is more dense near stack and it is less dense away from stack. Side edges near stack are also divided in 26 parts with bias factor of 16. Mesh is denser at center and it is less dense away from center. Geometry with mesh is shown in Figure 4.3.

Once the mesh is build, it is checked for mesh orthogonal quality. Orthogonal quality near to unity is considered as good quality. Therefore mesh orthogonal quality of current geometry is monitored and kept above 0.8. Names are given to the respective surfaces (air inlet, fuel inlet and outlet) by using Create Named Section command. The entire domain is meshed by using MultiZone and Edge Sizing command. The mesh used for simulation consists of 0.4 million cells. The simulation was performed on a system with Intel Quad core i5 processors, CPU at 3.2 GHZ and RAM of 8 GB.

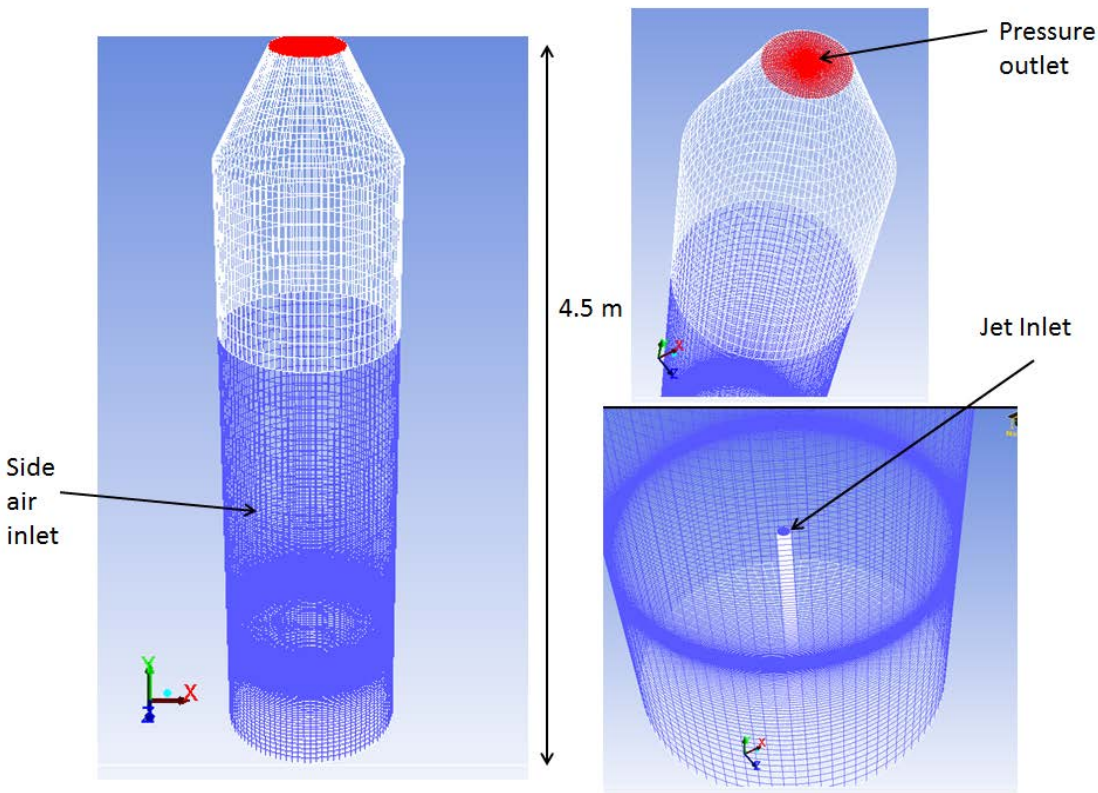

Figure 4.3: Computational domain with sloped mesh

4.2.1 Development of Chemical Mechanism LU 3.0.1 for Soot Analysis

A team at Lamar University already developed chemical mechanisms LU 1.0 and LU 2.0 to study the ethylene combustion and pollutant formations like Volatile Organic Compounds (VOCs) and NO_x. To develop mechanism suitable for soot analysis, a common 34 species set from both LU1.1 and LU2.0 was taken first for combustion of C_1-C_3 light hydrocarbons. Important VOC species (HCHO, CH_3CHO, CH_2CHO) were also included. Then, in order to include the soot precursor species (C_6H_6 and C_6H_5) for use in Fluent Moss-Brookes and Moss Brooks Hall models, the species required for formation of benzene ring were identified based on literature survey. Analysis of the important species was done as a first step by ranking the intermediate species based on their rates of production and destruction and then the reaction path analysis was done for both reactants and products. The final 50-species list suitable for the fluent EDC modeling is given below.

50 Species selected for reduced mechanism:

AR OH H_2O H O H_2 O_2 CO CO_2 HO_2 CH_3 HCO CH_2* CH_2 CH_2O N_2 CH_4 CH C_2H_2 C_2H_4 C_2H_3 C_2H_5 HCCO C_2H_6 C_2H_3CHO C nC_3H_7 CH_2OH C_3H_8 C_3H_6 aC_3H_5 C_3H_3 C_4H_{10} CH_2CO C_4H_81 pC_4H_9 H_2CC aC_3H_4 CH_3CHO CH_3O CH_3OH C_4H_6 CH_2CHO C_4H_4 C_4H_5-2 iC_4H_3 C_6H_5 C_5H_5 C_6H_6 C_6H_5O

To validate the afore-mentioned list, the full USC II mechanism was run as a reference combustion model in CHEMKIN. Finally, the new reduced USC II mechanism is validated successfully against literature data. Results of various key performance indicators for methane, ethylene and propene flames show that the simulation and experimental results are in good agreement.

4.2.2 FLUENT Setup and Soot Model

To run the FLUENT simulation, geometry mesh file and new LU 3.0.1 mechanism were imported in FLUENT domain, along with new thermodynamic data by using CHEMKIN import. New geometry is checked for its orthogonal mesh quality before beginning of setup procedure. At the beginning of setup, the energy equation is applied. Default least square cell based gradient option is used. Gravity is applied in negative Y-axis as -9.81 m/s². The standard k-ε model with standard wall functions is used as viscous model. SIMPLE algorithm is enabled for pressure-velocity coupling. The non-premixed combustion species model (PDF model) is used to simulate the combustion phenomenon. Then, the fuel composition, as given by experimental data (6 mix and Heavy 4-mix) is used as follows:

Table 4.1: Fuel Composition for lab-scale flares

Species	Purity (%)	Average 6-Mix (%)	Heavy 4-Mix (%)
Methane	99.0	85.24	74.54
Ethane	99.0	7.06	15.47
Propane	99.0	3.11	6.83
Butane	99.0	1.44	3.16
Carbon Dioxide	99.0	1.91	0
Nitrogen	99.999	1.24	0

Once fuel is specified, flamelets are generated until either the maximum number of flamelets is reached or the flamelets are extinguished. Extinguished flamelets are not included in library. In ANSYS Fluent, the flamelets can be either generated by the users or imported from other packages. The parameters used for flamelet generation are listed in Table 4.2. These parameters are limited by computer memory and a fatal error will occur if the parameters are increased beyond a certain level.

Table 4.2: Flamelet generation parameters

Number of grid points in flamelet	32
Maximum number of flamelets	10
Initial scalar dissipation (1/s)	0.01
Scalar dissipation step (1/s)	5

The grid refinement was used while generating the flamelets. ANSYS Fluent has the option for automated grid refinement of steady flamelets, where an adaptive algorithm inserts grid points so that the change of values as well as the change of slopes between successive grid points is less than user specified tolerances. During automated grid refinement, a steady solution is calculated on a coarse grid with a user specified initial number of grid points in flamelets. When it reaches to the convergence, a new grid point is inserted between a point i and its neighbor (i+1) if it satisfies the equation below.

$$|T_i - T_{i+1}| > \varepsilon_v(v_{max} - v_{min}) \tag{4.2}$$

where T_i is the value for each temperature and species mass fraction at grid point i, ε_v is a user specified maximum change coefficient, and v_{max}, v_{min} are the maximum, minimum values over all grid points. The parameters for automated grid refinement are listed in Table 4.3.

Table 4.3: Grid refinement parameters for flamelet

Initial number of grid points in flamelet	8
Maximum number of grid points in flamelet	64
Maximum change in value ratio	0.5
Maximum change in slope ratio	0.5

After the flamelets are generated, the flamelet profiles are convoluted with the assumed-shape PDFs as in Equation (4.3), and then tabulated for look-up in ANSYS Fluent.

$$\overline{\emptyset} = \iint \emptyset(f, \chi_{st}) p(f, \chi_{st}) df \, d\chi_{st} \tag{4.3}$$

where f is the mixture fractions, χ_{st} is the scalar dissipation rate, and $\emptyset$ is the species mass fraction or temperature. The parameters used to generate the PDF table are listed in Table 4.4.

Table 4.4: Parameters used to generate the PDF table

Number of mean mixture fraction points	31
Number of mixture fraction variance points	40
Maximum number of species	50
Number of mean enthalpy points	41
Minimum temperature (k)	298

In addition to those settings described above, the operating pressure, temperature and gravity need to be applied. Before starting each case, the solution was initialized from the co-flow inlet. An iso-surface (Z=0) parallel to X-Y plane was created at the center of domain. The maximum temperature at Z=0 plane was monitored during iteration. Once the temperature was stabilized and the solution was converged the results were saved for further analysis. The emission is measured at the top surface (outlet) of the domain.

Moss-Brookes Soot Model

FLUENT mainly comprises three basic soot models. One-Step Soot model, Two-Step Soot model and Moss-Brookes soot model. After careful analysis and more than hundred simulation runs, the Moss-Brookes model was chosen for simulation. The Moss-Brookes model solves transport equations for normalized radical nuclei concentration b^*_{nuc} and soot mass fraction Y_{soot}:

$$\frac{\partial}{\partial t}(\rho Y_{soot}) + \nabla \cdot (\rho \vec{v}\, Y_{soot}) = \nabla \cdot \left(\frac{\mu_t}{\sigma_{soot}} \nabla Y_{soot} \right) + \frac{\dot{a}M}{dt} \tag{4.4}$$

$$\frac{\partial}{\partial t}(\rho b^*_{nuc}) + \nabla \cdot (\rho \vec{v}\, b^*_{nuc}) = \nabla \cdot \left(\frac{\mu_t}{\sigma_{nuc}} \nabla b^*_{nuc} \right) + \frac{1}{N_{norm}} \frac{\dot{a}N}{dt} \tag{4.5}$$

Y_{soot} = soot mass fraction

M = soot mass concentration (kg/m^3)

b^*_{nuc} = normalized radical nuclei concentration

N = soot particle number density (particles/m^3)

$N_{norm} = 10^{15}$ particles

The instantaneous production rate of soot particles, subject to nucleation from the gas phase and coagulation in the free molecular regime, is given by

$$\frac{\dot{a}N}{dt} = \underbrace{C_\alpha N_A \left(\frac{X_{prec} P}{RT} \right)^l \exp\left\{ -\frac{T_\alpha}{T} \right\}}_{\text{Nucleation}} - \underbrace{C_\beta \left(\frac{24RT}{\rho_{soot} N_A} \right)^{1/2} d_p^{1/2} N^2}_{\text{Coagulation}} \tag{4.6}$$

Where C_α,C_β and l are model constants. Here N_A is the Avodgdro number and X_{prec} is the mole fraction of soot precursor (for methane, the precursor is assumed to be acetylene, whereas for

kerosene it is a combination of acetylene and benzene). The mass density of soot, ρ_{soot}, is assumed to be 1800 kg/m^3 and d_p is the mean diameter of a soot particle. The nucleation rate for soot particles is taken to be proportional to the local acetylene concentration for methane. The activation temperature T_α for the nucleation reaction is that proposed by Lindstedt [8].

The source term for soot mass concentration is modeled by the expression

$$\begin{aligned}\frac{dM}{dt} &= \underbrace{M_P C_\alpha \left(\frac{X_{prec}P}{RT}\right)^l \exp\left\{-\frac{T_\alpha}{T}\right\}}_{\text{Nucleation}} \\ &+ \underbrace{C_\gamma \left(\frac{X_{sgs}P}{RT}\right)^m \exp\left\{-\frac{T_\gamma}{T}\right\}\left[(\pi N)^{1/3}\left(\frac{6M}{\rho_{soot}}\right)^{2/3}\right]^n}_{\text{Surface Growth}} \\ &- \underbrace{C_{oxid} C_\omega \eta_{coll}\left(\frac{X_{CH}P}{RT}\right)\sqrt{T}\,(\pi N)^{1/3}\left(\frac{6M}{\rho_{soot}}\right)^{2/3}}_{\text{Oxidation}}\end{aligned} \tag{4.7}$$

where C_γ C_{oxid}, C_w, m, and n are additional model constants. The constant Mp is the mass of an incipient soot particle, here taken to consist of 12 carbon atoms. Even though the model is not found to be sensitive to this assumption, a nonzero initial mass is needed to begin the process of surface growth. Here X_{sgs} is the mole fraction of the participating surface growth species. For paraffinic fuels, soot particles have been found to grow primarily by the addition of gaseous species at their surfaces, particularly acetylene that has been found in abundance in the sooting region of laminar methane diffusion flames.

The set of constants proposed by Brookes and Moss for methane flames are given below:

C_α = 54 s^{-1}(model constant for soot inception rate)

T_α = 21000 K (activation temperature of soot inception)

C_β = 1.0 (model constant for coagulation rate)

$C\gamma$ = 11700 kg m kmols^{-1} s $^{-1}$ (surface growth rate scaling factor)

$T\gamma$ =12100 K (activation temperature of surface growth rate)

C_w =105.8125 kg m kmols^{-1}K$^{-1/2}$ s $^{-1}$ (oxidation model constant)

n_{coll} = 0.04 (collisional efficiency parameter)

C_{oxid} = 0.015 (oxidation rate scaling parameter)

The implementation of the Moss-Brookes model in ANSYS FLUENT uses the values listed above, except for C_{oxid}, which is set to unity by default.

4.3 Results and Discussion

4.3.1 Results for lab-scale flares test no. 20 to 23

By applying initial settings, as explained in above section, all cases with different fuel exit velocities simulated for CFD analysis. Test no. 20 to 23 (4 mix) with inlet diameter 50.8 mm were simulated for soot yield and combustion efficiency analysis. Figure 4.4 shows temperature contours, velocity vectors and soot contours of one of the tests.

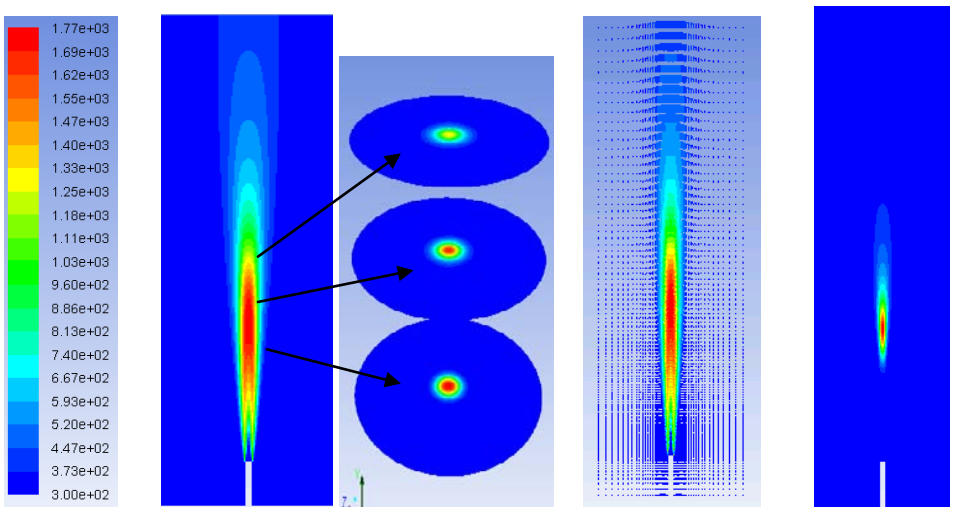

Figure 4.4: Temperature contours, velocity vectors and soot contours

Converged results are obtained after running all the test cases successfully. Maximum temperature of flares varies from 1766 K to 1802 K, as shown in Table 4.5. In post-processing, flow rate of soot is calculated at outlet, and flow rate of fuel is calculated at inlet. Soot yield (kg/kg) is calculated by using following formula:

$$\text{Soot Yield (kg/kg)} = \frac{\text{flow rate of soot at outlet (kg/s)}}{\text{flow rate of fuel at inlet (kg/s)}}$$

Table 4.5: Maximum flame temperature attained by flare

Test no.	Jet velocity (m/s)	Maximum Flame Temperature (K)
20	0.28	1766.2
21	0.56	1783.4
22	1.00	1797.4
23	1.67	1802.1

The soot yield results obtained after post processing are shown in Figure 4.5.

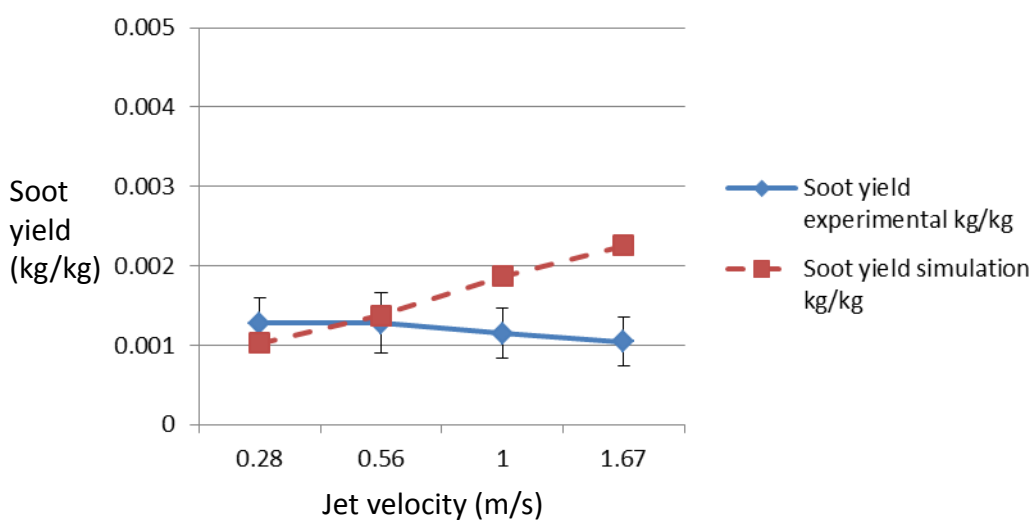

Figure 4.5: Soot yield results

As shown in Figure 4.5, soot results obtained by CFD simulation analysis are in agreement with experimental data for lower exit velocities, well within uncertainty limits. However, for higher fuel exit velocity, soot yield is slightly over-predicted by FLUENT-PDF model even though the prediction and data are still in good agreement in terms of the order of magnitude. Combustion efficiency (CE) of the flare is calculated by using following equation:

$$\%CE = \frac{CO_2}{CO_2 + CO + \text{Total Hydrocarbon Out} + \text{Soot}}$$

Results for combustion efficiency are given in Table 4.6.

Table 4.6: Simulated and experimental combustion efficiency

Test no.	Jet Velocity (m/s)	CE % Experimental	CE % Simulation
20	0.28	99.67 (+/-0.31)	99.96
21	0.56	99.70 (+/-0.06)	99.95
22	1.00	99.75 (+/-0.05)	99.93
23	1.67	99.75 (+/-0.04)	99.87

From Table 4.6, it can be inferred that combustion efficiencies obtained by FLUENT-PDF model for given flare tests are consistent with experimental results. Along with soot and CE, carbon-dioxide yield is also post-processed for current CFD analysis. The results for CO_2 yield are given in Table 4.7. These results are good match with experimental data. CO_2 yield is calculated by using following equation:

$$CO_2 \text{ Yield (kg/kg)} = \frac{\text{flow rate of } CO_2 \text{ at outlet (kg/s)}}{\text{flow rate of fuel at inlet (kg/s)}}$$

Table 4.7: CO_2 yield results

Test no.	Jet Velocity (m/s)	CO_2 yield experimental (kg/kg)	CO_2 yield simulation (kg/kg)
20	0.28	2.83	2.85
21	0.56	2.83	2.84
22	1.00	2.84	2.84
23	1.67	2.84	2.84

4.3.2 Results for lab-scale flares test no. 1 to 4 (6-mix) with model constant correction for high jet velocities

Moss-Brookes soot model mainly rely on two model constants, constant for soot inception rate (C_α) and constant for soot coagulation rate (C_β), which are determined through numerical modeling of a laminar flame for which experimental data exists. However, after simulating more than forty experiments, it is understood that these model constants may not hold for high velocity turbulent jet flame with Reynolds number above 4000. All simulation results suggest that as jet velocity increases, soot yield also increase. Experimental data suggests otherwise. Therefore, these model constants must be corrected for turbulent flame with higher jet velocities. Figure 4.6a shows soot yield results for tests 1 to 4 without any model constant correction. These test simulations use default values of model constant for soot inception rate (C_α) and soot coagulation rate (C_β) (Table 4.8a). Figure 4.6b gives soot yield results with model constant correction for C_α and C_β (Table 4.8b).

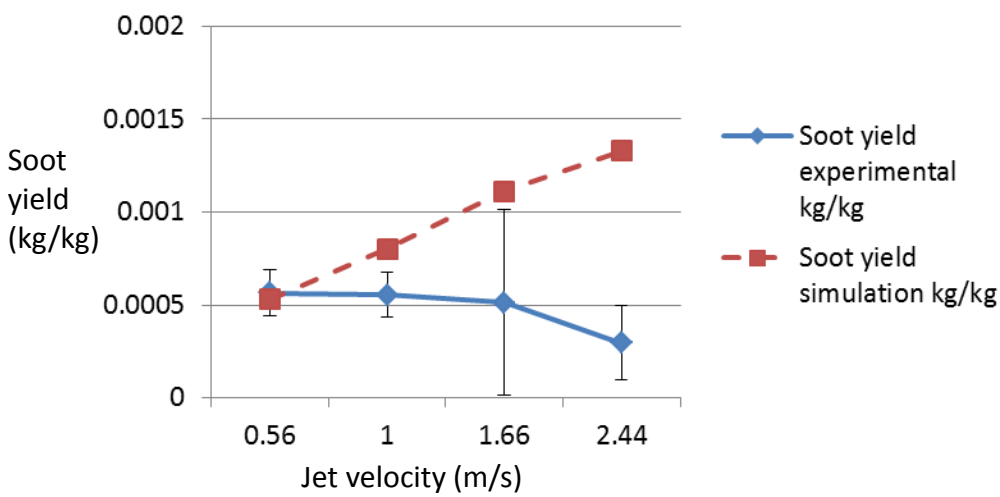

Figure 4.6a: Soot yield results without model constant correction

Table 4.8a: Default values of C_α and C_β (valid for low jet velocities Re<4000)

Soot inception rate C_α	54 s^{-1}
Soot coagulation rate C_β	1.0

Table 4.8b: Corrected values C_α and C_β for turbulent flame (higher jet velocities Re>4000)

Jet (m/s)	C_α	C_β
1.6	27	2
2.44	18	3

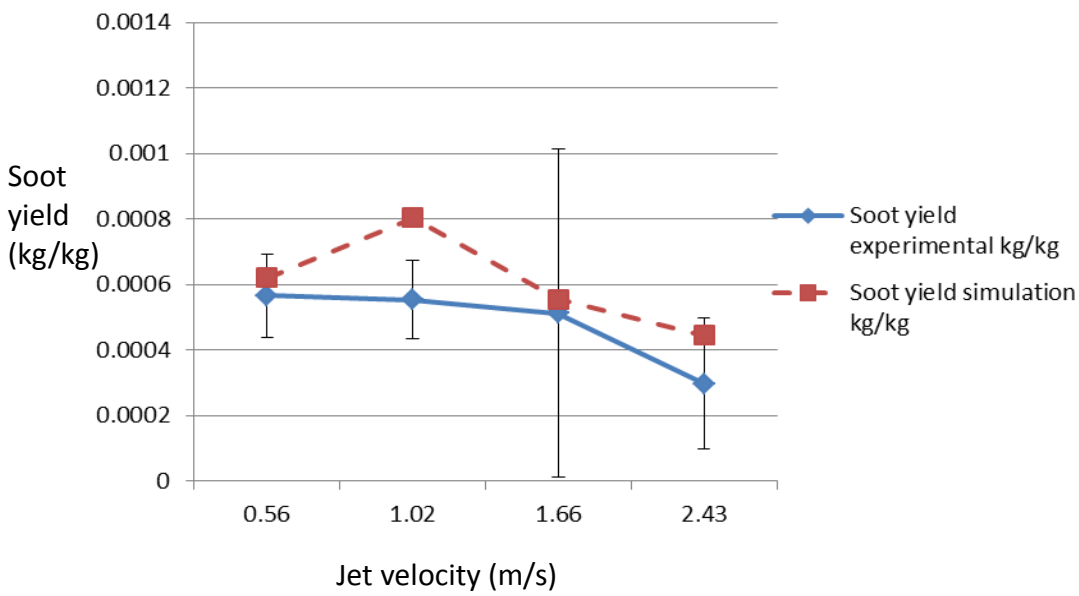

Figure 4.6b: Soot yield results with model constant correction for higher jet velocities

Figure 4.6a shows continues increase in soot-yield with increasing jet velocities, whereas experimental data suggests that soot-yield decrease for higher velocities. Figure 4.6b shows results with model constant correction, analogous with experimental analysis. By simulating more experiments, current model constant correction can be validated. Such validation of correction will be a part of immediate future work.

4.4 Conclusions

New chemical mechanism LU 3.0.1 validated successfully for soot analysis. Results of numerous significant performance indicators for methane mixture flames show that the simulation and experimental results are in good agreement. From soot yield CFD analysis, it can be concluded that soot yield measured with Fluent-PDF model is well within uncertainty limits for lower fuel exit velocities; however it slightly over-predicts soot for higher fuel exit velocities.

CO_2 yield measured by simulation is almost exact as experimental analysis. Combustion efficiency measured by this model is also equivalent to experimental analysis.

New approach of model constant correction in Moss-Brookes soot model can limit the over-prediction of soot for higher fuel-exit velocities (Reynolds number above 4000). However such correction must be dealt with careful analysis and validation.

4.5 Future Work

Along with soot yield and combustion analysis, experimental data from Carleton University also provides NO_x analysis. Unlike LU 1.1, new mechanism LU 3.0.1 does not include NO_x. However, FLUENT has its own in build NO_x models. Therefore, either by developing current mechanism further for NO_x species, or by using FLUENT NO_x model, these flare test simulations can be repeated to obtain NO_x yield results. For CO and VOC analysis Eddy Dissipation Concept (EDC) model can be explored. Also a new approach of soot model constant correction for turbulent flow will be a part immediate future work.

References Cited in This Section

[1] Elvidge, C. D.; Ziskin, D.; Baugh, K. E.; Tuttle, B. T.; Ghosh, T.; Pack, D. W.; Erwin, E. H.; Zhizhin, M. A Fifteen Year Record of Global Natural Gas Flaring Derived from Satellite Data. Energies 2009, 2, 595-622; doi: 10.3390/en20300595.

[2] Pope III, C. A.; Burnett, R. T.; Thun, M. J.; Eugenia, E. C.; Krewski, D.; Ito, K.; Thruston, G. D. Lung Cancer, Cardiopulmonary Mortality, and Long-term Exposure to Fine Particulate Air Pollution. JAMA: The Journal of the American Medical Association 2002, 287, 1132-1141; doi: 10.1001/jama.287.9.1132.

[3] US EPA Integrated Science Assessment for Particulate Matter EPA/600/R-08/139F; Washington, DC, 2010.

[4] IPCC Solomon, S.; Qin, D.; Manning, M.; Chen, Z.; Marquis, M.; Averyt, K. B.; Tignor, M.; Miller, H. L., Eds.; Cambridge University Press: Cambridge, UK and New York, USA, 2007; p. 996.

[5] Hansen, J.; Sato, M.; Ruedy, R.; Lacis, A.; Oinas, V. Global warming in the twenty-first century: An alternative scenario. Proceedings of the National Academy of Sciences of the United States of America 2000, 97, 9875-9880.

[6] Ramanathan, V.; Carmichael, G. Global and regional climate changes due to black carbon. Nature Geoscience 2008, 1, 221-227; doi: 10.1038/ngeo156.

[7] J.D.N. McEwen & M.R. Johnson, Black carbon particulate matter emission factors for buoyancy driven associated gas flares J. Air Waste Manage. Assoc., 62(3):307-321 (doi: 10.1080/10473289.2011.650040)

[8] R. P. Lindstedt. *In Proc. IUTAM Conf. on Aerothermo-Chemistry in Combustion*. Taipei, Taiwan1991

PART B: CFD Study of 2010 TCEQ Flare Test Data

4.6 Model Development for 2010 TCEQ Flare

4.6.1 General Information on 2010 TECQ Flare Test

Part of the scope of Task 4 is to model the flare tests conducted during September 2010 in John Zink test facility, Tulsa, Oklahoma, Figure 4.7 [1].

Fig. 4.7 Flare Plume Sampling System, John Zink test facility, Tulsa, Oklahoma [1]

A study was conducted by Aerodyne Research Mobile Laboratory on 2010 TCEQ flare tests to determine the flare combustion characteristics [2]. The scope of the analysis focused on the chemical composition and size of particles and differences in those parameters with the composition of the vent gas, as well as levels of steam and air assist. Propylene mix flares tested were found to have a significant Black Carbon (Soot) content, sensitive to air and steam assist levels. During 2011-2013, Lamar University acquired and modelled the operating and design

data of the flare tests conducted at John Zink facility [3,4]. These input data include the geometry of the flares used in the tests, meteorological data and the operating data available from the data acquisition system. The flare performance data provided primarily include soot yield (lb/MMBTU) and Combustion Efficiency (CE). Lamar University also acquired numeric soot emission data for certain test series reported in the 2010 TCEQ Flare Study –Particulate Appendix [2] from Aerodyne Research, Inc. These data sets serve as the foundation to check and possibly calibrate the CFD modelling for flare performance and soot/VOC emissions.

Combustion efficiency is defined as the percentage of flare emissions that are completely oxidized to CO_2. It can be written mathematically as:

$$\%CE = \frac{CO_2}{CO_2 + CO + THC + Soot} \times 100 \tag{4.8}$$

Where:

CO_2 — flow rate of carbon dioxide in kg/s

CO — flow rate of carbon monoxide in kg/s

THC — flow rate total hydrocarbon exiting from the flare in kg/s

Soot — flow rate of soot black carbon (soot) in kg/s

4.6.2 Governing Equations

ANSYS Fluent software contains the broad physical modelling capabilities needed to model flow, turbulence, heat transfer, and reactions for industrial applications. Steady-state or transient flows; heat transfer, including forced, natural, and mixed convection, conjugate (solid/fluid) heat transfer, and radiation; in viscid, laminar, and turbulent flows; and volumetric sources of mass, momentum, heat, and chemical species can be efficiently modelled using solver in ANSYS Fluent. Advanced solver technology provides fast, accurate CFD results, flexible moving and deforming meshes, and superior parallel scalability. The interactive solver setup, solution and post-processing capabilities of ANSYS Fluent make it easy to pause a calculation, examine results with integrated post-processing, change any setting, and then continue the calculation within a single application [5]. FLUENT can simulate the mixing and reaction of chemical species, including homogeneous and heterogeneous combustion models and surface deposition/reaction models. The Navier-Stokes equations and the equations for mass, energy and species transport are to be solved. The conservation equations of mass, momentum and energy are as follows[5]:

Mass balance equations:

The Equation for conservation of mass can be written as follows:

$$\frac{\partial \rho}{\partial t} + \nabla.(\rho\vec{v}) = S_m \tag{4.9}$$

Source term S_m is the mass added to the continuous phase from the dispersed second phase and any user defined phases.

Momentum balance equations:

Conservation of momentum in an inertial reference frame is described by

$$\frac{\partial}{\partial t}(\rho\vec{v}) + \nabla.(\rho\vec{v}\vec{v}) = -\nabla p + \nabla.(\bar{\bar{\tau}}) + \rho\vec{g} + \vec{F} \tag{4.10}$$

where p is the static pressure, $\bar{\bar{\tau}}$ is the stress tensor and $\rho\vec{g}$ and $\vec{F}$ are the gravitational body force and external body forces respectively.

The stress tensor $\bar{\bar{\tau}}$ is given by

$$\bar{\bar{\tau}} = \mu\left[\left(\nabla\vec{v} + \nabla\vec{v}^T\right) - \frac{2}{3}\nabla.\vec{v}\, I\right] \tag{4.11}$$

where μ is the molecular viscosity, I is the unit tensor, and the second term on the right hand side is the effect of volume dilation.

Energy balance equations:

ANSYS FLUENT solves the energy equation in the following form:

$$\frac{\partial}{\partial t}(\rho E) + \nabla.\left(\vec{v}(\rho E + p)\right) = \nabla.\left(k_{eff}\nabla T - \sum_j h_j\vec{J_j} + (\overline{\overline{\tau_{eff}}}.\vec{v})\right) + S_h \tag{4.12}$$

where k_{eff} is the effective conductivity and $\vec{J_j}$ is the diffusion flux of species j. The three terms on the right hand side represent

$k_{eff}\nabla T$ is conductive energy transfer,

$\sum_j h_j\vec{J_j}$ is diffusion of species and

$\overline{\overline{\tau_{eff}}}.\vec{v}$ is viscous dissipation.

S_h includes the heat of chemical reaction and any other defined volumetric sources.

Here,

$$E = h - \frac{p}{\rho} + \frac{v^2}{2} \tag{4.13}$$

where sensible enthalpy h is defined for ideal gases as

$$h = \sum_j Y_j h_j \tag{4.14}$$

and for incompressible flows as

$$h = \sum_j Y_j h_j + \frac{p}{\rho} \tag{4.15}$$

Y_j is the mass fraction of species j and

$$h_j = \int_{T_{ref}}^{T} c_{p,j} dT \text{ where } T_{ref} \text{ is 298.15 K.} \tag{4.16}$$

When the non adiabatic non-premixed combustion model is enabled, ANSYS FLUENT [5b] solves the total enthalpy form of the equation:

$$\frac{\partial}{\partial t}(\rho H) + \nabla.(\rho \vec{v} H) = \nabla.\left(\frac{k_t}{c_p} \nabla H\right) + S_h \tag{4.17}$$

The conduction and species diffusion terms together sum-up to give the first term on the right-hand side of the equation above while the second term contributes to the viscous dissipation. The total enthalpy H is defined as

$$H = \sum_j Y_j H_j \tag{4.18}$$

where Y_j is the mass fraction of species j and

$$H_j = \int_{T_{ref,j}}^{T} c_{p,j} dT + h_j^0 \left(T_{ref,j}\right) \tag{4.19}$$

$h_j^0 \left(T_{ref,j}\right)$ is the formation enthalpy of species j at the reference $T_{ref,j}$

Species balance equations:

The conservation equation for chemical species is solved by predicting the local mass fraction of each species, Y_i, through the solution of a convection-diffusion equation for the ith species. This conservation equation takes the general form:

$$\frac{\partial}{\partial t}(\rho Y_i) + \nabla.(\rho \vec{v} Y_i) = -\nabla.\vec{J_i} + R_i + S_i \tag{4.20}$$

R_i is the net rate of production of species *i* by chemical reaction and S_i is the rate of creation by addition from the dispersed phase plus any user-defined sources. An equation of this form will be solved for N-1 species where N is the total number of fluid phase chemical species present in the system. To minimize numerical error, N^{th} species should be selected as the species with the overall largest mass fraction, such as N_2 when the oxidizer is air.

4.6.3 Geometry

The detailed side and top view of flare stack and tip is shown in Figure 4.8**.** A three-dimensional geometry with rectangular domain is constructed in ANSYS-Workbench[5 e] design modular. Its rectangular fluid domain and mesh structure is shown in Figure 4.9. The geometry

has the fuel inlet lifted slightly by 20 cm above the air-assist inlet (Figure 4.9c). Slopped mesh for this geometry is created by using MultiZone and Edge sizing method in meshing module of ANSYS Workbench. Crosswind inlet is given to left side of the geometry, and pressure outlet is given right and right top of the geometry. Both flow rate and velocity in the simulation are matched to the actual test values. Mesh structure is made denser at stack inlet for better combustion analysis (Figure 4.9d). Orthogonal quality of mesh is kept at 0.76 and grid size is around 0.8 million. The mesh is successfully checked for good skewness.

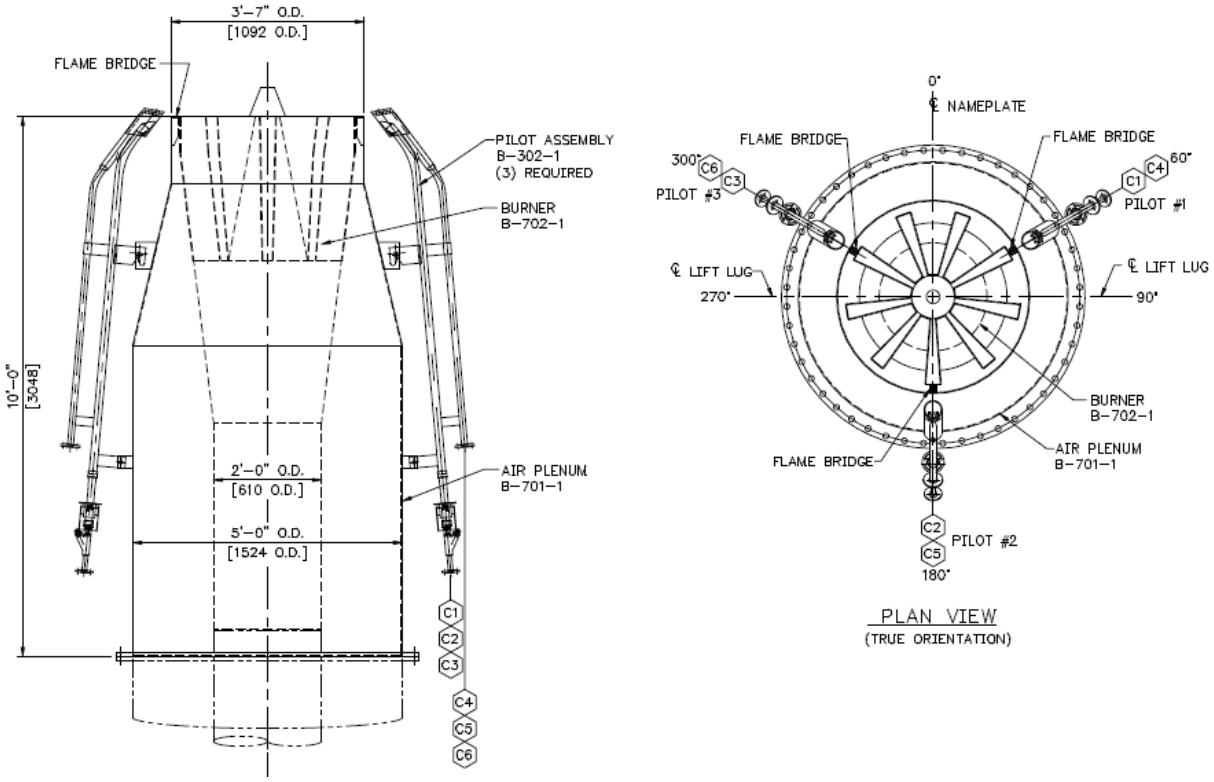

Fig. 4.8 :Air assisted flare stack and flare tip

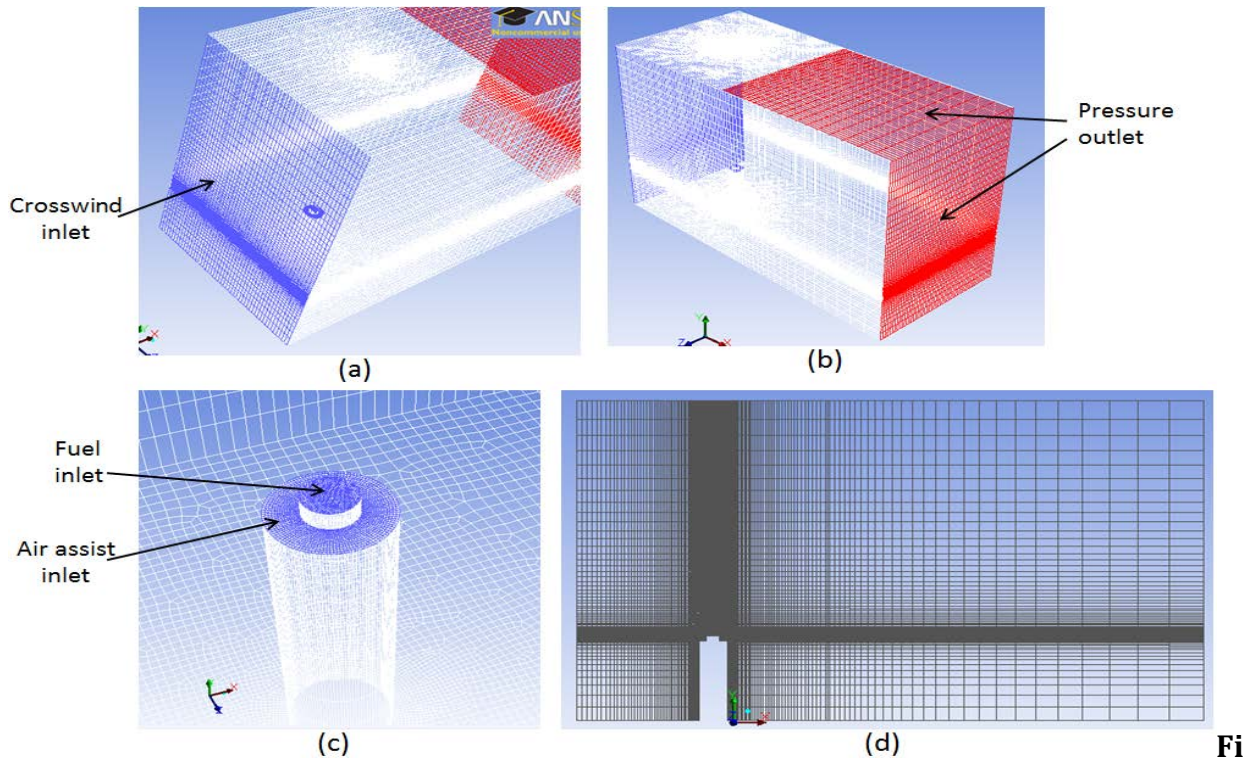

Fig. 4.9: Computational domain and mesh view

4.6.4 Turbulence and Chemistry Models

Physical and turbulence models

In general, the flare flow is turbulent as the exit diameter is large and jet velocity is high. The flow can be predicted more accurately with the Reynolds number. Turbulent flows are characterized by high-frequency fluctuating velocity fields, which result in the Reynolds stresses. The turbulence boosts the mixing of transported quantities such as momentum, energy, and species concentration, and affects the chemical reaction process. Therefore, a turbulence model is needed to simulate the flare with the chemical kinetics playing a dominative role in flare reactions.

There are many turbulence models available in the commercial software package FLUENT[5 b]. The standard k-ε model is considered the most robust for a wide range of applications. One of the more successful recent developments is the realizable k-ε model. The realizable k- ε model is significantly better than the standard k- ε model for many applications. In flare simulation, the cross wind can impose a significant effect on the shape as well as the

efficiency of flare. Besides, the downwash of a flare jet can be very important to sustain the flare. To predict the effect of cross winds and downwash of flame, the realizable k- ε model is used in this study, and is expected to produce more reasonable results.

Chemistry models

Two types of combustion/chemical reaction models are being considered: Eddy-dissipation finite-rate also known as Eddy-dissipation Concept (EDC) model and non-premixed combustion also known as Probability Density Function (PDF) model.

To run the cases in non-premixed combustion model pre-PDF is created and it contains the required mean mixture fractions of each species involved in combustion. PDF table is made up from number of flamelets. These flamelets are embedded together to generate PDF table. The fuel composition is given during the generation of flamelets. But in the EDC model the species equations are solved for each species. The new reduced mechanism LU3.0.1 is used for both models.

Problem Setup in FLUENT

New geometry is checked for its orthogonal mesh quality before beginning of setup procedure. Steady state pressure-based solver is used for all the test cases . The realizable k-ε turbulent model with standard wall functions is used for the viscous model. SIMPLE scheme is used for the pressure-velocity coupling.

4.7 Results for 2010 TCEQ flare tests

4.7.1. Non-Premixed Combustion (PDF)

Probability Density Function (PDF) model settings are applied to six cases of 2010 TCEQ air-assist flare study with Moss-Brookes soot model. In Moss-Brooks soot model, C_2H_2 and C_6H_6 are used as soot precursors along with Fenimore-Jones Oxidation model.

Figure 4.10 shows temperature contours for the case A4.1. For this case, crosswind of 4.69 m/s is given from left inlet. Fuel exit velocity is 0.5791 m/s and its major composition consists of propylene and nitrogen. Highest temperature attained by this flare is around 2050K. Carbon balance error for these preliminary simulations for current PDF model varies case to case

from 0.04% up to 20%. Boundary conditions and LHV data for all six cases are given in Table 4.9. Initial results for the soot and combustions efficiency for these tests are given in Tables 4.10-4.11 and Figures 4.11-12, respectively.

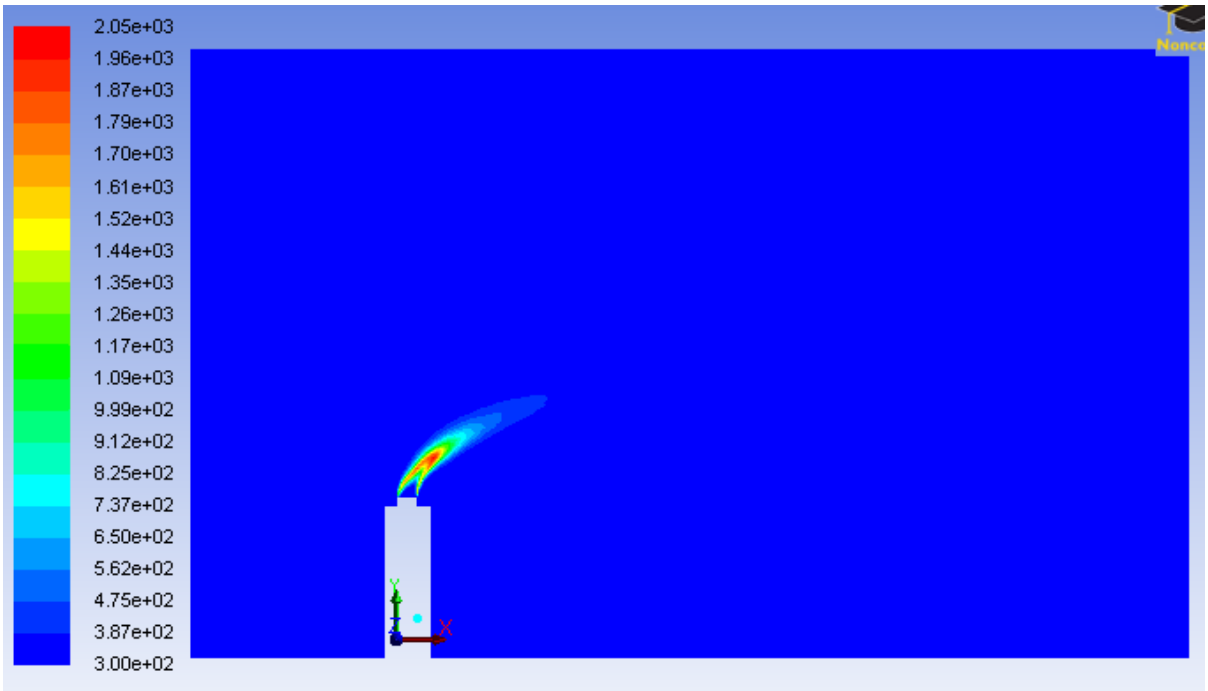

Figure 4.10: Temperature Contours for Test A4.1

Table 4.9: Input Conditions for Simulated Air-Assist Cases

Case no.	Propylene (kg/s)	TNG (kg/s)	Nitrogen (kg/s)	Total (kg/s)	Temp (^{O}F)	Actual Vent gas LHV (Btu/scf)	Exit velocity (m/s)	Air flow rate (kg/s)	Crosswind (m/s)
A1.1	0.1158	0.0000	0.0000	0.1158	87	2108.00	0.43	18.80	5.68
A2.1	0.0446	0.0000	0.0000	0.0446	94	2120.00	0.15	10.54	5.81
A3.1	0.0229	0.0024	0.0885	0.1138	95	339.00	0.61	2.48	5.08
A4.1	0.0383	0.0039	0.0746	0.1168	84	569.00	0.58	6.34	4.69
A5.1	0.0092	0.0009	0.0344	0.0445	88	345.33	0.24	1.05	2.06
A6.1	0.0149	0.0015	0.0278	0.0442	99	585.00	0.21	1.42	7.13

Table 4.10: Soot Results for 2010 TCEQ flare study

Case no.	BC Experiment (lb/MMBTU)	log BC Experiment (lb/MMBTU)	BC simulation (lb/MMBTU)	log BC Simulation (lb/MMBTU)	Error, a factor of
A1.1	3.05	0.48	4.22	0.63	1.38
A2.1	4.6	0.66	6.19	0.79	1.35
A3.1	3.95	0.6	1.86	0.27	2.12
A4.1	2.68	0.43	1.22	0.09	2.2
A5.1	3.45	0.54	1.55	0.19	2.23
A6.1	8.05	0.91	11.46	1.06	1.42
Avg.					1.78

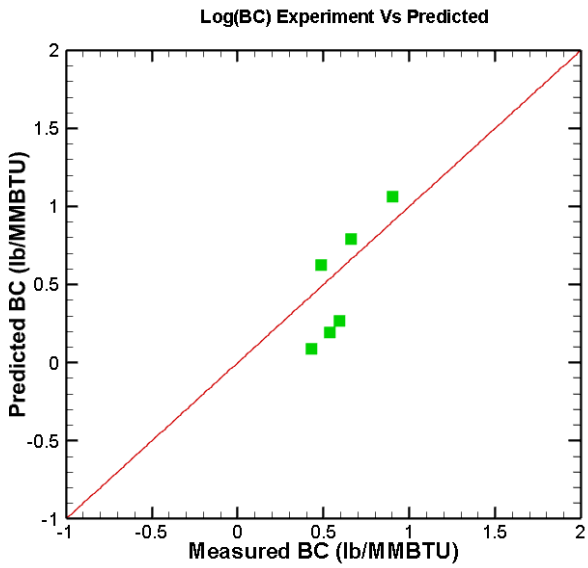

Fig. 4.11: Measured vs. Predicted black carbon

Table 4.11: Combustion Efficiency

Case no.	CE Experiment (%)	CE Simulation (%)	% error
A1.1	96.9	96.93	0.03
A2.1	95.9	95.09	0.84
A3.1	98.3	98.88	0.59
A4.1	97.1	99.23	2.19
A5.1	95.9	99.37	3.62
A6.1	99.4	92.9	6.54
Avg.			2.3

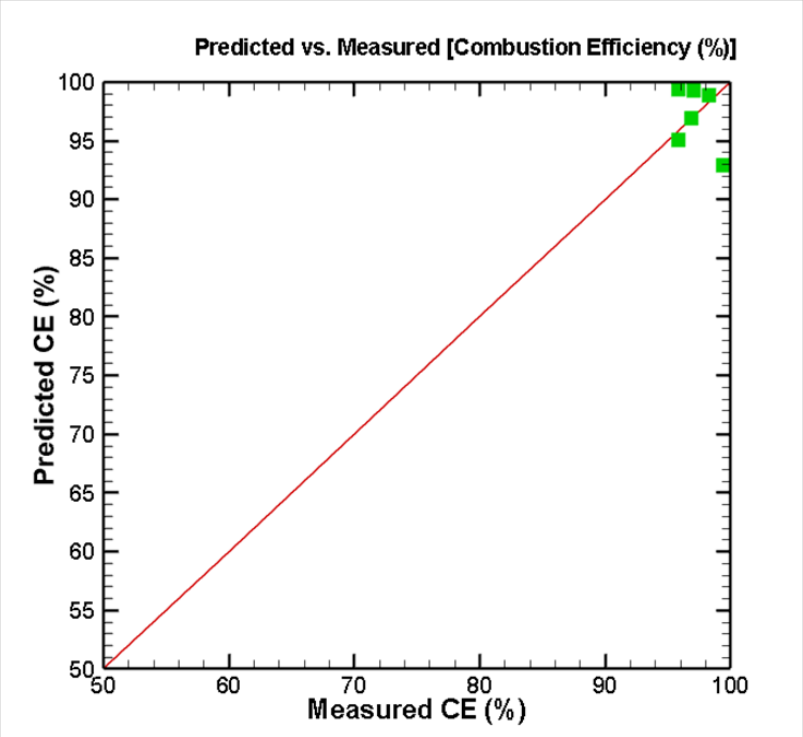

Fig. 4.12: Measured vs. predicted Combustion efficiency

It can be seen that soot yields can be predicted within a factor of 2.2 (with an average of 1.8) while CEs are predicted within 6.5% (with an average of 2.3%) for the air-assisted flare cases in 2010 TCEQ Flare Study.

4.7.2 Species Transport Model — Eddy Dissipation Concept (EDC)

Detailed Arrhenius chemical kinetics can be incorporated in turbulent flames. However, typical reaction mechanisms are invariably stiff and their numerical integration is computationally costly. Hence, the model should be used only when the assumption of fast chemistry is invalid

Eddy Dissipation Concept settings was applied to one air-assisted flare test case with Moss-Brookes soot model. The standard k-ε realizable turbulent model with standard wall functions was used as viscous model. SIMPLE algorithm was enabled for pressure-velocity coupling. For soot model, C_2H_2 and C_6H_6 are used as precursors along with Fenimore-Jones Oxidation model [2 b]. Soot and CE results for EDC model for case A1.1 are given in Tables 4.12 and 4.13.

Table 4.12: Soot Results with the EDC model

Case no.	Soot Experiment (lb/MMBTU)	Soot simulation (lb/MMBTU)
A1.1	3.05	2.06

Table 4.13: Combustion efficiency with the EDC model

Case no.	CE Experiment (%)	CE Simulation (%)
A1.1	96.9	82.64

4.8 Future Work

The group has been using GAMBIT for geometry and meshing until recent 2013 but this part of the simulation has been moved into ANSYS Workbench [5 d] [5 e]. Gambit is much more convenient and simple to use when compared to workbench geometry and meshing with FLUENT 13.0 and 14.0[5 c] [5 d]. Mesh generation has been a challenge to the group given the time and the large complex geometry. The convergence time with the new mechanism and the overall carbon balance error has been found to be increased which might be due to the inclusion of the soot precursors and soot modeling in FLUENT. In the near future, new geometry for air assist cases will be modified to best suit the experimental set up. The EDC model for the dilute fuel mixtures having low LHV will be simulated. Steam assisted test cases will be simulated with a simpler geometry with PDF model and then the same will be modeled in EDC along with the soot model to best match the experimental data.

References for This Section

[1] David T. Allen and Vincent M. Torres, 2010 TCEQ Flare Study Final Report, The University of Texas at Austin, The Center for Energy and Environmental Resources, TCEQ PGA No. 582-8-86245-FY09-04 and Task Order No. UTA10-000924-LOAT-RP9, Aug. 1, 2011.

[2] Appendix: Aerodyne Research Mobile Laboratory Particulate Measurements TCEQ 2010 Flare Study http://www.Tceq.Texas.Gov/Assets/Public/Implementation/Air/Rules/Flare/2010flarestudy/2010-Flare-Study-Final-Appendices-Particulates.Pdf

[3] Daniel Chen et al., “Final Report: AQRP Project#10-022 Development of Speciated Industrial Flare Emission Inventories for Air Quality Modeling in Texas, Dec 2011”

[4] Kanwar Devesh Singh, Preeti Gangadharan, Daniel Chen, Helen H. Lou, Xianchang Li, P. Richmond, “CFD Modeling of Laboratory Flames and an Industrial Flare,” *Journal of the Air & Waste Management Association* (in Press, 2014).

[5] ANSYS FLUENT Inc.
a. ANSYS FLUENT User's Guide Release 14.0 ; November 2011. ANSYS,Inc.
b. ANSYS FLUENT Theory Guide Release 14.0 ; November 2011. ANSYS, Inc.
c. *ANSYS® Academic Research, Release 13.0,*
d. *ANSYS® Academic Research, Release 14.0*
e. *ANSYS FLUENT in ANSYS Workbench User's Guide Release 14.0; November 2011*.

5. RESPONSE SURFACE MODELING OF FLARE TESTS DATA (TASK 5)

5.1. Background

Control of soot and VOC emissions from combustion processes are important issues in flaring. Although the USEPA states that destruction efficiency for normal industrial flaring practices is 98%, these assumptions are currently under scrutiny by the agencies [1-2]. Further, current EPA regulations (40 CFR60.18) requires smokeless flaring, which motivates flare operators to over-steam or over-air to suppress smoke at the expense of combustion efficiency (CE) or carbon conversion Efficiency (CCE). It is also well known that incipient smoke point (ISP) is a good indicator for good combustion, but the phenomena is neither well understood nor scientifically defined. Since many factors affect soot emission and unburned/ produced VOC emissions, there is a lack of clear guidelines as to how to operate the flares in order to achieve the optimal over-all environmental performance.

Not only current field measurements (such as FTIR, MEMS, EI, LIF and REMPI) for estimating flare efficiency are costly, but also difficult to deploy on site. Detailed computational fluid dynamics modeling of flaring based on rigorous kinetic mechanisms are also comparatively expensive and time consuming (requiring parallel computing with high-performance clusters). As a result, this task seeks to use easy-to-use response surface models to predict the flare performance.

5.2. Methodology for This Section

In the first part of this section, the calculation procedure for CCE and its relation to CE is discussed. A step by step procedure used in the development of Soot/CE/DRE response surfaces is discussed in the later part of this section.

5.2.1 Calculation of Combustion Efficiency

$$Combustion\ Efficiency\ (CE) = \frac{Mass\ of\ Carbon\ converetd\ to\ CO2}{Mass\ of\ Carbon\ originally\ fed\ as\ fuel} * 100 \qquad (5.1)$$

As defined above, combustion efficiency is equivalent to carbon conversion efficiency. CE is also calculated based on the concentration ratios in the field by the following equation:

$$CE\ \% = \frac{CO_2\ (Plume)}{CO_2\ (plume) + CO\ (plume) + \Sigma hydrocarbons\ (plume) + soot} * 100 \qquad (5.2)$$

where

CO_2 (plume) ……. mole % of carbon dioxide in the plume,

CO (plume) …….. mole % of carbon monoxide in the plume;

Σhydrocarbons (plume) … …mole % of all the unburned hydrocarbons in the plume multiplied by the number of carbons in the hydrocarbon;

Soot …… mole % as carbon in the plume.

CE can also be used interchangeably with carbon conversion efficiency. According to the TCEQ report, the reported CE was calculated without considering the soot emissions. In order to develop model equations based on soot emissions and to find the relation between Soot/CE, corrected combustion efficiency (CCE) was calculated taking soot emissions into account. CCE can also be regarded as the real carbon conversion efficiency. The procedure for calculation of CCE is explained in Appendix . A word of caution needs to be given here that the soot data collected by ARI indicated a high degree of variability. Given the measurement errors of soot are in the range of 15% - 20%, not accounting for the sampling errors [1], the actual uncertainty may be bigger. As a result, the corrected CE or CCE values need to be taken with due caution.

Originally reported CE and Corrected CE values were plotted for all steam and air cases as shown in Figures 5.1 & 5.2. It was observed for the steam assist cases that CE values greater than 95% required an adjustment about 1- 8% to satisfy the carbon balance, when the soot emissions were taken into account. For test cases S4.2.A (2010 TCEQ Report) and test cases 4 & 8 (1983 McDaniel Report), CCE lowered by about 8% due to higher soot emissions of about 2.7 to 3.4 lb/MMBTU.

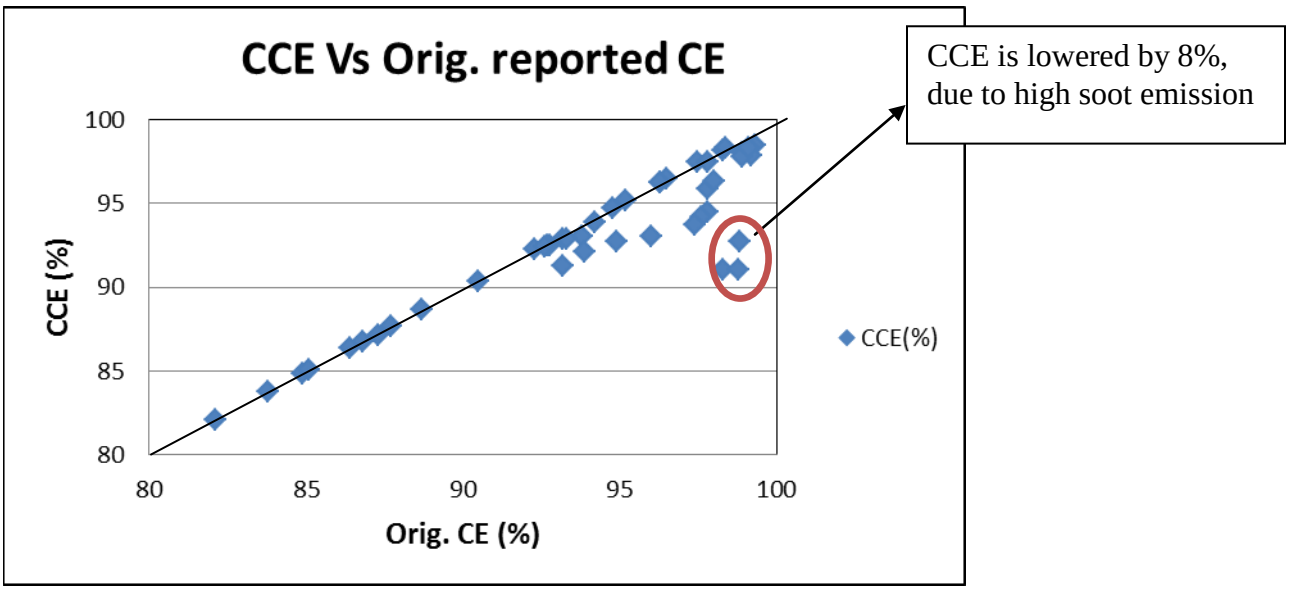

Fig. 5.1 CCE vs. Originally reported CE for all steam assisted cases

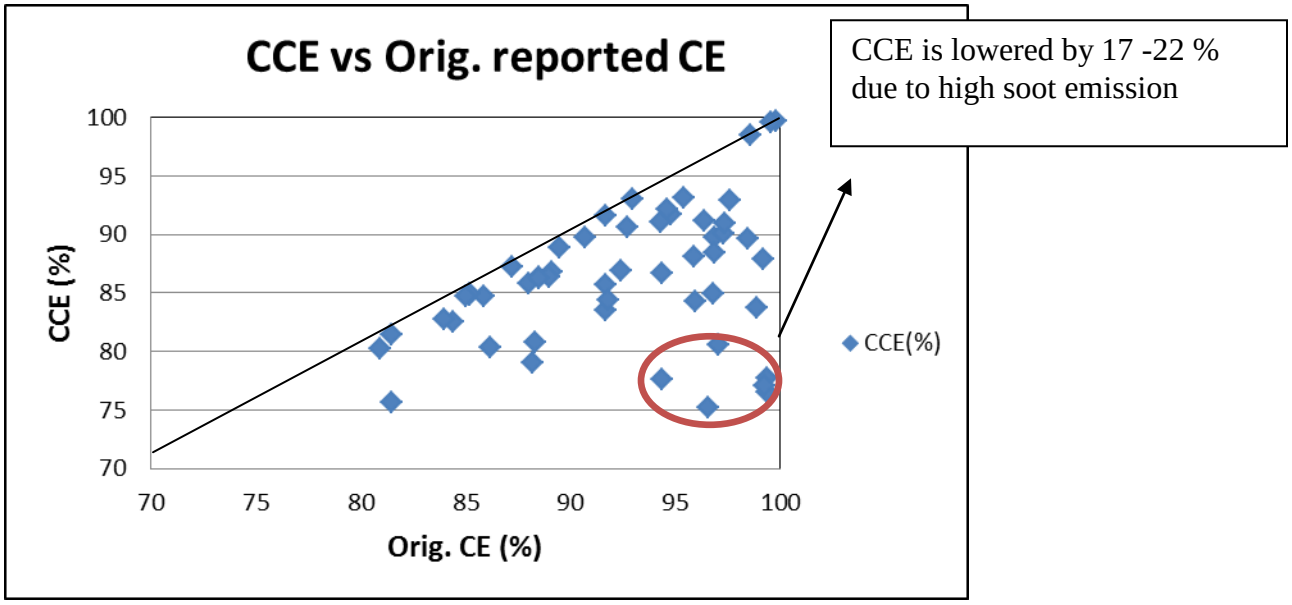

Fig. 5.2 CCE vs. Originally reported CE for all air assisted cases

For all air assist test cases in 2010 TCEQ Final Report, with soot emissions higher than 2 lb/MMBTU, the CCE is by about 5 – 23% lower compared to CE.

5.2.2 Effect of Soot emissions on Combustion Efficiencies

To study the effect of soot on combustion efficiencies, soot yield was plotted in terms of log BC against CCE and CE for the steam assist cases. In this case, data from 1983 and 2010 reports (shown in Appendix) were used since soot emissions were not accounted for calculating CE. The results were shown in Figures 5.3 and 5.4. The data points encircled in black moved to lower CE values (as shown in Fig.5.3) due to higher soot emissions. The original CE has to be adjusted about 3 – 8% in order to satisfy the carbon balance. The test series S5 shows an increasing trend in CE up to 98% as shown in Fig. 5.4, whereas the increasing trend stops at 96% due to the adjustment for higher CE values when soot emissions were considered. The test cases S4.2.A, S4.4.1, S4.6.1, S8.1.1, S8.2.1 and S8.3.1 produced more soot, because of low steam flow compared to high vent gas supply.

Also, the test cases S4.4.1 and S8 had no center steam flow. Two test cases 4 and 8 reported in 1983 were operated at higher vent gas flow with no steam. These factors might have influenced high soot production. The data encircled in red were found to have higher CE and lower soot emissions. They did not require any adjustment in CE even after considering the soot value in combustion efficiency calculations.

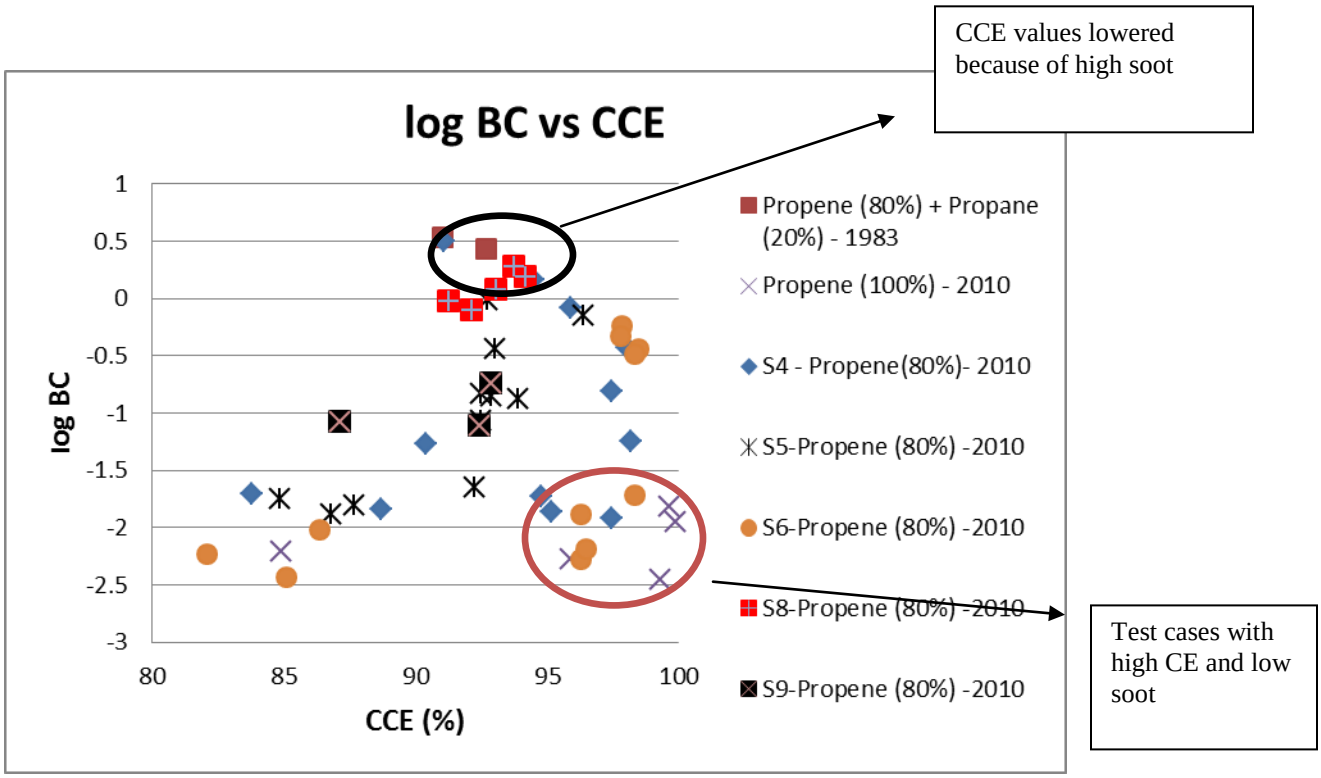

Fig. 5.3 Log BC vs. CCE (Steam assist 1983/2010 test cases with CE >80%)

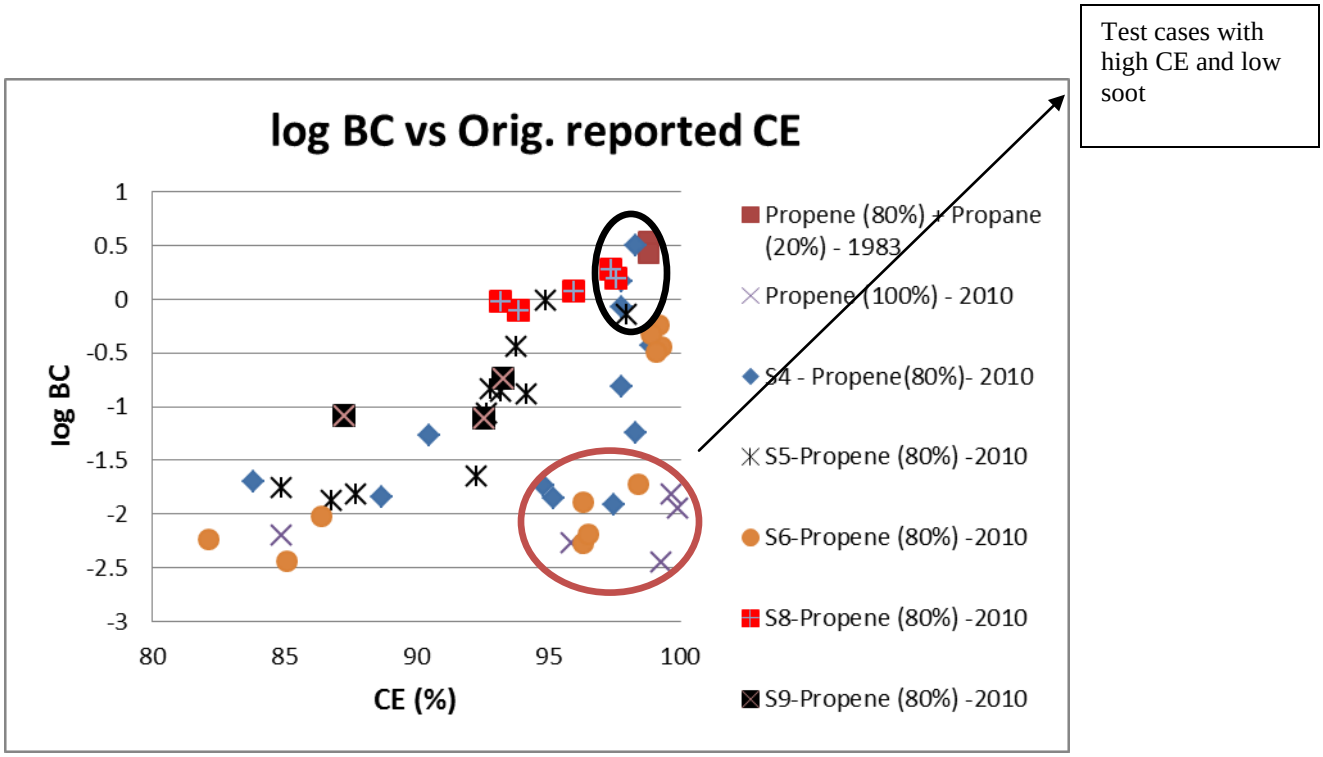

Fig. 5.4 Log BC vs. Originally reported CE (Steam assist **1983/2010** test cases with CE >80%)

5.2.3 Data Sources

Experimental data for the response surface modeling were collected from the following sources:

i. Flare efficiency study by Marc McDaniel - 1983 [2]

ii. Evaluation of efficiency of Industrial flares: Test results by Industrial Environmental Research Laboratory - 1984 [3]

iii. TCEQ 2010 Flare study final report by David Allen and Vincent Torres [4]

5.2.4 Response Surface Methodology for Soot/CE/DRE

Generalized response surface models were established using Microsoft Excel and Minitab. Initially, a simple quadratic response model with two input variables (X, Y) was developed with limited data from 2010 TCEQ report as shown below:

$$Z = a_0 + a_1*X + a_2*Y + a_3*X*Y + a_4*X^2 + a_5*Y^2; \quad (5.3)$$

where Z = Soot/DRE/CE.

The response surface models were developed using MINITAB statistics tool box [5]. The developed multi-dimensional response surface models were then used to identify the optimal

operating zones. The sequential procedure followed in developing a response surface is given below.

Data collection

In the first stage, all the available data with soot/DRE/CE values were collected from TCEQ 2010 flare study report. Then the data from 1983 and 1984 were added to the data pool. The data collected from the literature include the geometry of the steam-assist and air-assist flares used in the test, meteorological data (cross-wind speed/direction, humidity, and temperature), operating data (aeration, steaming, exit velocity, waste gas/pilot fuel species), flare efficiencies, and soot emission data. These data were tabulated in Excel spreadsheets as shown in Appendix .

Identification of important variables

Soot, DRE, and CE are the response variables, while LHV, V, U, D, S, A, and VG are the independent variables in this study. An automatic tool was considered to be an appropriate option for picking the best regression model with multiple parameters. Minitab software an automatic tool to select the best regression model in a specific category. Useful predictors for model building were identified based on the Best Subsets Regression method [6-7]. This technique compares all possible linear models using a specified set of predictors, and displays the best-fitting models that contain one predictor, two predictors, and so on. The end result is a number of models and their summary statistics. Based on our requirements, we can compare and choose one.

Fitting a model

In the next step, a model is developed using the identified variables to fit the data. Initially, a linear model is developed and then the model is validated based on Adjusted R^2, Predicted R^2 and residual plots [7-9]. If the linear model is not appropriate, then a quadratic model is used. Then the interaction terms were added to make a good fit to the data. The detailed procedure for model validation and selection of interaction terms are shown in Appendix .

5.3. Results and Discussion

5.3.1 Effect of steam on Combustion efficiencies

The effect of steam assist (lb/MMBTU) on originally reported CE & the corrected CE was shown in Figures 5.5 & 5.6. All available steam assist test data from 1983 & 2010 were used in this case. In the 1984 EPA study, CE value was calculated by considering soot emissions. Hence, those data were not used in this section. Both plots show a decreasing trend with increase in steam assist.

In Fig. 5.5, the encircled region shows an approx. constant CE (around 98%) at lower steam assist but the same was not observed in Fig. 5.6 because the soot emission is higher at low steam assists. After considering soot emissions in calculation of CCE, higher efficiency was observed in the range of 70 -140 lb/MMBTU of steam assist. The test cases S1.5.1, S1.6.1 and S1.7.1 with 100% propene produced less soot, so their CE and CCE values remain unchanged. When steam flow increases, CE decreased because of higher production of hydrocarbons as seen in the cases S5.3, S 6.4.2, S6.4.3 and S1.9.1. The data points marked in blue were taken from 1983 flare efficiency study, which shows decrease in CE value of about 6 – 7 %, because of higher soot emissions with no steam injection.

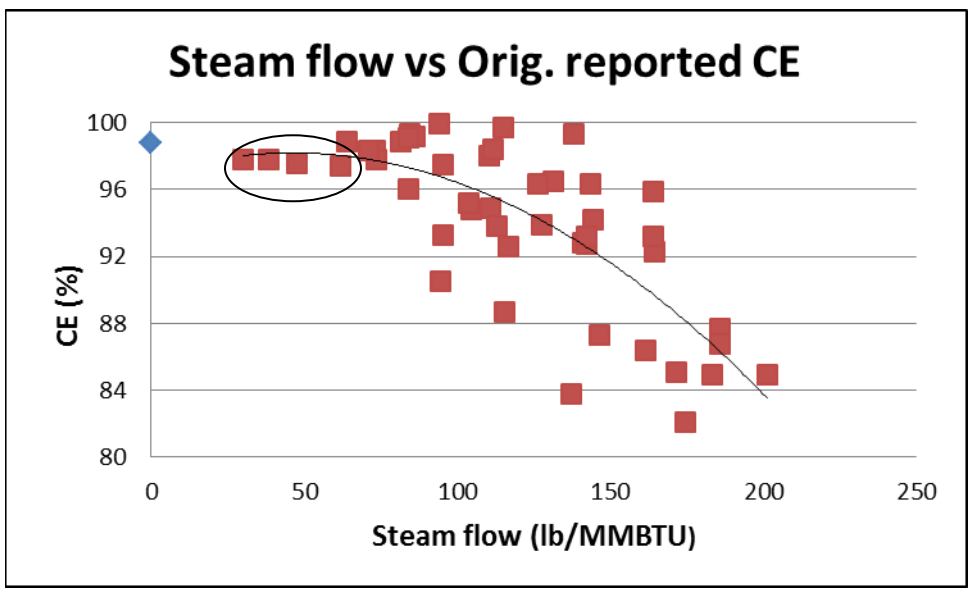

Fig. 5.5 Steam flow vs. Combustion Efficiency as originally reported (Steam assist test cases with CE >80%; The data points marked in blue were taken from 1983 EPA study)

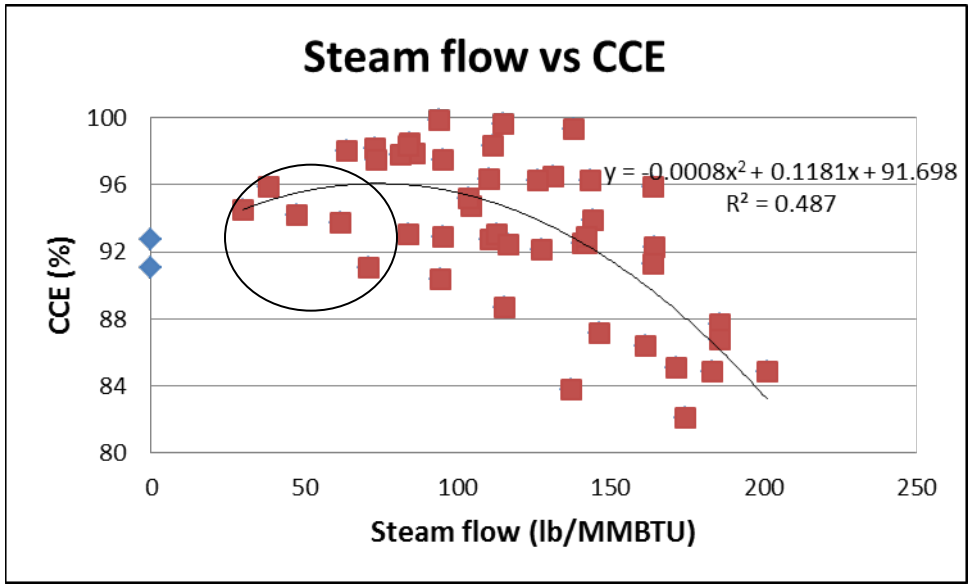

Fig. 5.6 Steam flow vs. CCE (Steam assist test cases with CCE >80%; The data points marked in blue were taken from 1983 EPA study)

The univariate relation between the CCE and steam flow is given by the following quadratic model:

$$CCE = 91.698+0.1181*S -0.0008*S*S \quad (5.4)$$

5.3.2 Identification of Incipient Smoke point for steam assisted flares tests

According to the 2010 Flare study report, TCEQ have identified the test cases S1.5, S3.1, S4.1, S5.1, S6.1 and S8.3 as Incipient smoking point (shown in Fig. 5.7). Steam assist required at incipient smoke points were determined from the relation between steam assist and soot emissions. Table 5.1 shows the average of soot values available as BC (lb/MMBTU) and steam assist (lb/MMBTU) for the identified test cases as ISP.

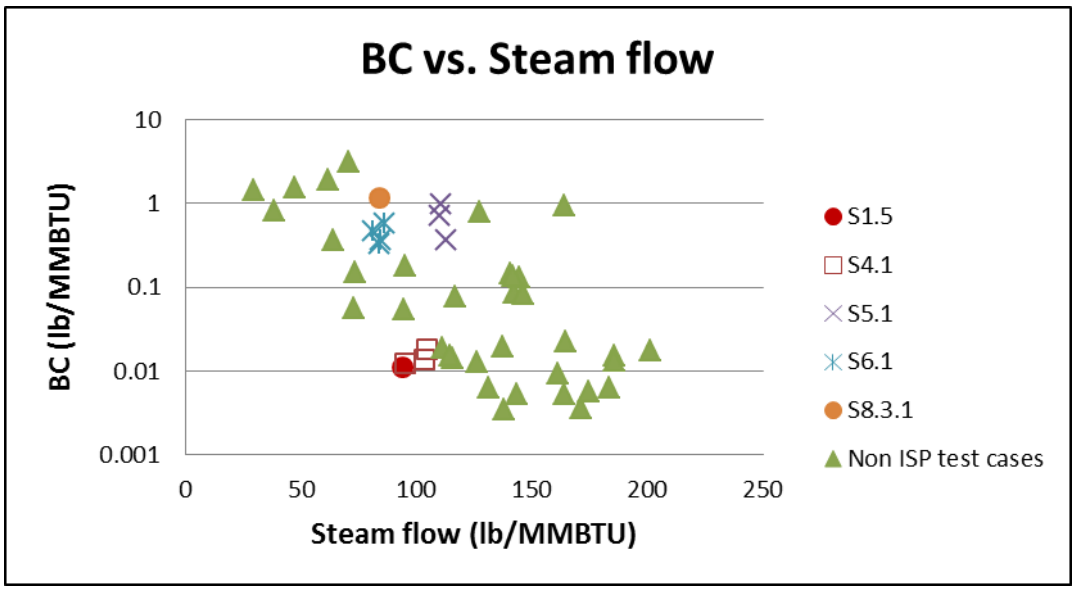

Fig. 5.7 Steam flow vs. Soot produced (at ISP)

From the figure, it is clear that steam flow in the range of 80 – 110 lb/MMBTU produce minimum soot at the incipient smoke point.

Table: 5.1 Incipient smoke points for steam assisted flare tests

Test case	S1.5	S4.1	S5.1	S6.1	S8.3
Report Year	2010	2010	2010	2010	2010
Steam Flow (lb/MMBTU)	94	101	111	84	84.85
Soot (lb/MMBTU)	0.011	0.015	0.683	0.431	1.171

5.3.3 Identification of Incipient Smoke point for Air assisted flares tests

For air assist flare tests, the test cases A1.1, A2.1, A3.1, A4.1, A5.1, A6.1 and A7.1 were identified as incipient smoking point (shown in Fig. 5.8). Air assist required at Incipient smoke points were determined as earlier. Table 5.2 shows the average of soot values available as BC (lb/MMBTU) and air flow (lb/MMBTU) for the identified test cases as ISP. It can be seen from the figure that air assist in range of 4000 – 13000 lb/MMBTU produced minimum soot at the incipient smoke point.

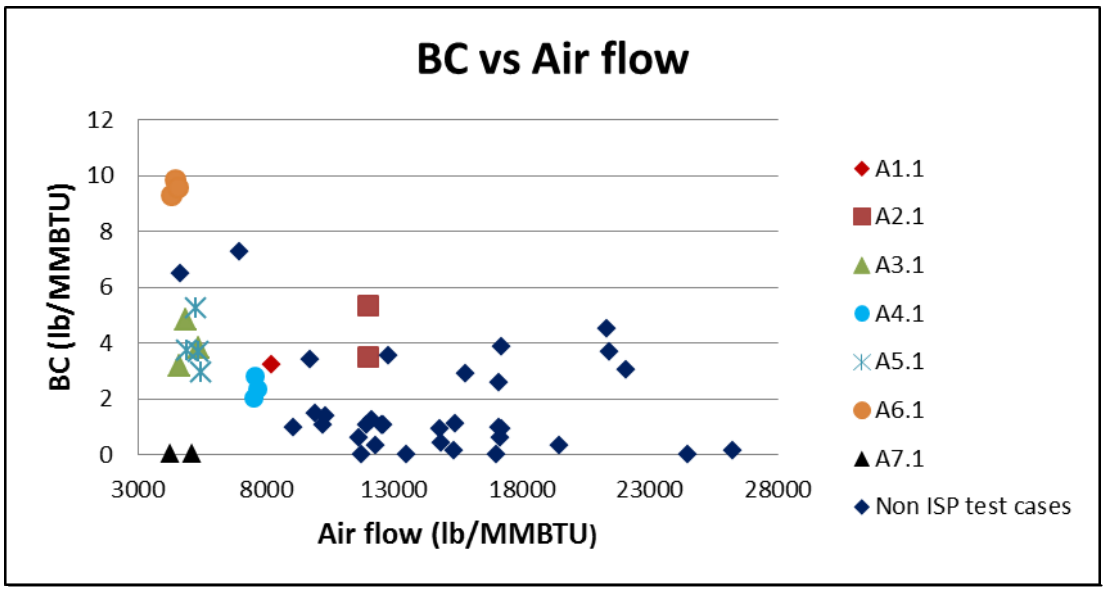

Fig. 5.8 Air flow vs. Soot produced (at ISP)

Table: 5.2 Incipient smoke points for air assisted flare tests

Test case	A1.1	A2.1	A3.1	A4.1	A5.1	A6.1	A7.1
Report Year	2010	2010	2010	2010	2010	2010	2010
Air Flow (lb/MMBTU)	8247	12000	4950	7600	5250	4440	4679
Soot (lb/MMBTU)	3.24	4.44	3.95	2.40	3.90	9.57	0.07

5.3.4 Response Surface models

5.3.4a Response Surface model for soot emissions

Steam assist flare data with soot/CE/DRE values were collected from 1983 and 1984 flare efficiency study reports and included in the data set. Since, the 1984 flare test has been studied using propane as a major component in vent gas stream and all other flare tests were carried out with propylene mixtures, a new variable was introduced for the presence of double bond (DB). The table containing all steam assist data with soot/CE/DRE values is shown in Appendix . Important variables were identified by the best subsets regression method. LHV, S, VG and DB were identified as important variables which have significant effect on soot emissions (response variable). Initially, a simple linear model was developed and checked for model adequacy [10]. Since the linear model with interactions and simple quadratic model were inadequate, a quadratic model with interactions was developed and validated against the model

validation criteria as explained in Appendix . In each step, outliers were removed and then recursive regression was performed to develop the final model. The quadratic model with soot as response and LHV, S, VG, DB as predictors is given below:

$$\log BC = -2.567 + 0.002904\ LHV - 0.4747\ S - 0.1679\ VG + 4.321\ DB - 0.000001\ LHV*LHV + 0.000078\ LHV*VG - 0.001005\ LHV*DB + 0.4575\ S*DB \quad (5.5)$$

Model Summary

Std. Error	R-sq	R-sq(adj)	R-sq(pred)
0.494077	87.78%	86.72%	84.97%

Table 5.3 Steam assist data range used in developing the quadratic model equation Eq. 5.5 [Source: 1983, 1984, & 2010 Flare study reports]

No. of data points	BC	V	S	VG	DB	LHV
	lb/MMBTU	ft/s	lb/MMBTU	MMBTU/hr		BTU/scf
101	0 – 3.41	0.2 – 1509	0 – 202	0.12 – 48.6	0 / 1	290 – 2350

Similarly, a response surface model was developed for soot emissions with all available air assisted flare data from 1983. Air flow was in the range of 0 – 26200 lb/MMBTU compared to other variables. So, they were normalized by subtracting the mean from the observed value and then divided by the standard deviation. The final model developed is given below:

$$\log BC = -2.350 - 0.000001\ LHV*LHV + 0.0501\ A*A + 0.000115\ LHV*D + 0.000187\ LHV*A - 0.01579\ D*A - 0.01203\ D*V + 0.07571\ D*DB - 0.1208\ A*V \quad (5.6)$$

Model Summary

Std. Error	R-sq	R-sq(adj)	R-sq(pred)
0.150489	97.01%	96.45%	79.04%

Table 5.4 Air assist data range used in developing the quadratic model equation Eq. 5.6 [Source: 1983, 1984, & 2010 Flare study reports]

No. of data points	BC	V	A	VG	DB	LHV	D
	lb/MMBTU	ft/s	lb/MMBTU	MMBTU/hr		BTU/scf	inch
51	0.002 - 9.8	0.5 – 72	0 – 26200	1.5 – 21	0 / 1	330 – 2180	18 – 24

5.3.4b Response Surface model for CCE

A response model was developed with CCE as response for all steam (or air) assist data. The final model developed for the steam assist flares is given below**:**

$$CCE = 98.78 + 0.1088\ S - 0.001152\ LHV - 0.00771\ V + 0.0862\ VG - 0.023\ D - 0.000741\ S*S - 0.00620\ D*D - 0.001299\ S*VG + 0.000169\ LHV*D \quad (5.7)$$

Model Summary

Std. Error	R-sq	R-sq(adj)	R-sq(pred)
2.06495	78.20%	76.12%	72.35%

Table 5.5 Steam assist data range used in developing the quadratic model equation Eq. 5.7 [Source: 1983, 1984, & 2010 Flare study reports]

No. of data points	BC	V	S	VG	DB	LHV	D
	lb/MMBTU	ft/s	lb/MMBTU	MMBTU/hr		BTU/scf	inch
104	0 – 3.41	0.2 – 1509	0 – 202	0.12 – 48.6	0 / 1	290 – 2350	3 – 36

The final model developed with CCE as response variable for all the available air assist data is given below:

$$CCE = 107.24 - 0.04917\ LHV - 3.18\ A + 1.773\ VG - 6.79\ DB + 0.000021\ LHV*LHV - 1.396\ A*A - 0.000980\ LHV*VG - 0.649\ A*VG + 5.66\ A*DB \quad (5.8)$$

Model Summary

S	R-sq	R-sq(adj)	R-sq(pred)
2.56821	82.84%	78.78%	64.64%

Table 5.6 Air assist data range used in developing the quadratic model equation Eq. 5.8 [Source: 1983, 1984, & 2010 Flare study reports]

No. of data points	BC	V	A	VG	DB	LHV	D
	lb/MMBTU	ft/s	lb/MMBTU	MMBTU/hr		BTU/scf	inch
48	0.002 - 9.8	0.5 – 72	0 – 26200	1.5 – 21	0 / 1	330 – 2180	18 – 24

5.3.4c Response surface model for DRE

Response surface model were developed with DRE as response for all available steam and air assist data. The final model developed for the steam assist flares is given below**:**

$$DRE = 99.561 - 0.000708\ LHV + 0.0363\ S + 0.0287\ VG - 0.0860\ D - 0.000448\ S*S + 0.000129\ LHV*D - 0.000740\ S*VG \quad (5.9)$$

Model Summary

S	R-sq	R-sq(adj)	R-sq(pred)
1.56725	78.99%	77.45%	73.96%

Table 5.7 Steam assist data range used in developing the quadratic model equation Eq. 5.9 [Source: 1983, 1984, & 2010 Flare study reports]

No. of data points	BC	V	S	VG	DB	LHV	D
	lb/MMBTU	ft/s	lb/MMBTU	MMBTU/hr		BTU/scf	inch
103	0 – 3.41	0.2 – 1509	0 – 202	0.12 – 48.6	0 / 1	290 – 2350	3 – 36

The final model developed with DRE as response variable for all the available air assist data is given below:

$$DRE = 92.835 + 0.002843\ LHV - 5.192\ A - 0.1971\ VG + 0.000983\ LHV*A \quad (5.10)$$

Model Summary

S	R-sq	R-sq(adj)	R-sq(pred)
1.21495	92.39%	91.67%	90.48%

Table 5.8 Air assist data range used in developing the quadratic model equation Eq. 5.10 [Source: 1983, 1984, & 2010 Flare study reports]

No. of data points	BC	V	A	VG	DB	LHV	D
	lb/MMBTU	ft/s	lb/MMBTU	MMBTU/hr		BTU/scf	inch
47	0.002 - 9.8	0.5 – 72	0 – 26200	1.5 – 21	0 / 1	330 – 2180	18 – 24

5.3.4d Regression model for Steam flow vs. Log BC and CCE

Simultaneous minimization of soot yield and maximization of flare efficiencies is one of the objectives of this study. For better flare operations, higher combustion efficiency and lower soot emissions are expected. In order to estimate the value of each independent variable at higher CCE and lower soot emission, regression models were developed to present operating variables as a function of performance variables. In other words, air assist and steam assist which are normally considered as independent variables were used as the response, while log BC and CCE were treated as the predictors.

Model Equation

$$S = -2718 - 28.3\ \log BC + 69.8\ CCE - 5.80\ \log BC*\log BC - 0.427\ CCE*CCE \qquad (5.11)$$

Model Summary

S	R-sq	R-sq(adj)	R-sq(pred)
44.9268	52.91%	51.06%	48.40%

Table 5.9 Steam assist data range used in developing the quadratic model equation Eq. 5.11 [Source: 1983, 1984, & 2010 Flare study reports]

No. of data points	BC	V	S	VG	DB	LHV	D
	lb/MMBTU	ft/s	lb/MMBTU	MMBTU/hr		BTU/scf	inch
107	0 – 3.41	0.2 – 1509	0 – 202	0.12 – 48.6	0 / 1	290 – 2350	3 – 36

A 2-D contour plot was constructed for the model developed as shown in Fig.5.9. From the figure, it is clear that steam flow in the range of 20 -70 (lb/MMBTU) is required for low soot emissions (log BC < –1 or BC <0.1 lb/MMBTU) and high CE (>96%). The region of higher CE

and lower soot is marked by red circle (used in all plots in this report to show best operating regime).

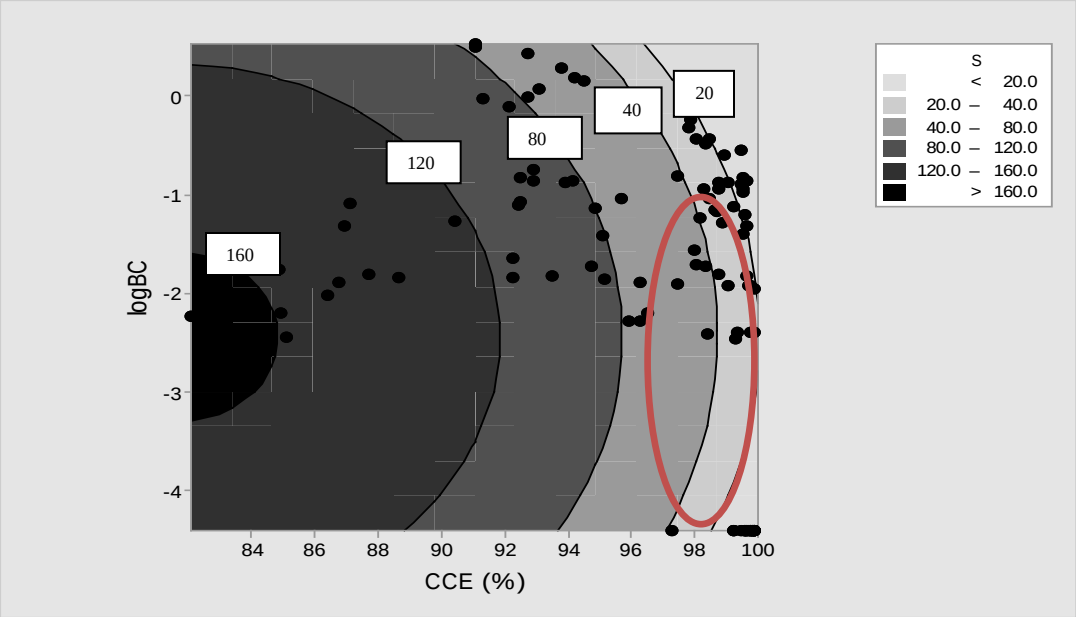

Fig. 5.9 2-D Contour plot for the model Steam flow vs. log BC, CCE

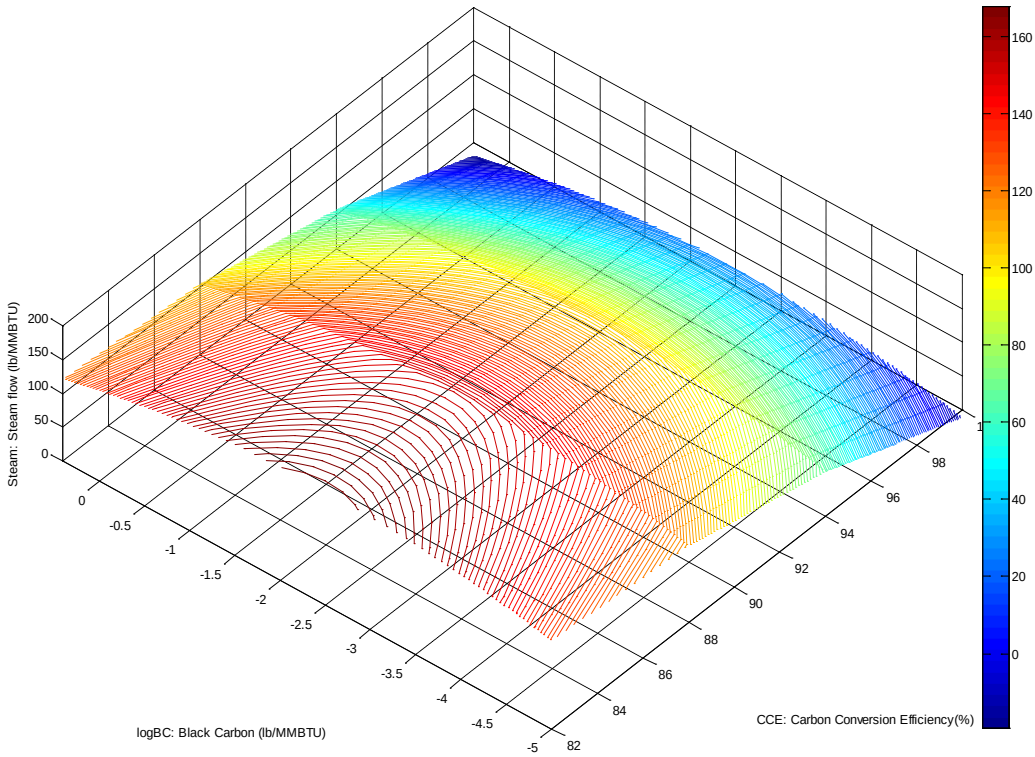

Fig. 5.10 3-D Contour plot for the model Steam flow vs. log BC, CCE

A 3-D contour plot was developed using MATLAB statistics toolbox [11] for the model as shown in Fig. 5.10. Low soot emission (log BC <–1 or BC < 0.1 lb/MMBTU) and high CE (>96%) exist simultaneously in the steam assist range of 20 – 70 lb/MMBTU. On comparing the two plots, it is observed that that the common range of steam required for best operating regime is 20 – 70 lb/MMBTU.

5.3.4e Regression model for Air Assist vs. Log BC and CCE

As mentioned earlier, to find the optimum air assist required for high combustion efficiency and low soot emission, a regression model was developed with air flow (A) as response, while log BC and CCE are predictors. In this model, Air flow was not normalized and the actual values were used.

Model Equation

$$A = -252570 - 6968\ \log BC + 6806\ CCE - 2166\ \log BC*\log BC - 43.0\ CCE*CCE \quad (5.12)$$

Model Summary

S	R-sq	R-sq(adj)	R-sq(pred)
4161.59	54.50%	50.71%	41.64%

Table 5.10 Air assist data range used in developing the quadratic model equation Eq. 5.12 [Source: 1983, 1984, & 2010 Flare study reports]

No. of data points	BC	V	A	VG	DB	LHV	D
	lb/MMBTU	ft/s	lb/MMBTU	MMBTU/hr		BTU/scf	inch
53	0.002 - 9.8	0.5 – 72	0 – 26200	1.5 – 21	0 / 1	330 – 2180	18 – 24

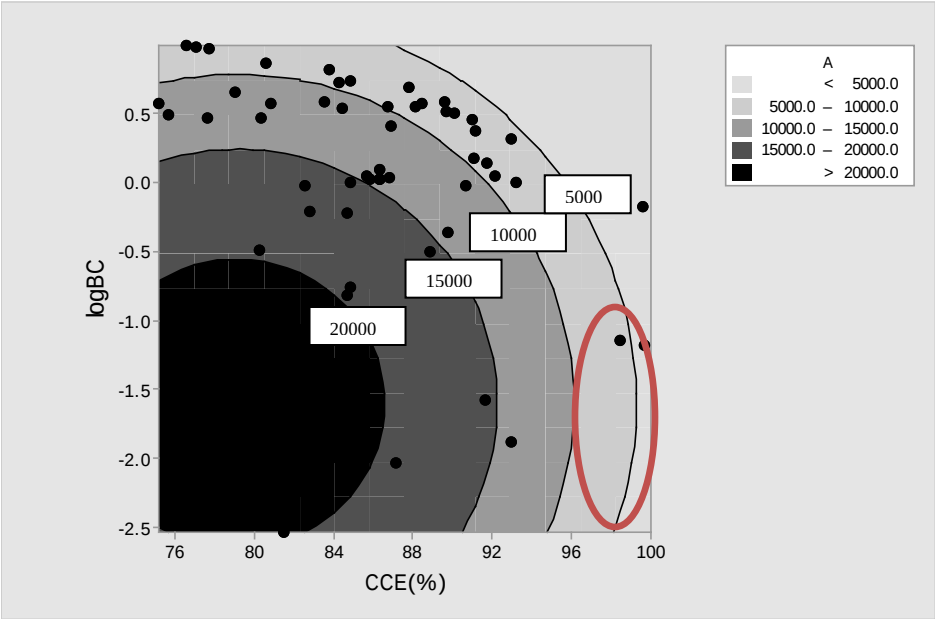

Fig. 5.11 2-D Contour plot for the model Air flow vs. log BC, CCE

From the 2-D contour plot shown in Fig. 5.11, it is clear that air flow in the range of 4000 -10000 (lb/MMBTU) is required for low soot emissions (log BC < –1 or BC <0.1 lb/MMBTU)) and high CE (>96%). A 3-D contour plot for the model Eq. 5.12 is shown in Fig. 5.12. Low soot emission (log BC <–1 or BC < 0.1 lb/MMBTU) and high CE (>96%) exist simultaneously in the air assist range of 4000 – 10000 lb/MMBTU. The common range of air assist for low soot and high CE exists in the range of 4000 – 10000 lb/MMBTU.

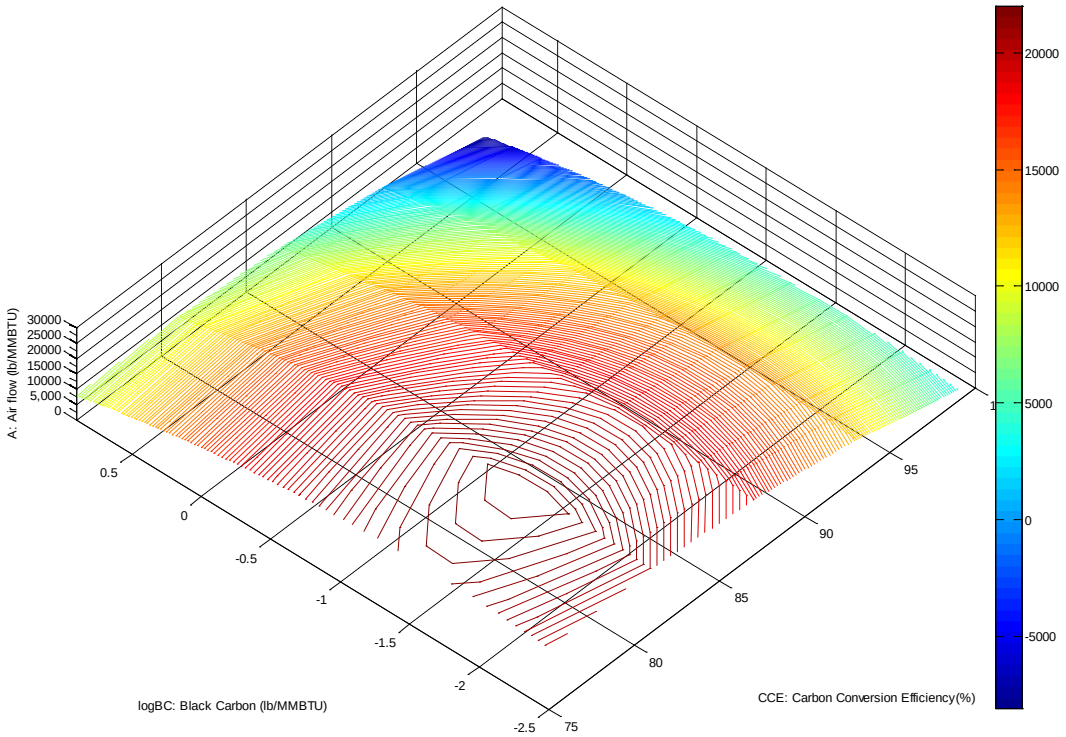

Fig.5.12 3-D Contour plot for the model Air flow vs. log BC, CCE

5.3.4f Regression model for LHV vs. Log BC and CCE

A regression model was developed with LHV as response, while log BC and CCE are predictors for steam and air assisted data. The model equation for steam assist data is given below:

Model Equation

$$LHV = 86074 + 2143\ logBC - 1844\ ACE + 9.96\ ACE*ACE - 22.0\ logBC*ACE \quad (5.13)$$

Model Summary

S	R-sq	R-sq(adj)	R-sq(pred)
542.535	24.36%	21.39%	14.42%

Table 5.11 Steam assist data range used in developing the quadratic model equation Eq. 5.13 [Source: 1983, 1984, & 2010 Flare study reports]

No. of data points	BC	V	S	VG	DB	LHV	D
	lb/MMBTU	ft/s	lb/MMBTU	MMBTU/hr		BTU/scf	inch
107	0 – 3.41	0.2 – 1509	0 – 202	0.12 – 48.6	0 / 1	290 – 2350	3 – 36

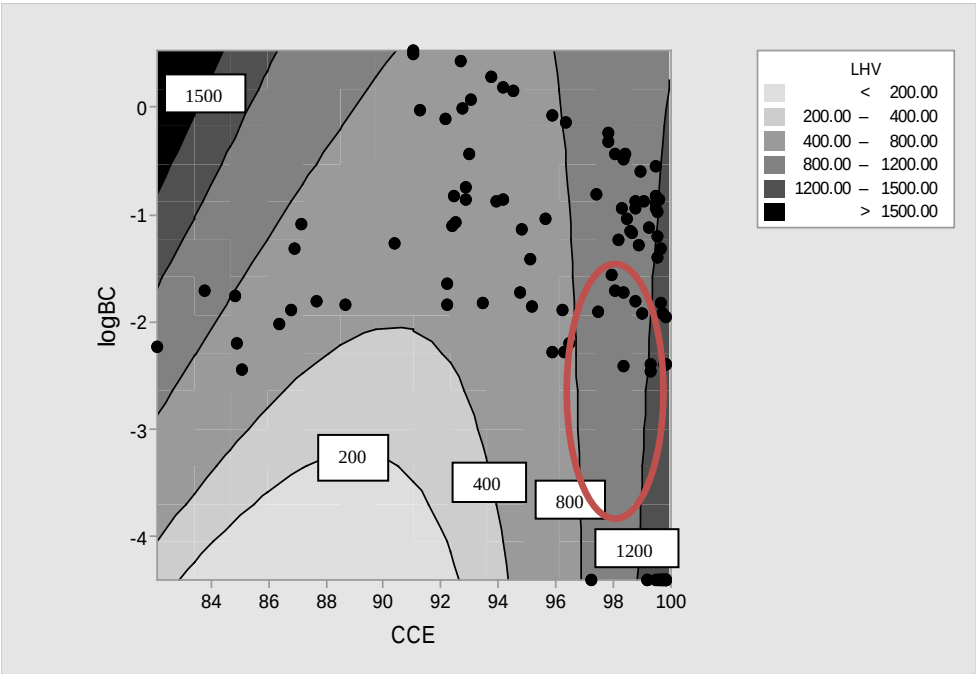

Fig. 5.13 2-D Contour plot for the model LHV Vs log BC, CCE (Steam assisted flares)

From the 2-D contour plot shown in Fig. 5.13, it is clear that LHV in the range of 700 – 1300 (BTU/scf) is required for low soot emissions (log BC < –1 or BC <0.1 lb/MMBTU)) and high CE (>96%). The peak value of soot exists at 0.53 lb/MMBTU with corresponding CCE at 91%.

The model equation for all air assist data is given below:

Model Equation

$$LHV = -1274 + 475\ logBC + 22.0\ ACE + 143\ logBC*logBC \quad (5.14)$$

Model Summary

S	R-sq	R-sq(adj)	R-sq(pred)
612.429	14.11%	8.86%	3.50%

Table 5.12 Air assist data range used in developing the quadratic model equation Eq. 5.14 [Source: 1983, 1984, & 2010 Flare study reports]

No. of data points	BC	V	A	VG	DB	LHV	D
	lb/MMBTU	ft/s	lb/MMBTU	MMBTU/hr		BTU/scf	inch
53	0.002 - 9.8	0.5 – 72	0 – 26200	1.5 – 21	0 / 1	330 – 2180	18 – 24

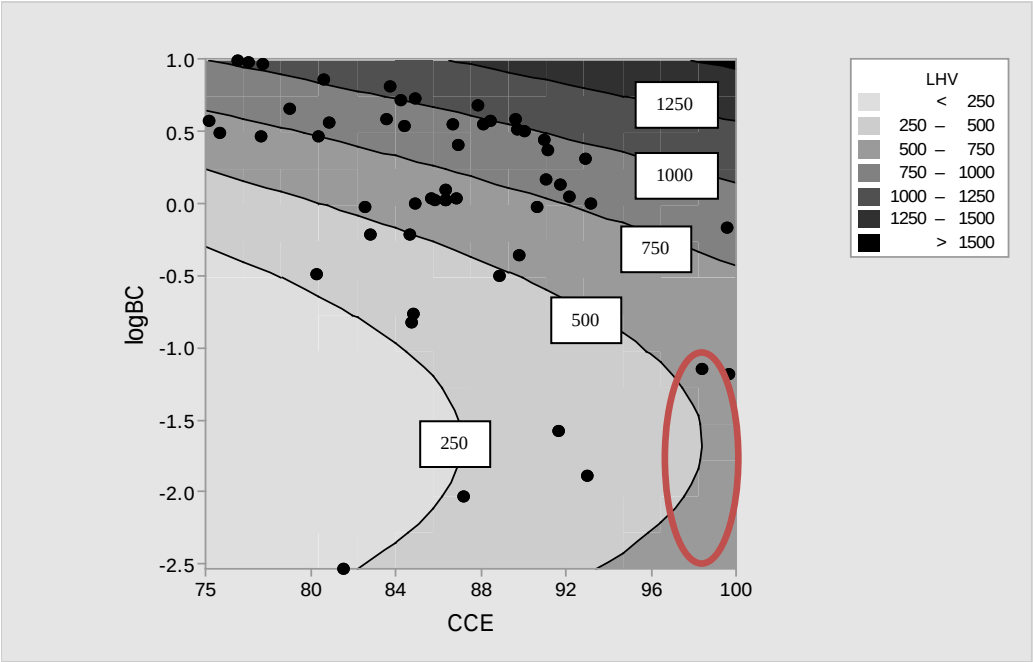

Fig. 5.14 2-D Contour plot for the model LHV Vs log BC, CCE (Air assisted flares)

It is clear from the above figure, that LHV in the range of 400 – 600 (BTU/scf) is required for low soot emissions (log BC < –1 or BC <0.1 lb/MMBTU)) and high CE (>96%). The peak value of soot exists at 0.99 lb/MMBTU with corresponding CCE at 78%. R^2 values for the model were too low since these variables have less significant effect on soot emission and CE when considered alone and they have significant effect while interacting with other operating variables.

5.3.4g Regression model for Vent gas heat flow vs. Log BC and CCE

The optimum vent gas heat flow required for high CE and low soot emissions was identified by the developing regression models with VG as response, while Log BC and CCE are predictors for all available steam and air assisted flare test data. The model equation for steam assisted flare tests given below:

Model Equation

$$VG = 1211 + 42.8\ \log BC - 25.1\ ACE + 0.1309\ ACE*ACE - 0.456\ \log BC*ACE \quad (5.15)$$

Model Summary

S	R-sq	R-sq(adj)	R-sq(pred)
11.9461	13.70%	10.31%	4.32%

Table 5.13 Steam assist data range used in developing the quadratic model equation Eq. 5.15 [Source: 1983, 1984, & 2010 Flare study reports]

No. of data points	BC	V	S	VG	DB	LHV	D
	lb/MMBTU	ft/s	lb/MMBTU	MMBTU/hr		BTU/scf	inch
107	0 – 3.41	0.2 – 1509	0 – 202	0.12 – 48.6	0 / 1	290 – 2350	3 – 36

Figure 5.15 shows the 2D contour plot for the model with VG as response. From the figure, it is clear that VG in the range of 11 – 20 (MMBTU/hr) is required for low soot emissions (log BC < –1 or BC <0.1 lb/MMBTU)) and high CE (>96%).

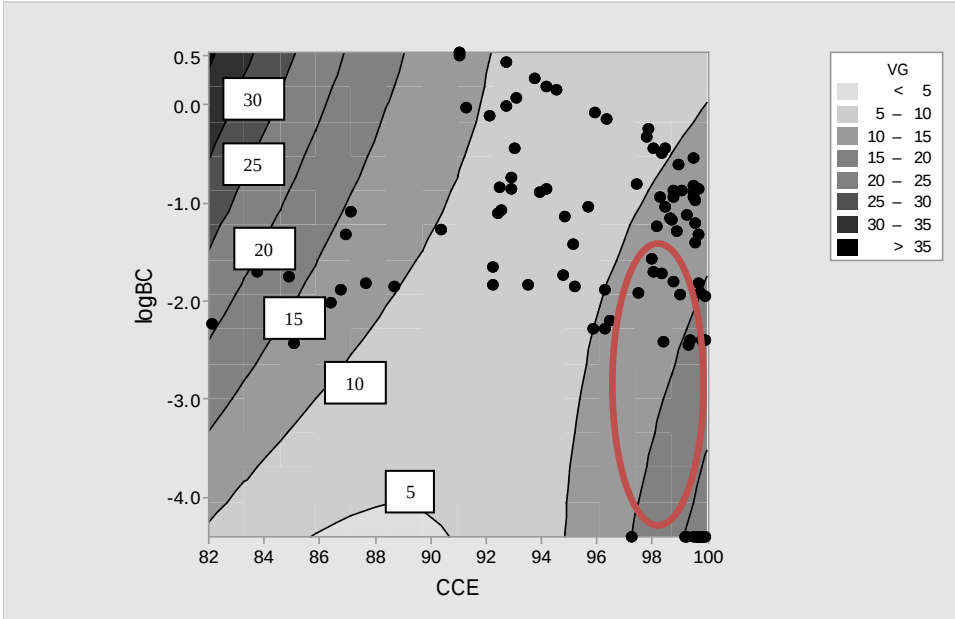

Fig. 5.15 2-D Contour plot for the model VG vs. log BC, CCE (Steam assisted flares)

The model equation for all air assist data is given below:

Model Equation

$$VG = -18.09 - 14.64\ \log BC + 0.2675\ ACE + 0.1905\ \log BC * ACE \quad (5.16)$$

Model Summary

S	R-sq	R-sq(adj)	R-sq(pred)
3.25358	25.98%	21.45%	12.73%

Table 5.14 Air assist data range used in developing the quadratic model equation Eq. 5.16 [Source: 1983, 1984, & 2010 Flare study reports]

No. of data points	BC	V	A	VG	DB	LHV	D
	lb/MMBTU	ft/s	lb/MMBTU	MMBTU/hr		BTU/scf	inch
53	0.002 - 9.8	0.5 – 72	0 – 26200	1.5 – 21	0 / 1	330 – 2180	18 – 24

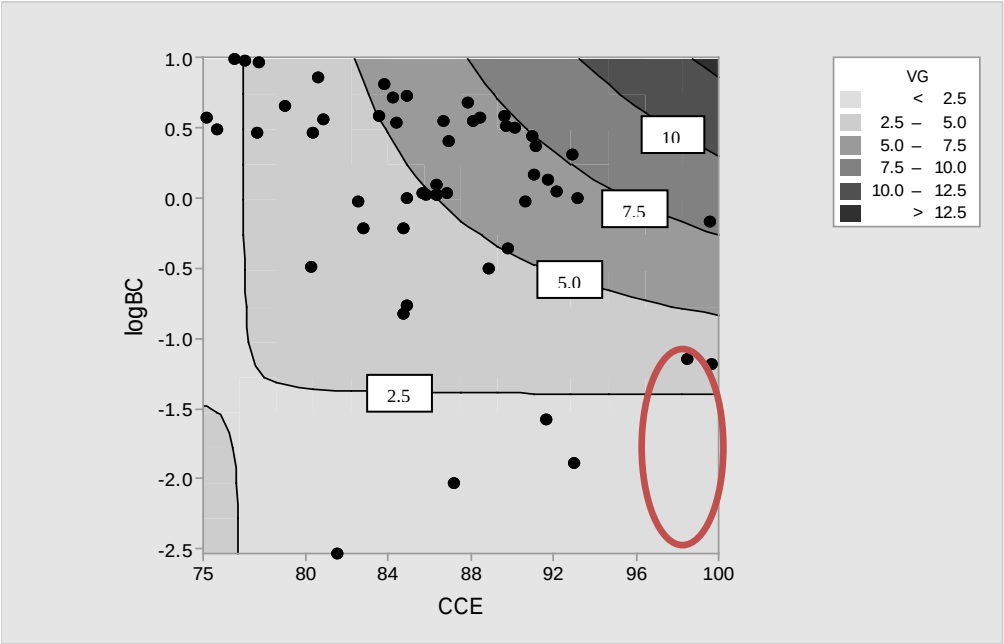

Fig.5.16 2-D Contour plot for the model VG vs. log BC, CCE (Air assisted flares)

From the figure, it is clear that VG in the range of 1.5 – 4 (MMBTU/hr) is required for low soot emissions (log BC < –1 or BC <0.1 lb/MMBTU)) and high CE (>96%).

5.4. Conclusions

- CCE decreased about 3 – 8% (steam assist) and 17 – 22% (air assist) when soot emissions were taken into account for calculation of combustion efficiency.
- Steam flow in the range of 80 – 110 lb/MMBTU and air flow in the range of 4000 – 13000 lb/MMBTU produce minimum soot at the incipient smoke point according to 2010 TCEQ data.
- Response surface models for soot/CCE/DRE as response were developed for steam assist and air assist flare tests for both Propane and Propene mixtures using all available flare test data from 1983 till 2010.
- Optimal range of LHV, VG, S and A for simultaneously high CE and low soot emissions were estimated from 2D and 3D contour plots.

5.5 Future Work

Inverse response models of S (or A, VG, LHV) can also be developed as a function of Log BC and DRE (instead of CE). The use of dimensionless groups or normalized variables may improve the robustness of the developed response surface models. Further study is needed to characterize the ISP in terms of absorbance, absorptance, and soot emissions and to investigate the effect of feed gas composition and soot particle size on soot opacity at the incipient smoke point for steam and air assisted flares.

Reference Cited in this Section

[1] David T. Allen and Vincent M. Torres, 2010 TCEQ Flare Study Final Report, The University of Texas at Austin, The Center for Energy and Environmental Resources, TCEQ PGA No. 582-8-86245-FY09-04 and Task Order No. UTA10-000924-LOAT-RP9, Aug. 1, 2011.

[2] McDaniel, M., Flare Efficiency study, EPA-600/2-83-052, July 1983. http://www.epa.gov/ttn/chief/old/ap42/ch13/s05/reference/ref_01c13s05_jan1995.pdf

[3] Pohl, J., R. Payne, and J. Lee. 1984. Evaluation of the efficiency of industrial flares: Test Results. EPA-600/2-84-095. Prepared for U.S. EPA Office of Research and Development by Energy and Environmental Research Corporation (May).

[4] David T. Allen and Vincent M. Torres, "TCEQ 2010 Flare Study Final Report--Appendices," August 1, 2011, http://www.tceq.texas.gov/assets/public/implementation/air/rules/Flare/2010flarestudy/2010-flare-study-final-appendices.pdf

[5] Minitab 17 User Guide.

[6] https://onlinecourses.science.psu.edu/stat501/node/89

[7] http://www2.hawaii.edu/~taylor/z632/MTBmodelseln.pdf

[8] https://onlinecourses.science.psu.edu/stat501/node/36

[9] http://blog.minitab.com/blog/adventures-in-statistics/multiple-regession-analysis-use-adjusted-r-squared-and predicted-r-squared-to-include-the-correct-number-of-variables

[10] Kathleen M. Carley, Natalia Y. Kamneva, and Jeff Reminga. Response Surface Methodology. CASOS Technical Report, Oct. 2004.

[11] Matlab R2010a user manual.

[12] Pilat and Ensor .1970. Plume opacity and particulate mass concentration. Atmospheric Environment. Vol.4. 163 – 173.

[13] https://hplc.chem.shu.edu/NEW/Undergrad/Molec_Spectr/Lambert.html

[14] Fortner, Brooks, Onasch, Canagaratna, Massoli, Jayne, Franklin, Knighton, Wormhoudt, Worsnop, Kolb, and Herndon (2012). Particulate Emissions Measured During the TCEQ Comprehensive Flare Emission Study. Industrial and Engineering Chemistry Research. 51. 12586 - 12592.

6. SUMMARY REMARKS AND FUTURE WORK

Summary Remarks

As indicated in recent TCEQ and EPA reports, the flare destruction and removal efficiency (DRE) and combustion efficiency (CE) can drop below the 98% threshold under certain high air/steam-assisted conditions even in compliance with 40 CFR 60.18. Basic combustion chemistry indicates that many intermediate species including VOCs, HO_x, NO_x, CO, and soot may be formed and emitted during the combustion process in addition to CO_2 and water. Flare operators have a special concern about soot emission, i.e., to avoid visible smoke to comply with EPA's visibility regulations. From an operations standpoint, this means there are dual objectives for flares to accomplish: full destruction of hydrocarbons and negligible soot emission. In this project, the challenge of simultaneously addressing these two goals is examined. This project aims to study important flare operating parameters, while summarizing the knowledge base in simple response surface contour maps, and seeking optimal operating regimes for design, operation, and regulatory purposes. The project is to 1) Generate DRE/CE /soot emission data for various fuel/nitrogen mixes by conducting large-scale laboratory flare experiments; 2) Develop CFD methodology that is validated/calibrated with controlled flare data and is capable of predicting DRE/CE/soot emission; and 3) Search for the acceptable operating window in terms of steam/air injection and makeup fuel in the face of operating variables such as vent gas composition, exit velocity, and crosswind.

Experimental measurements of flare efficiency and species emission rates were performed at the Carleton University flare facility using flares of three different diameters (38.1 mm, 50.8 mm, and 76.2 mm), for a range of flare gas compositions. Separate methodologies based on closing the overall carbon mass balance and based on metered injection of tracer into the plume and sampling system were employed, and full mathematical details of these methods in conjunction with detailed uncertainty analysis procedures have been separately submitted for peer-reviewed journal publication. These methodologies permitted quantitative measurements of flare efficiency, soot emission rates and NOx emission rates as reported with the results. Efficiencies were generally high as expected given the quality of the fuels and the quiescent crossflow conditions. Efficiencies for flares burning methane-based natural gas mixtures were all above 99%. Efficiencies were lower when burning ethylene, predominantly

due to increased soot emissions. Overall, soot emission rate results were shown to have strong dependence on fuel chemistry and comparatively negligible dependence on flare diameter. By contrast, NOx emission rates were shown to have little dependence on fuel chemistry and scaled directly with the fuel consumption rate.

In this project, a new reduced mechanism (LU3.0.1) was developed and validated successfully against literature data. LU 3.0.1 contains important soot precursor species and can handle C_1-C_4 hydrocarbons. The important C_4-species included in this mechanism are n-butane, 1-butene and 1,3-butadiene while the soot precursor species included are acetylene, ethylene and benzene. The new mechanism (LU3.0.1) performs much better in the case of ignition delay and adiabatic flame temperature as compared to the LU 1.0 and LU1.1 mechanisms. In the case of laminar flame speed, LU3.0.1 shows a relatively high deviation from the experimental data, but nonetheless, it is comparable to the full USC II mechanism which has an error percentage of 14.78 %. Overall, the results show that the simulation and experimental literature results are in good agreement for light hydrocarbons.

The new chemical mechanism is further applied to CFD simulation, which can test the mechanism in action along with turbulence and turbulence-chemistry interaction models.The latter like non-premixed PDF model and eddy-dissipation concept (EDC) model in Ansys FLUENT were used to simulate air assisted flare tests for which DRE/CE/soot data are available (Carleton University's large scale laboratory flares and 2010 TCEQ tests). From soot yield CFD analysis, it can be concluded that soot yield predicted with Fluent-PDF model is well within uncertainty limits. The CO_2 yield and combustion efficiency (CE) predicted is almost exact when compared to experimental data. New approach of model constant correction in the Moss-Brookes soot model can better fit the trend of soot emission versus fuel-exit velocity. However such correction must be dealt with careful analysis and validation. For 2010 study data, the PDF model provided good predictions for soot yield and CE.

Since soot emission was not considered for the CE calculations in the 2010 flare study, corrections were made and expressed as "corrected CE" or CCE using data provided by ARI. CCE decreased about 3 – 8% (steam assist) and 17 – 22% (air assist) when soot emissions were taken into account for calculation of combustion efficiency. Data analysis based on 107 steam assisted flare data and 53 air assisted flare data reveal that incipient smoke points in general lie within steam flow range of 80 – 110 lb/MMBTU and air flow range of 4000 – 13000

lb/MMBTU. Response surface models for soot/CCE/DRE as response were developed for steam assist and air assist flare tests from 1983 till 2010 for which both soot and CE data are available (These tests dealt with propane and Propene mixtures). Optimal range of LHV, VG, S and A for high CE and low soot emissions were estimated from 2D and 3D contour plots.

Future Work

Carleton University can expand the experimental work to cover different fuel mixes to include H2, propylene. Exploring the limiting exit velocity and air mixes are another possibility to investigate minimum smoke.

The Moss-Brookes soot model's constants will be corrected to best fit the trend of soot yield versus fuel exit velocity (or mass flow rate) partly due to the data revisions made in Task 2. Along with soot yield and combustion analysis, experimental data from Carleton University also provide NO_x analysis. FLUENT's built-in NO_x models can be used to predict and compare with Task 2's NOx data. Since the VOC yields are nearly non-existent when the PDF model is used, for CO and VOC analysis the Eddy Dissipation Concept (EDC) model will be further explored in the future.

New geometry for air assist cases will be modified to best suit the experimental set up. Further, steam assisted test cases will be simulated with a simpler geometry with PDF model and then the same will be modeled in EDC along with the soot model to best match the experimental data.

Inverse response models of S (or A, VG, LHV) can also be developed as a function of Log BC and DRE (instead of CE). The use of dimensionless groups or normalized variables may improve the robustness of the developed response surface models. Further study is needed to characterize the ISP in terms of absorbance, absorptance, and soot emissions and to investigate the effect of feed gas composition and soot particle size on soot opacity at the incipient smoke point for steam and air assisted flares. Response surface models need to be validated by specifying soot emission at the ISP level and solving for DRE/CE for a given steam/air assist.

NOMENCLATURES

A	Air assist flow (lb/MMBTU)
BTU	British Thermal Unit
BC	Black Carbon (soot, lb/MMBTU)
CCE	Carbon Conversion efficiency, %
CE	Combustion efficiency, %
CFD	Computational Fluid Dynamics
CO	Carbon monoxide
CO_2	Carbon dioxide
CZHV	Combustion Zone Heating Value (BTU/scf)
D	Flare tip diameter, inch
DB	Double bond (C=C, Logic Variable, 1/0))
DRE	Destruction and removal efficiency, %
EDC:	Eddy Dissipation Concept (Fluent species transport model)
EPA	U.S. Environmental Protection Agency
ISP	Incipient Smoke Point
lb/hr	Pounds per hour
LHV	Lower Heating Value (BTU/scf)
LU:	Lamar University
MMBTU	Millions of BTU
MMscf	Millions of standard cubic feet per hour
PDF:	Probability Density Function (Fluent species transport model)
S	Steam assist flow (lb/MMBTU)
scf	Standard cubic feet
SNCR:	Selective Non-Catalytic Reduction
SST:	Shear Stress Transport
TCEQ	Texas Commission on Environmental Quality
THC:	Total Hydrocarbons
TI:	Turbulence Intensity
TNG	Tulsa Natural Gas
V	Exit Velocity (ft/s)
VOC:	Volatile Organic Carbon
VG	Vent Gas heat flow (MMBTU/hr)

APPENDIX

A.1 Calculation of Corrected Combustion Efficiency (CCE):

Initially, flare tests with steam assist for which the soot values were reported by Aerodyne, were considered in modeling. The sample calculation of corrected combustion efficiency for test case S4.4.1 is given below:

Original CE % (reported by TCEQ)	=	97.8%
Mass of C in the feed (VG)	=	476.67 (lb/hr)
Mass of soot (reported by ARI)	=	16.0348 (lb/hr)
Actual mass of C in feed (reported as feed by TCEQ)	=	476.67 -16.0348
	=	460.63 (lb/hr)

On substituting the actual mass of C in feed and CE (%) in Eq.1,

Mass of C converted to CO_2	=	450.50 (lb/hr)

Corrected combustion efficiency which is equivalent to CE is calculated by the following equation,

$$Corrected\ Combustion\ Efficiency\ (CCE) = \frac{Mass\ of\ Carbon\ converetd\ to\ CO2}{Mass\ of\ Carbon\ originally\ fed\ as\ fuel} * 100 \qquad (A.1)$$

After substituting these values in Eq. B.1, we get

$$CCE = (450.5) / (476.67) * 100 = 94.51\%$$

Likewise, CCE was calculated for all the steam assist flare test data series. Table B.1 shows the CCE values for all steam assist flare test cases which have soot values as reported by Aerodyne Research Inc.

Table A.1 Corrected Combustion Efficiency for Steam Assist Flare Test Cases [1]

Test case	BC (lb/hr)	CE (%)	Total Carbon in feed (lb/hr)	Mass of C in feed – BC (lb/hr)	Mass of C converted to CO_2 (lb/hr)	CCE (%)
S1.5.1	0.516	99.9	2003.14	2002.63	2000.62	99.87
S1.6.1	0.703	99.7	2006.57	2005.87	1999.85	99.67
S1.7.1	0.161	99.3	2006.57	2006.41	1992.37	99.29
S1.8.1	0.245	95.9	2004.00	2003.76	1921.60	95.89
S1.9.1	0.287	84.9	2003.14	2002.86	1700.42	84.89
S4.1.1	0.129	97.5	452.10	451.97	440.67	97.5
S4.1.2	0.193	94.8	447.58	447.38	424.12	94.8
S4.1.3	0.148	95.2	453.43	453.28	431.53	95.2
S4.2.1	0.603	98.3	452.72	452.12	444.43	98.2
S4.2.2	1.598	97.8	447.01	445.41	435.61	97.5
S4.2.3	3.886	98.9	452.50	448.62	443.68	98.1
S4.4.1	16.034	97.8	476.67	460.63	450.50	94.5
S4.5.1	0.551	90.5	472.83	472.28	427.41	90.4
S4.6.1	9.242	97.8	476.33	467.09	456.81	95.9
S4.7.1	0.158	88.7	473.76	473.60	420.08	88.7
S4.8.1	0.218	83.8	471.54	471.32	394.97	83.8
S5.1.1	4.992	98.0	298.68	293.69	287.81	96.4
S5.1.2	6.665	94.9	292.52	285.86	271.28	92.7
S5.1.3	2.435	93.8	287.73	285.30	267.61	93.0
S5.3.1	0.107	87.7	296.17	296.06	259.65	87.7
S5.3.2	0.089	86.8	290.38	290.29	251.97	86.8
S5.3.3	0.118	84.9	286.02	285.90	242.73	84.9
S5.5.1	0.154	92.3	295.95	295.80	273.02	92.3
S5.6.1	0.905	94.2	295.02	294.12	277.06	93.9
S5.6.2	0.996	92.8	290.45	289.45	268.61	92.5
S5.6.3	0.577	92.7	287.09	286.51	265.60	92.5
S5.6.A	0.940	93.2	290.85	289.91	270.20	92.9
S6.1.1	6.478	99.3	765.26	758.78	753.47	98.5
S6.1.2	10.399	99.2	768.50	758.10	752.03	97.9
S6.1.3	8.799	98.9	803.76	794.96	786.21	97.8
S6.1.A	5.876	99.1	779.17	773.29	766.33	98.4
S6.3.1	0.092	96.3	745.34	745.25	717.67	96.3
S6.3.2	0.117	96.5	780.39	780.27	752.96	96.5
S6.3.3	0.242	96.3	795.69	795.45	766.02	96.3
S6.4.2	0.068	85.1	796.47	796.40	677.73	85.1
S6.4.3	0.107	82.1	793.91	793.80	651.71	82.1
S6.5.1	0.359	98.4	767.29	766.93	754.66	98.4
S6.6.1	0.173	86.4	780.39	780.21	674.10	86.4
S8.3.1	8.289	96.0	272.35	264.06	253.50	93.1
S8.4.1	3.456	93.9	184.83	181.38	170.31	92.1
S8.5.1	3.122	93.2	152.87	149.74	139.56	91.3
S9.1.1	1.937	93.3	455.61	453.68	423.28	92.9
S9.2.1	0.675	92.6	371.33	370.65	343.22	92.4
S9.3.1	0.547	87.3	283.93	283.38	247.39	87.1

Table A.2 Corrected combustion Efficiency for Air Assist Flare Test cases [1]

Test case	BC (lb/hr)	CE (%)	Total Carbon in feed (lb/hr)	Mass of C in feed – BC (lb/hr)	Mass of C converted to CO_2 (lb/hr)	CCE (%)
A1.1.1	58.56	96.9	787.71	729.16	706.55	89.70
A2.1.1	37.11	96.8	301.71	264.60	256.13	84.89
A2.1.2	24.63	95.9	304.29	279.66	268.19	88.14
A2.3.1	24.62	94.4	301.71	277.10	261.58	86.70
A2.4.1	25.60	88.3	302.57	276.97	244.56	80.83
A2.4.2	31.63	88.2	303.43	271.80	239.73	79.01
A2.5.1	18.01	92.4	304.29	286.27	264.52	86.93
A2.5.2	26.83	91.7	302.57	275.74	252.86	83.57
A3.1.1	12.64	97.3	170.19	157.56	153.30	90.08
A3.1.2	19.33	99.2	168.76	149.43	148.24	87.84
A3.1.3	15.20	98.5	168.62	153.42	151.12	89.63
A3.3.1	0.68	85.2	168.47	167.79	142.96	84.86
A3.5.1	3.94	95.4	168.47	164.53	156.97	93.17
A3.6.1	1.25	89.5	168.62	167.36	149.79	88.84
A3.6.2	4.29	89.1	168.76	164.48	146.55	86.84
A3.6.3	2.39	85.9	168.33	165.94	142.54	84.68
A4.1.1	19.24	97.4	292.89	273.63	266.52	91.00
A4.1.2	15.32	96.4	279.61	264.28	254.77	91.12
A4.1.3	13.25	97.6	277.38	264.14	257.80	92.94
A4.3.1	8.97	94.8	279.31	270.33	256.28	91.75
A4.3.2	7.12	91.7	278.23	259.92	238.35	85.66
A4.3.3	9.62	94.3	277.52	267.90	252.63	91.03
A4.4.1	6.94	88.5	280.17	273.23	241.81	86.31
A4.4.2	6.89	88	276.59	269.71	237.34	85.81
A4.4.3	8.28	89	276.81	268.53	238.99	86.34
A4.4.A	6.92	88.5	277.86	270.94	239.78	86.30
A4.5.1	6.12	84.4	278.09	271.98	229.55	82.55
A4.5.2	3.98	84	279.09	275.07	231.06	82.79
A4.5.3	6.52	85.2	278.67	277.67	236.57	84.89
A4.6.1	42.34	98.9	276.52	234.18	231.61	83.76
A5.1.1	4.67	94.4	68.08	55.98	52.84	77.62
A5.1.2	6.01	96.6	69.65	54.23	52.39	75.22
A5.1.3	5.79	96.9	66.36	60.58	58.70	88.46
A5.1.A	8.33	96	68.03	59.70	57.31	84.25
A5.3.2	0.24	85	67.15	66.91	56.87	84.70
A5.4.1	0.51	80.9	67.15	66.64	53.91	80.29
A5.5.1	0.68	90.7	66.36	65.68	59.57	89.77
A5.5.2	1.47	92.7	66.22	64.75	60.02	90.65
A5.5.3	1.73	94.6	67.15	65.41	61.88	92.16
A6.1.1	25.22	99.4	109.76	84.55	84.04	76.57
A6.1.2	24.01	99.4	110.05	86.09	85.58	77.76
A6.1.A	24.59	99.3	109.98	85.37	84.77	77.08
A6.2.1	8.86	91.8	109.91	101.07	92.78	84.42
A6.3.1	18.66	97.1	109.91	91.24	88.59	80.61
A6.4.1	7.47	86.2	109.91	102.43	88.30	80.34
A6.5.1	7.87	81.5	109.91	102.04	83.16	75.66

Table A.3 Steam Assist Flare Test cases with BC, CE, CCE, LHV, V, S, D, DB and VG [1-3]

Report year	Test case no.	BC (lb/MMBTU)	CE (%)	CCE (%)	DB	LHV (BTU/scf)	V (ft/s)	S (lb/MMBTU)	VG (MMBTU/hr)	D (inch)
1984	1	0.28290	99.49	99.49	0	1311	0.5	0	0.115368	3
1984	3	0.13396	98.77	98.77	0	1309	0.5	0	0.115192	3
1984	4	0.13439	99.06	99.06	0	1311	0.5	0	0.115368	3
1984	6	0.07176	94.84	94.84	0	1314	2	0	0.463842	3
1984	7	0.13910	99.64	99.64	0	1314	2	0	0.463842	3
1984	8	0.24934	98.95	98.95	0	1314	2	0	0.463842	3
1984	10	0.06681	98.69	98.69	0	1316	10	0	2.325372	3
1984	11	0.09150	95.66	95.66	0	1323	10	0	2.337741	3
1984	12	0.11422	98.78	98.78	0	1323	10	0	2.337741	3
1984	77	0.03785	95.11	95.11	0	1316	39.6	0	9.575561	3
1984	78	0.00391	98.4	98.40	0	1325	80	0	19.47686	3
1984	79	0.00000	99.66	99.66	0	1307	118.5	2.817406	28.45818	3
1984	80	0.00000	99.2	99.20	0	1255	168.2	0.728804	38.7867	3
1984	81	0.00000	97.27	97.27	0	837	26.8	7.236575	4.121672	3
1984	82	0.00395	99.33	99.33	0	1107	99.3	1.506112	20.19808	3
1984	83	0.00000	99.87	99.87	0	2350	57.8	6.3654	24.95795	3
1984	92	0.00000	99.6	99.60	0	2350	79.3	2.91545	34.24161	3
1984	93	0.00000	99.74	99.74	0	2348	39.2	5.927198	16.91209	3
1984	94	0.00397	99.83	99.83	0	2350	79.3	2.964041	34.24161	3
1984	95	0.00000	99.87	99.87	0	792	53.1	4.227136	7.727391	3
1984	96	0.00000	99.85	99.85	0	1043	126.8	1.361065	24.30058	3
1984	97	0.00000	99.72	99.72	0	1156	39.7	6.901093	8.4326	3
1984	98	0.00000	99.87	99.87	0	1133	79.7	3.449036	16.5921	3
1984	99	0.00000	99.88	99.88	0	1027	198.1	0.874592	37.38248	3
1984	100	0.00000	99.84	99.84	0	1149	158.7	0.971944	33.50504	3
1984	101	0.00000	99.73	99.73	0	1807	39.7	4.422133	13.18141	3
1984	102	0.00000	99.74	99.74	0	1805	78.7	3.886836	26.10148	3
1984	103	0.00397	99.88	99.88	0	1795	120.3	2.9161	39.6774	3
1984	104	0.00000	99.81	99.81	0	921	173.7	1.117832	29.39494	3
1984	105	0.00397	99.77	99.77	0	2350	112.6	2.380951	48.6205	3
1984	28	0.13904	94.15	94.15	0	1318	2.9	0	2.636	6
1984	29	0.06345	99.56	99.56	0	1318	2.9	0	2.636	6
1984	30	0.09025	98.47	98.47	0	1323	2.9	0	2.646	6
1984	31	0.05118	98.9	98.90	0	1316	10.1	0	9.302804	6
1984	35	0.04847	86.93	86.93	0	451	3.1	0	0.902	6
1984	36	0.01948	98.06	98.06	0	454	3.1	0	0.908	6
1984	37	0.01468	92.24	92.24	0	451	3.1	0	0.902	6
1984	38	0.01572	98.76	98.76	0	613	11.7	0	4.333297	6
1984	72	0.01489	93.49	93.49	0	345	2.9	0	0.69	6
1984	73	0.02732	97.97	97.97	0	291	1	0	0.205737	6
1984	74	0.01182	99.02	99.02	0	350	2.9	0	0.7	6
1984	75	0.04759	99.66	99.66	0	1321	2.9	0	2.642	6
1984	76	0.10716	99.54	99.54	0	1311	1	0	0.926877	6
1984	39	0.11390	98.29	98.29	0	1309	0.2	0	0.740894	12
1984	40	0.07528	99.24	99.24	0	1323	2	0	7.481565	12
1984	41	0.11528	99.5	99.50	0	1314	4.1	0	14.86134	12

1984	42	0.12722	99.48	99.48	0	1314	4	0	14.86134	12
1984	43	0.14728	99.5	99.50	0	1318	4.1	0	14.90658	12
Report year	Test case no.	BC (lb/MMBTU)	CE (%)	CCE (%)	DB	LHV (BTU/scf)	V (ft/s)	S (lb/MMBTU)	VG (MMBTU/hr)	D (inch)
1984	44	0.01194	99.73	99.73	0	378	2.1	0	2.13759	12
1984	46	0.07089	98.62	98.62	0	451	0.2	0	0.255266	12
1984	84	0.03961	99.54	99.54	0	1276	1.9	0	7.21578	12
1984	85	0.00000	99.65	99.65	0	1316	4	0	14.88396	12
1984	86	0.00000	99.48	99.48	0	1314	0.2	0	0.743724	12
1984	87	0.00000	99.58	99.58	0	1314	4	0	14.86134	12
1984	88	0.00000	99.21	99.21	0	317	2	0	1.792635	12
1984	89	0.01190	99.72	99.72	0	303	4.1	0	3.42693	12
1984	90	0.00000	99.59	99.59	0	315	0.2	0	0.17829	12
1984	91	0.00000	99.84	99.84	0	1311	3.9	21.43346	14.82741	12
1983	4	3.40120	98.8	91.05	1	2183	1509	0	37.067	8.625
1983	8	2.69200	98.81	92.70	1	2183	837	0	20.564	8.625
2010	S4.1.1	0.01220	97.5	97.47	1	348	2	95.30322	10.54209	36
2010	S4.1.2	0.01849	94.8	94.76	1	346	2	104.7355	10.45676	36
2010	S4.1.3	0.01383	95.2	95.17	1	350	2	103.5734	10.60041	36
2010	S4.2.1	0.05721	98.3	98.17	1	349	2	72.93011	10.5846	36
2010	S4.2.2	0.15323	97.8	97.45	1	345	2	73.70121	10.43087	36
2010	S4.2.3	0.36763	98.9	98.05	1	349	2	64.0901	10.56967	36
2010	S4.2.A	3.15600	98.3	91.06	1	348	1.97	70.9	10.535	36
2010	S4.4.1	1.44709	97.8	94.51	1	363	1.4	29.81683	11.13499	36
2010	S4.5.1	0.05354	90.5	90.39	1	360	1.9	94.3958	11.02519	36
2010	S4.6.1	0.83431	97.8	95.90	1	362	1.8	38.41602	11.13473	36
2010	S4.7.1	0.01429	88.7	88.67	1	361	1.9	115.5285	11.07966	36
2010	S4.8.1	0.01980	83.8	83.76	1	360	1.9	137.303	11.03312	36
2010	S5.1.1	0.71511	98	96.36	1	594	1	110.3796	6.980948	36
2010	S5.1.2	0.97449	94.9	92.74	1	592	1	110.8244	6.838984	36
2010	S5.1.3	0.36207	93.8	93.01	1	588	1	112.8657	6.725851	36
2010	S5.3.1	0.01540	87.7	87.67	1	594	1	185.9416	6.931854	36
2010	S5.3.2	0.01311	86.8	86.77	1	590	1	185.7252	6.801125	36
2010	S5.3.3	0.01767	84.9	84.86	1	588	1	201.1239	6.703729	36
2010	S5.5.1	0.02230	92.3	92.25	1	594	1	164.4365	6.916994	36
2010	S5.6.1	0.13132	94.2	93.91	1	593	1	144.4152	6.892029	36
2010	S5.6.2	0.14668	92.8	92.48	1	590	1	140.9884	6.792273	36
2010	S5.6.3	0.08575	92.7	92.51	1	590	1	142.2517	6.723609	36
2010	S5.6.A	0.13817	93.2	92.90	1	591	1	142.1033	6.805263	36
2010	S6.1.1	0.36257	99.3	98.46	1	609	1.9	84.43708	17.89621	36
2010	S6.1.2	0.57943	99.2	97.86	1	607	1.9	86.20571	17.9462	36
2010	S6.1.3	0.46880	98.9	97.82	1	625	1.9	81.33001	18.76909	36
2010	S6.1.A	0.32312	99.1	98.35	1	613	1.9	84.04867	18.1868	36
2010	S6.3.1	0.00530	96.3	96.29	1	594	1.9	143.2878	17.40604	36
2010	S6.3.2	0.00642	96.5	96.49	1	612	1.9	131.5406	18.2111	36
2010	S6.3.3	0.01303	96.3	96.27	1	619	1.9	126.2328	18.57812	36
2010	S6.4.2	0.00365	85.1	85.09	1	621	1.9	171.393	18.59474	36
2010	S6.4.3	0.00579	82.1	82.09	1	618	1.9	174.6657	18.54734	36
2010	S6.5.1	0.01914	98.4	98.35	1	606	1.9	111.5162	17.92594	36
2010	S6.6.1	0.00950	86.4	86.38	1	613	1.9	161.531	18.22563	36
2010	S8.1.1	1.53090	97.6	94.18	1	356	1.5	47.66	11.071	36
2010	S8.2.1	1.88800	97.4	93.76	1	349	1.1	61.84	8.431	36
2010	S8.3.1	1.17105	96	93.08	1	348	0.9	84.1081	6.376247	36

2010	S8.4.1	0.78614	93.9	92.14	1	351	0.6	127.3641	4.320261	36
2010	S8.5.1	0.93217	93.2	91.30	1	373	0.4	164.0905	3.34981	36
Report year	Test case no.	BC (lb/MMBTU)	CE (%)	CCE (%)	DB	LHV (BTU/scf)	V (ft/s)	S (lb/MMBTU)	VG (MMBTU/hr)	D (inch)
2010	S9.1.1	0.18184	93.3	92.90	1	347	1.4	95.41707	10.64983	36
2010	S9.2.1	0.07778	92.6	92.43	1	356	1.1	116.8755	8.675539	36
2010	S9.3.1	0.08255	87.3	87.13	1	359	0.9	146.2416	6.625556	36
2010	S1.5.1	0.01122	99.9	99.87	1	2145	1.52	94.00767	45.9904	36
2010	S1.6.1	0.01525	99.7	99.67	1	2149	1.52	114.8191	46.07823	36
2010	S1.7.1	0.00350	99.3	99.29	1	2148	1.51	138.2208	46.06773	36
2010	S1.8.1	0.00532	95.9	95.89	1	2146	1.5	164.1339	46.00962	36
2010	S1.9.1	0.00623	84.9	84.89	1	2144	1.5	183.4402	45.99086	36

Table A.4 Air Assist Flare Test cases with BC, CE, CCE, LHV, DB, V, A, VG, and D [1-3]

Report year	Test case no.	BC (lb/MMBTU)	CE (%)	CCE (%)	DB	LHV (BTU/scf)	V (ft/s)	A (lb/MMBTU)	VG (MMBTU/hr)	D (inch)
2010	A1.1.1	3.23743	96.9	89.70	1	2108	1.4	8247.231	18.09	24
2010	A2.1.1	5.35828	96.8	84.89	1	2108	0.5	12002.87	6.93	24
2010	A2.1.2	3.52522	95.9	88.14	1	2125	0.5	11998.23	6.99	24
2010	A2.3.1	3.55398	94.4	86.70	1	2108	0.5	12819.32	6.93	24
2010	A2.4.1	3.6846	88.3	80.83	1	2113	0.5	21412.92	6.95	24
2010	A2.4.2	4.54009	88.2	79.01	1	2120	0.5	21324.23	6.97	24
2010	A2.5.1	2.578	92.4	86.93	1	2124	0.5	17113.14	6.99	24
2010	A2.5.2	3.86086	91.7	83.57	1	2115	0.5	17191.53	6.95	24
2010	A3.1.1	3.175	97.3	90.08	1	339	1.9	4620.06	3.98	24
2010	A3.1.2	4.855	99.2	87.84	1	339	1.9	4868.305	3.98	24
2010	A3.1.3	3.822	98.5	89.63	1	339	1.9	5366.981	3.98	24
2010	A3.3.1	0.174	85.2	84.86	1	334	1.9	15363.79	3.91	24
2010	A3.5.1	1.000089	95.4	93.17	1	336	1.9	9075.458	3.94	24
2010	A3.6.1	0.31549	89.5	88.84	1	339	1.9	12299.7	3.97	24
2010	A3.6.2	1.078041	89.1	86.84	1	338	1.9	11948.36	3.97	24
2010	A3.6.3	0.604442	85.9	84.68	1	337	1.9	11630.93	3.95	24
2010	A4.1.1	2.8129	97.4	91.00	1	584	1.9	7569.266	6.84	24
2010	A4.1.2	2.347121	96.4	91.12	1	564	1.9	7691.279	6.53	24
2010	A4.1.3	2.0411	97.6	92.94	1	560	1.9	7541.211	6.49	24
2010	A4.3.1	1.3737	94.8	91.75	1	564	1.9	10353.88	6.53	24
2010	A4.3.2	1.094832	91.7	85.66	1	563	1.9	10224.7	6.50	24
2010	A4.3.3	1.48245	94.3	91.03	1	561	1.9	9940.524	6.49	24
2010	A4.4.1	1.058267	88.5	86.31	1	564	1.9	12543.77	6.56	24
2010	A4.4.2	1.063882	88	85.81	1	561	1.9	12575.97	6.48	24
2010	A4.4.3	1.236089	89	86.34	1	559	1.9	12154.25	6.70	24
2010	A4.4.A	1.063882	88.5	86.30	1	561	1.9	12560.53	6.50	24
2010	A4.5.1	0.9387	84.4	82.55	1	563	1.9	17208.69	6.52	24
2010	A4.5.2	0.6104	84	82.79	1	562	1.9	17172.01	6.52	24
2010	A4.5.3	1.000934	85.2	84.89	1	561	1.9	17122.57	6.52	24
2010	A4.6.1	6.51685	98.9	83.76	1	559	1.9	4646.293	6.50	24
2010	A5.1.1	2.93437	94.4	77.62	1	344	0.8	5496.008	1.59	24
2010	A5.1.2	3.7153	96.6	75.22	1	351	0.8	4907.135	1.62	24

2010	A5.1.3	3.7136	96.9	88.46	1	341	0.8	5348.12	1.56	24
2010	A5.1.A	5.2462	96	84.25	1	345	0.8	5253.949	1.59	24
Report year	Test case no.	BC (lb/MMBTU)	CE (%)	CCE (%)	DB	LHV (BTU/scf)	V (ft/s)	A (lb/MMBTU)	VG (MMBTU/hr)	D (inch)
2010	A5.3.2	0.150124	85	84.70	1	344	0.8	26237.81	1.57	24
2010	A5.4.1	0.325247	80.9	80.29	1	340	0.8	19465.84	1.57	24
2010	A5.5.1	0.43768	90.7	89.77	1	340	0.8	14839.12	1.56	24
2010	A5.5.2	0.9396	92.7	90.65	1	341	0.8	14794.09	1.56	24
2010	A5.5.3	1.10844	94.6	92.16	1	342	0.8	15421.13	1.56	24
2010	A6.1.1	9.835	99.4	76.57	1	584	0.7	4446.902	2.56	24
2010	A6.1.2	9.2998	99.4	77.76	1	586	0.7	4315.818	2.58	24
2010	A6.1.A	9.5675	99.3	77.08	1	585	0.7	4558.182	2.57	24
2010	A6.2.1	3.4323	91.8	84.42	1	586	0.7	9716.692	2.58	24
2010	A6.3.1	7.275423	97.1	80.61	1	584	0.7	6960.549	2.57	24
2010	A6.4.1	2.9076	86.2	80.34	1	585	0.7	15793.24	2.57	24
2010	A6.5.1	3.0679	81.5	75.66	1	584	0.7	22061.23	2.57	24
2010	A7.1.1	0.070837	98.6	98.43	0	376	0.8	5104.47	1.78	24
2010	A7.1.2	0.0658	99.8	99.65	0	356	0.8	4255.064	1.67	24
2010	A7.2.1	0.013091	93	92.97	0	357	0.8	13506.96	1.67	24
2010	A7.2.2	0.026177	91.7	91.64	0	356	0.8	11733.8	1.67	24
2010	A7.3.1	0.002883	81.5	81.49	0	355	0.8	24503.5	1.67	24
2010	A7.5.1	0.00933	87.2	87.18	0	356	0.8	17019.62	1.68	24
1983	65	0.6734	99.57	99.57	1	2183	72	0	20.83	18.25

A.2 Model Validation

This section explains the model validation procedure and identification the important variables in response surface methodology using best subsets regression method.

The regression model is validated based on the following factors:

1. Adjusted R-squared:

The adjusted R-squared factor compares the explanatory power of regression models that contain different numbers of predictors. It is a modified version of R-squared that has been adjusted for the number of predictors in the model. The adjusted R-squared increases only if the new term improves the model. It decreases when a predictor improves the model by less than expected by chance. It is always lower than the R-squared [4].

2. Predicted R-squared:

The predicted R-squared shows how well a regression model predicts the responses for new observations. This statistic helps you determine when the model fits the original data but is

less capable of providing valid predictions for new observations. A key benefit of predicted R-squared is that it can prevent you from over fitting a model [4].

3. Mallow's Cp-statistic:

Mallow's Cp-statistic estimates the size of the bias that is introduced into the predicted

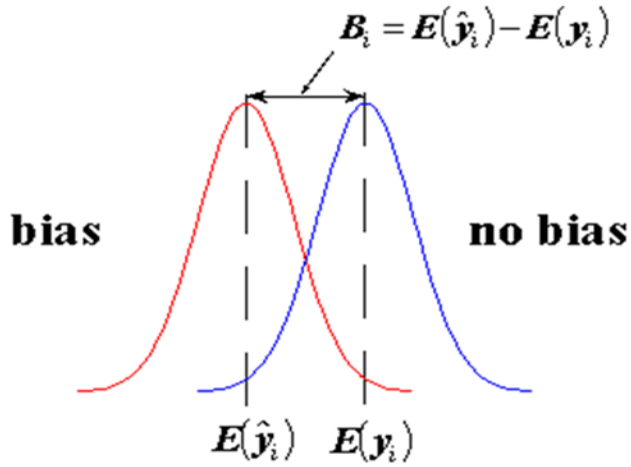

responses by having an underspecified model [5].

when the C-p value is ...
... near p, the bias is small (next to none); (p denotes the number of parameters in the model)
... much greater than p, the bias is substantial;
... below p, it is due to sampling error, interpret as no bias;

For the largest model containing all of the candidate predictors, Cp = p (always). Therefore, you shouldn't use Cp to evaluate the fullest model.

4. PRESS: (Prediction Sum of Squares)

In general, the smaller the PRESS value, the better the model's predictive ability. PRESS is used to calculate the predicted R^2, which is generally more intuitive to interpret. Both of them can help prevent overfitting the model because it is calculated using observations not included in model estimation. Overfitting refers to the models that appear to explain the relationship between the predictor and response variables for the data set used for model calculation but fail to provide valid predictions for new observations [6].

5. Residual Plots:

Residual Plots are used to assess the quality of a regression. When conducting a residual analysis, a "residuals versus fits plot" is the most frequently created plot. It is a scatter plot of

residuals on the y axis and fitted values (estimated responses) on the x axis. The plot is used to detect non-linearity, unequal error variances, and outliers. For a linear regression model, the following criteria may be followed for validation [7]:

i. The residuals "bounce randomly" around the 0 line. This suggests that the assumption that the relationship is linear is reasonable.
ii. The residuals roughly form a "horizontal band" around the 0 line. This suggests that the variances of the error terms are equal.
iii. No one residual "stands out" from the basic random pattern of residuals. This suggests that there are no outliers.
iv. The histogram and the normal probability plot should show the normal distribution of the residuals around the mean ($\mu = 0$).

A.3 Best Subsets Regression: log BC versus LHV, VG, V, S, DB, D, MF

In order to find the best model with Soot (log BC) as the response and LHV, VG, V, S, DB, D, MF as the predictors, best subsets regression methods was used. The best model was then determined based on Mallows C-p value (which should be closer to the number of regressors), PRESS (Lower the better) and the R^2 (adj) and R^2 (pred). Fig. A.1 shows that the best model can be developed with LHV, S, DB and VG as the predictors. Higher the value of R^2 (adj), better will be the model. But, R^2 (adj) is always lower than the actual R^2. R^2 (Pred) helps in preventing the overfitting of the model. When the predictors do not have significant effect on the response, the R^2 (Pred) does not increase with increase in the number of variables in the model. The model should have a R^2 (Pred) value closer to the R^2 and R^2 (adj), to be considered as a best model.

Response is logBC

Vars	R-Sq	R-Sq (adj)	PRESS	R-Sq (pred)	Mallows Cp	S	LHV	S	V	VG	B	D	MF
1	23.5	22.8	179.6	20.7	68.0	1.2843					X		
1	19.5	18.7	188.8	16.6	76.9	1.3173						X	
1	19.5	18.7	188.6	16.7	76.9	1.3174							X
1	10.6	9.8	209.9	7.3	96.7	1.3881				X			
1	9.1	8.3	213.8	5.6	100.0	1.3994	X						
2	39.8	38.7	144.0	36.4	33.4	1.1444				X	X		
2	33.7	32.5	155.9	31.1	47.0	1.2008		X			X		
2	32.1	30.8	162.3	28.3	50.7	1.2155				X		X	
2	27.4	26.0	171.6	24.2	61.3	1.2574		X				X	
2	27.1	25.7	174.5	22.9	61.9	1.2597				X			X
3	50.1	48.6	120.6	46.7	12.6	1.0475		X		X	X		

3	45.0	43.4	134.4	40.6	23.9	1.0996	X			X	X			
3	43.1	41.5	139.5	38.4	28.1	1.1180				X	X	X		
3	43.0	41.4	138.7	38.7	28.3	1.1189			X	X	X			
3	41.2	39.4	144.6	36.1	32.5	1.1371				X	X			X
4	**54.9**	**53.1**	**111.3**	**50.8**	**3.7**	**1.0002**	**X**	**X**		**X**	**X**			
4	51.0	49.0	122.3	46.0	12.5	1.0431		X		X	X			X
4	50.4	48.4	122.4	45.9	13.9	1.0494		X		X	X	X		
4	50.1	48.2	126.7	44.0	14.4	1.0519		X	X	X	X			
4	46.7	44.6	132.5	41.5	22.2	1.0880	X		X	X	X			
5	55.5	53.3	113.4	49.9	4.5	0.99884	X	X		X	X			X
5	55.0	52.8	114.2	49.6	5.5	1.0039	X	X		X	X	X		
5	55.0	52.8	118.9	47.5	5.5	1.0040	X	X	X	X	X			
5	51.1	48.7	124.8	44.9	14.3	1.0471		X		X	X	X	X	
5	51.0	48.6	129.3	42.9	14.5	1.0478		X	X	X	X			X
6	55.7	53.0	120.1	46.9	6.0	1.0015	X	X	X	X	X			X
6	55.6	52.9	116.4	48.6	6.2	1.0024	X	X		X	X	X	X	
6	55.0	52.3	126.6	44.1	7.4	1.0088	X	X	X	X	X	X		
6	51.8	48.9	122.3	46.0	14.7	1.0446	X	X	X	X		X	X	
6	51.1	48.1	141.1	37.7	16.3	1.0523		X	X	X	X	X	X	
7	55.7	52.6	129.2	42.9	8.0	1.0065	X	X	X	X	X	X	X	

Best set of variables

Fig. A.1 Best subsets regression results for log BC vs LHV, VG, V, S, DB, D, MF

A.4 Removal of outliers:

After finding the set of important variables, a simple linear model is built and checked for adequacy. Since the simple linear model and the model with interactions were not adequate a full quadratic model was developed for all available data using Minitab software. Residual analysis showed the presence of outliers. Initially, the outlier far from the fitted zero line was removed and full quadratic model was developed again. In this way, a recursive regression was performed. The following table shows the list of outliers removed.

Table A.5 List of outliers removed in developing response surface model for log BC for all steam assist data

Test No	D (inch)	CE (%)	LHV (BTU/scf)	S (lb/MMBTU)	Log BC (lb/MMBTU)	V (ft/s)	VG (MMBTU/hr)	Year of Study
86	12	99.48	1314	0	-4.403	0.2	0.744	1984
91	12	99.84	1311	21.43	-4.401	3.9	14.83	1984
85	12	99.65	1316	0	-4.402	4	14.88	1984
87	12	99.58	1314	0	-4.403	4	14.86	1984
90	12	99.59	315	0	-4.403	0.2	0.178	1984
88	12	99.21	317	0	-4.404	2	1.792	1984

Table A.6 Change in model summary after stepwise removal of outliers during recursive regression.

Step	R^2	R^2 (Adj)	R^2 (Pred)	Data points	Std. Error
1	69.91	67.45	48.56	107	0.8336
2	74.48	72.09	51.96	106	0.7641
3	78.5	76.71	74.65	105	0.6904
4	80.86	79.25	77.05	104	0.6440
5	83.62	82.22	79.83	103	0.5886
6	85.61	84.37	82.2	102	0.5445
7	87.78	86.72	84.97	101	0.4947

A.5 Validation of the model log BC vs. LHV, S, VG, DB

Eq. 5.5 (or E.1) discussed in section 5.3.4a with log BC versus LHV, VG, S, DB as predictors is validated based on the residual plots shown in Fig. A.2, in addition to R^2 (adj) and Pred R^2.

The normal probability plot and the histogram show that the residuals are normally distributed around the mean 0. There is a pattern observed in the residual vs. fitted plots which were due to set of data with zero soot emissions reported in 1984 flare study report. They should be further tested for heteroskedasticity and managed using weighted least squares method in future. The Predicted log BC vs. Actual log BC was plotted for the final model without outliers using the fitted line plot in Minitab software as shown in Fig. A.3. It shows almost all the data lies within 95% prediction band. Most of the data points were close to the fitted line, which shows that this model is a better fit for the data.

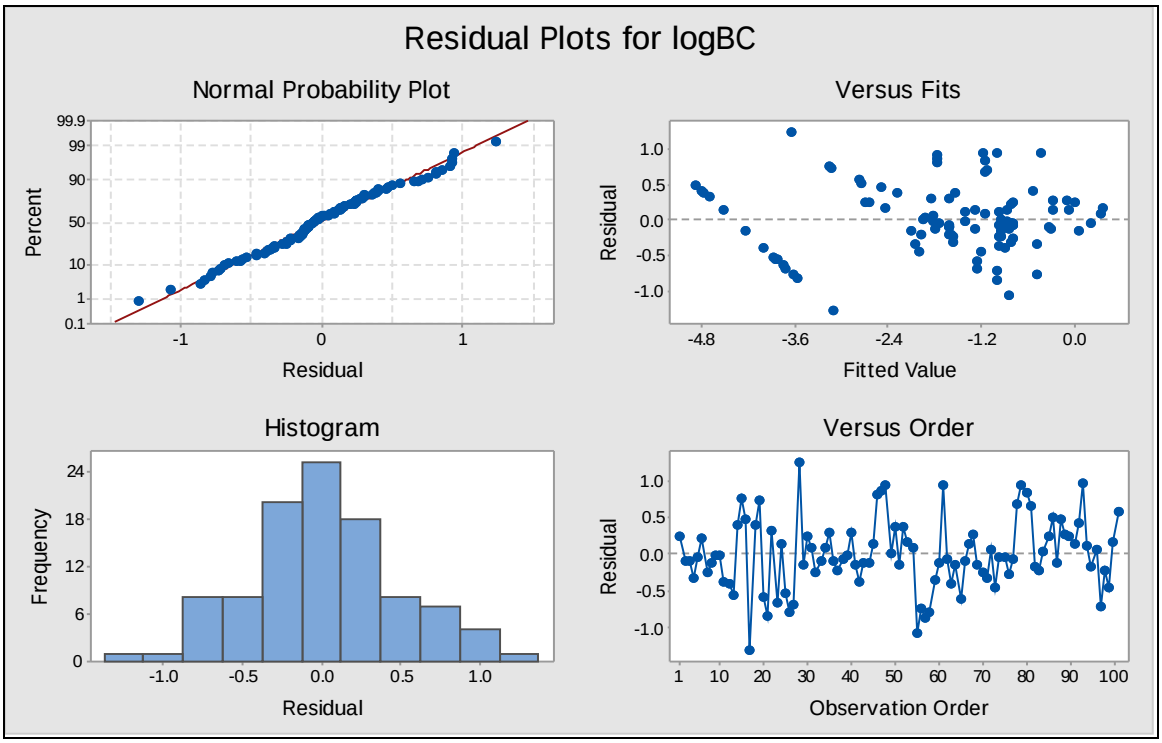

Fig. A.2 Residual plots for the model log BC vs. LHV, VG, S, DB

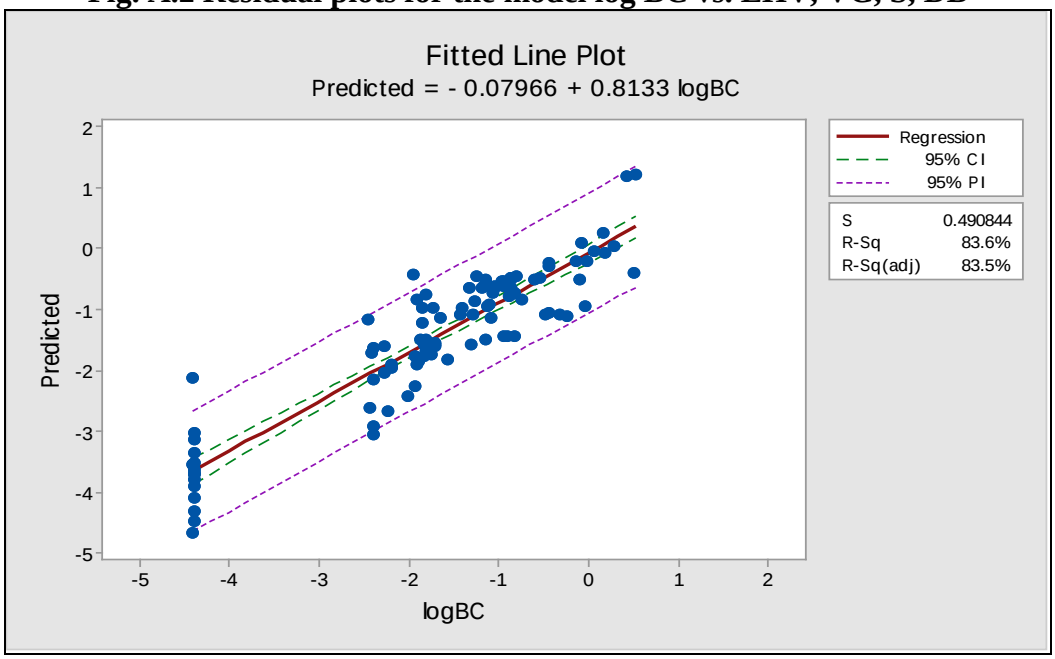

Fig. A.3 Fitted line plot for the Predicted log BC vs. Actual log BC

The predicted vs. actual plots using MS Excel without outliers is shown in Fig. A.4. It can be observed that more than 80% of the data were closer to the diagonal line (y=x). Hence, it

is clear that the model can predict more than 80 % of the data with log BC values in the range of -5 to 2.

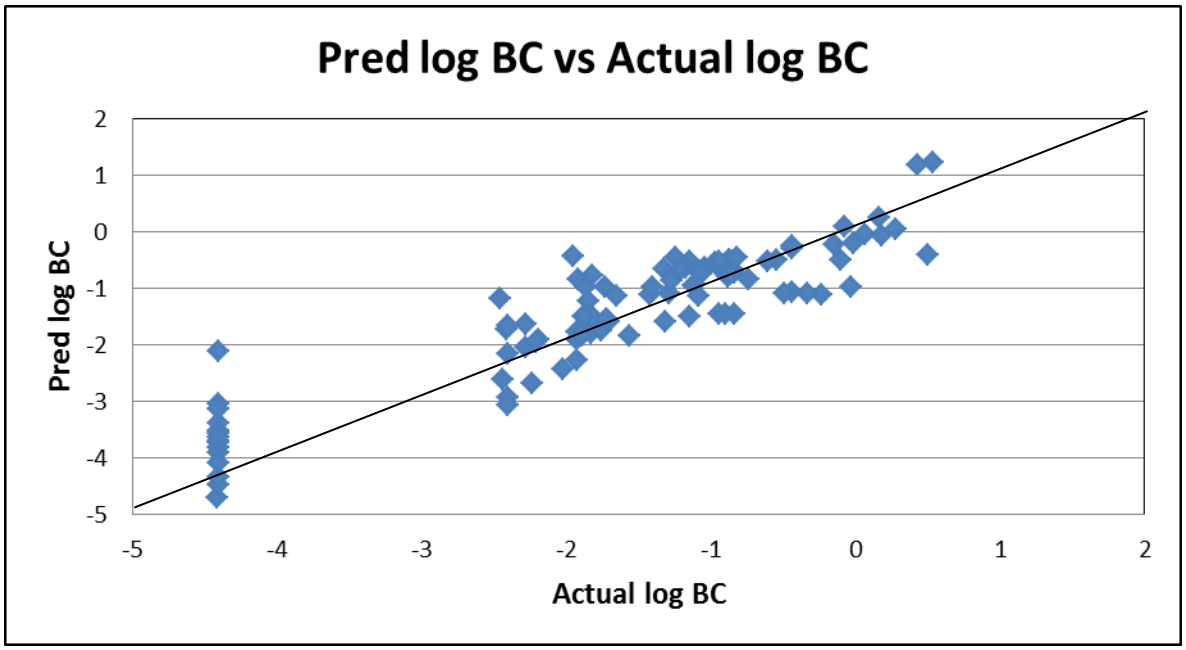

Fig. A.4 Predicted log BC vs. Actual log BC for the model log BC vs. LHV, S, VG, DB w/o outliers

References

[1] David T. Allen and Vincent M. Torres, "TCEQ 2010 Flare Study Final Report--Appendices," August 1, 2011, http://www.tceq.texas.gov/assets/public/implementation/air/rules/Flare/2010flarestudy/2010-flare-study-final-appendices.pdf

[2] McDaniel, M., Flare Efficiency study, EPA-600/2-83-052, July 1983. http://www.epa.gov/ttn/chief/old/ap42/ch13/s05/reference/ref_01c13s05_jan1995.pdf

[3] Pohl, J., R. Payne, and J. Lee. 1984. Evaluation of the efficiency of industrial flares: Test Results. EPA-600/2-84-095. Prepared for U.S. EPA Office of Research and Development by Energy and Environmental Research Corporation (May).

[4] http://blog.minitab.com/blog/adventures-in-statistics/multiple-regession-analysis-use-adjusted-r-squared-and predicted-r-squared-to-include-the-correct-number-of-variables

[5] https://onlinecourses.science.psu.edu/stat501/node/89

[6] http://www2.hawaii.edu/~taylor/z632/MTBmodelseln.pdf

[7] https://onlinecourses.science.psu.edu/stat501/node/36